Title

Molecular understanding of enzyme stabilization toward functional enzymatic materials

Author

DelRe, Christopher

Publication Date

2020

Peer reviewed|Thesis/dissertation

Molecular understanding of enzyme stabilization toward functional enzymatic materials

By
Christopher DelRe

A dissertation submitted in partial satisfaction of the
requirements for the degree of
Doctor of Philosophy
in
Engineering – Materials Science and Engineering
in the
Graduate Division
of the
University of California, Berkeley

Committee in charge:
Professor Ting Xu, Chair
Professor Kevin Healy
Professor Niren Murthy

Fall 2020

Molecular understanding of enzyme stabilization
toward functional enzymatic materials

Abstract

Molecular understanding of enzyme stabilization
toward functional enzymatic materials

By

Christopher DelRe

Doctor of Philosophy in Materials Science and Engineering

University of California, Berkeley

Professor Ting Xu, Chair

Enzymes are powerful natural catalysts that have long been promising as building blocks for functional materials. However, enzymes are only marginally stable in their natural environments—moderate temperature and aqueous solvents—so any perturbations to these ideal conditions tend to denature and/or deactivate enzymes. This instability in nonnatural environments has severely hindered the technological relevance of enzymes.

Here, I used amphiphilic random heteropolymers (RHPs) as a platform to understand and mediate enzyme stability in various nonnatural environments. RHPs are designed so that their compositions and sequences facilitate noncovalent interactions that are strong enough to stabilize the native state of enzymes while remaining soft enough so as to not outcompete the primary forces that govern enzyme folding. While RHPs were initially designed to stabilize enzymes in organic solvents, their versatility is such that they can modulate enzymes' stability, activity, and reaction mechanisms in a variety of situations.

RHPs can stabilize enzymes over long time periods in organic solvents, enabling versatile material fabrication techniques via electrospinning, film casting, spin coating, and 3-D printing. The ensuing enzyme-based functional materials can serve as reusable catalysts with exceptional stability due to confinement in a polymeric matrix.

RHPs can mediate the local microenvironment of enzymes in water as they adsorb to hydrophobic interfaces. Enzymes like organophosphorus hydrolase (OPH) and chymotrypsin become unstable as their hydrophobic substrates phase separate at high concentrations, likely because the enzymes' binding site loops are susceptible to local conformational changes at hydrophobic interfaces. RHPs provide sufficient short-range interactions to stabilize the native state conformation of these enzymes, facilitating efficient two-phase catalysis in water.

RHPs can drive adsorption of enzymes from the organic phase to an oil/water interface, where the enzymatic behavior changes significantly from that in the bulk solvent. RHPs form nanoscopic clusters with enzymes in organic solvents, and the amphiphilicity of RHPs makes these clusters particularly surface active. The low dielectric of nonpolar organic solvents can be

exploited to maintain enzyme latency in the pure organic solvent and trigger activation as conformational changes occur during adsorption to the oil/water interface.

Finally, RHPs can modulate the behavior of embedded enzymes when the confining polymer matrix is also a macromolecular substrate of the enzyme. This behavior enables fabrication of bioactive plastics with on-demand degradation in water. The embedded enzyme's active site determines the degradation pathway and rate, while the matrix's hierarchical and single-chain structure offer thermodynamic and kinetic control over degradation. The RHP not only interacts with the embedded enzymes but can also interact with the polymer matrix, causing degradation recalcitrance that can be overcome by exploiting synergistic enzyme mechanisms.

The results discussed in this dissertation offer new scientific insights into enzyme stability and may lead to functional materials with immediate technological relevance.

Molecular understanding of enzyme stabilization toward functional enzymatic materials

Table of Contents

Acknowledgements

I first acknowledge my family and friends, whose continued love and support has helped me persevere through difficult times throughout my life and especially during my PhD. I acknowledge my mentor, Professor Ting Xu, whose guidance has been instrumental in my personal and scientific growth. I will miss working in Ting's group, but I am sure that the many lessons I have learned will serve me well throughout my career. I acknowledge my labmates, mentors, collaborators, and mentees, who have been so generous with their time and effort in helping me to learn, expand my skillset, and finish my PhD! It has been an absolute pleasure to work with so many kind and talented people. Finally, I acknowledge Sam, without whom none of this would be possible.

Chapter 1:
Enzymes as promising material building blocks

1.1 Introduction: enzymes are powerful natural catalysts

Enzymes are natural molecules that rapidly and selectively catalyze a broad spectrum of chemical reactions.[1] Many enzymes are such powerful catalysts that they approach the diffusion-limited maximum catalytic efficiency ($k_{cat}/K_M \approx 1 \times 10^9\ M^{-1}\ s^{-1}$, where k_{cat} is the substrate turnover rate and K_M is the Michaelis binding affinity parameter).[2] The catalytic power of enzymes comes directly from their well-defined folds and three-dimensional structure,[3] which balance favorable intermolecular interactions (primarily the hydrophobic effect and hydrogen bonding) with a large unfavorable entropic penalty associated with restricting the enzyme to a specific conformation.[4] The native state of an enzyme typically gives rise to a well-defined active site, where the substrate binds and the reaction occurs.[5] Although alternative explanations have been put forth to explain the catalytic origin of enzymes,[6] it is generally accepted that the majority of enzymes' catalytic power comes from preorganization energy.[7] The amino acids that comprise the enzyme active site are preorganized due to the enzyme's specific fold; thus, the electronic transition state of a chemical reaction in the active site is easily stabilized and has a substantially lower activation barrier compared to the uncatalyzed reaction in bulk solvent (which has a high energetic penalty for reorganizing the solvating molecules during the reaction) (**Figure 1.1**). Clearly, an enzyme's function is directly tied to its structure, so a detailed understanding of enzyme structure is crucial.

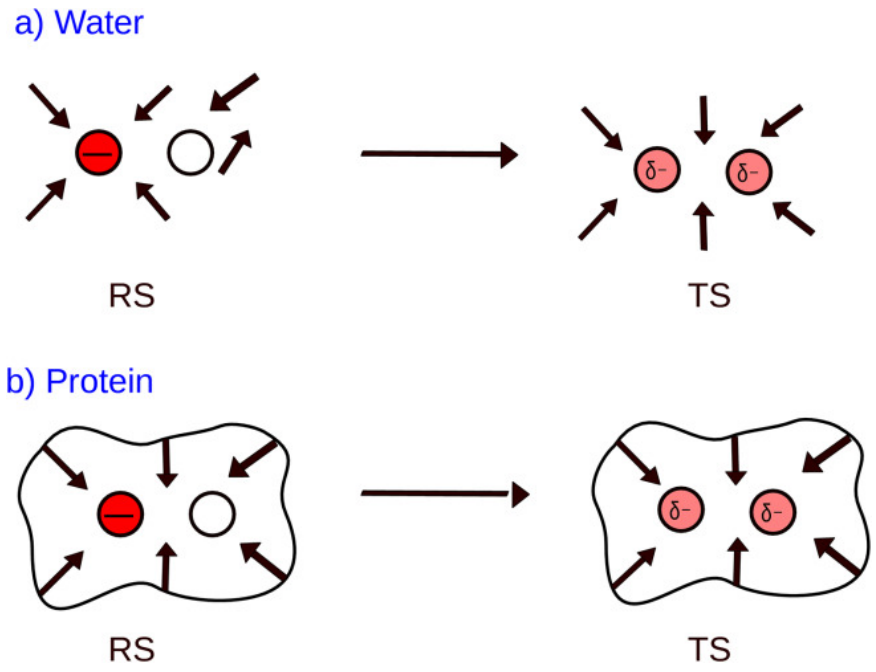

Figure 1.1 *Preorganization of charged groups in enzyme active site lowers the activation barrier of a reaction compared to that in bulk solvent by stabilizing the electronic transition state (adapted from ref [8])*

1.2 Enzymes are chemically diverse, hierarchically structured, and dynamic

Enzymes are biopolymers composed of amino acids. The twenty amino acids that typically exist in natural enzymes span a wide variety of functional groups, conferring a rich array of chemical diversity from which evolution has used to optimize enzymatic catalysis. The amino acid residues can be grouped into five general categories: positively-charged basic (arginine, histidine, and lysine), negatively-charged acidic (aspartic acid and glutamic acid), polar uncharged (serine, threonine, asparagine, glutamine, tyrosine, and tryptophan), and nonpolar (alanine, valine, isoleucine, leucine, methionine, and phenylalanine). The fifth category is a "special case" group of uncharged, nonpolar residues: cysteine is typically used to form disulfide bridges, glycine confers flexibility to the backbone due to the small hydrogen side group, and proline confers kinks in the backbone due to the rigid ring formed between the alpha carbon and the amine nitrogen.

Like synthetic polymers, enzymes are typically long-chain molecules with 100-400 amino acid monomers. Unlike synthetic copolymers, enzymes' primary structure—or the order in which the constituent amino acids are tethered together—is well-defined. This primary sequence encodes hierarchical structure in enzymes: the backbone carbonyl and amine groups form hydrogen bonds that stabilize alpha helices or beta sheets, called the secondary structure. Coils or loops are other important secondary structure motifs that provide flexibility to enzymes, but these motifs typically possess less defined structure in their domains. Packing of secondary structural motifs give rise to a three-dimensional conformation, called the tertiary structure. Formation of the tertiary structure gives rise to the enzyme active site, and thus maintaining this structure is typically crucial for enzyme activity. Tertiary structure is driven primarily by hydrophobic forces, as burial of nonpolar amino acids provides a large entropic gain by releasing water molecules. Finally, enzymes can dimerize or oligomerize to form even more complex three-dimensional structures, called quarternary structure. A general schematic of enzymes' structural hierarchy is presented in **Figure 1.2**.

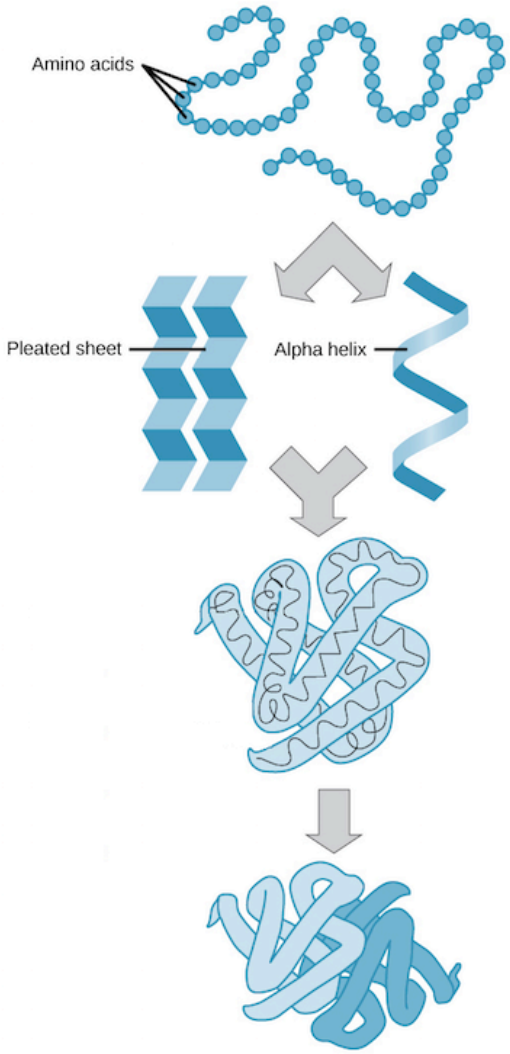

Figure 1.2 *Four levels of hierarchical structure in enzymes from primary structure (top) to quaternary structure (bottom) (image taken from khanacademy.org)*

Although the native state of enzymes is depicted as a well-defined structure, it has been known since the 1970s via experiment[9] and simulation[10] that the native state is in fact highly dynamic. Through relating structure via Fourier transform-infrared spectroscopy (FTIR) and neutron scattering to activity via common substrate binding assays, it was shown that the native state of myoglobin exists in three rapidly-interconverting conformers.[11] In a separate set of experiments, flash photolysis showed that the substrate rebinding process for myoglobin exhibited a broad distribution of activation energies for each of the three conformers rather than a single or narrow distribution,[9] suggesting the existence of many substates within the three conformers. Combined results from these studies and others led to the concept of the "conformational energy landscape" depicted in **Figure 1.3**.[12] While these early studies on the ensemble behavior of enzymes were instrumental in developing our initial understanding of dynamics, they were unable to distinguish between the existence of static heterogeneity—i.e. many different semi-permanent conformations within an ensemble at any given time—and dynamic fluctuations of single enzyme

molecules due to the ensemble nature of the experiments. More recently, it was shown using sophisticated single-molecule electron transfer experiments that dynamic fluctuations of single molecules indeed dominate the enzyme dynamics landscape.[13] Other fluorescence experiments suggested that single enzyme molecules have a conformational memory effect: substrate turnover is dependent on previous turnover steps because of fluctuations in protein dynamics.[14]

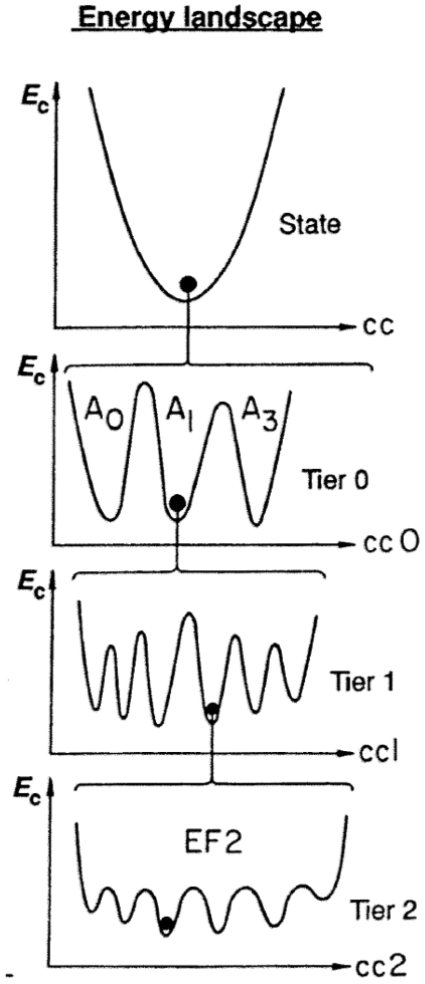

Figure 1.3 *Conformational energy landscape of enzymes, where tier 0 represents the three native state conformers of myoglobin and each subsequent tier represents the distribution of substates within the preceding energy minima (adapted from ref[12])*

The role of conformational dynamics on the actual catalytic power of enzymes is currently an actively studied topic. Many groups have provided evidence that conformational dynamics are linked to crucial steps in enzymatic catalysis cycles,[6, 15] but others (led primarily by the Warshel group) argue using detailed thermodynamic and computational analyses that dynamics play either no role or a minor role in catalyzing reactions[8, 16-17] and that the majority of catalytic power comes solely from the preorganization effect previously described. While more evidence is required to determine the extent to which conformational fluctuations affect catalytic power, it is indisputable

that enzymes are highly dynamic molecules that rapidly interconvert among a spectrum of substates. The potential role of conformational dynamics on enzyme (in)stability will be discussed later in Chapter 2.

1.3 Enzyme instability is an obstacle for functionality

The excellent catalytic efficiency and environmentally-benign nature of enzymes makes them desirable building blocks for a variety of functional catalytic applications. For instance, enzymes can neutralize acutely-toxic chemicals,[18] degrade plastics,[19] and catalyze the synthesis of pharmaceutically-relevant small molecules.[20] Functional enzyme-embedded polymer materials could thus find use as smart fabrics to protect against toxins or plastics with on-demand programmable degradation in water. However, enzymes are inherently unstable: the native state of most enzymes in aqueous environments is only ~5-20 kcal/mole more stable than unfolded states.[4] With such marginal energetic stability, even seemingly-minor perturbations like mildly elevated temperatures (~40-60 °C) or the presence of hydrophobic interfaces make many enzymes susceptible to denaturation and/or aggregation in water. Furthermore, enzymes are insoluble[21] and commonly unstable[22] in organic solvents, which hinders the fabrication of enzyme-polymer hybrid materials since most polymers are solution-processed from organic solvent. To improve the technological relevance of enzymes in aqueous environments under non-ideal conditions and enable development of new enzyme-functionalized polymeric materials, the inherent instability of enzymes must be overcome.

1.4 Previous enzyme stabilization approaches have had limited success

Enzyme stabilization has been explored for decades with a variety of approaches having limited successes. A simple approach involves blending osmolytes like glycerol, sugars, or salts in aqueous solution with the enzyme.[23-25] The proposed mechanism of stabilization in aqueous media involves preferential hydration: the osmolyte is "strongly excluded" from the protein's surface due to unfavorable interactions, leaving the solvent water molecules to preferentially hydrate the enzyme's surface. Since the enzyme forms net thermodynamically-unfavorable contacts with the osmolyte, the enzyme surface will tend to minimize its surface area.[23] The native folded state is more compact than unfolded states, so the presence of osmolytes tends to push the folded-unfolded equilibrium toward the folded state and therefore energetically stabilize enzymes. While this approach is successful for some enzymes in raising the thermal stability in buffer, it does not address the incompatibility with polymer processing solvents because most osmolytes are also only water-soluble and hence cannot disperse enzymes in organic solvents.

Blending small molecule or polymer surfactants with enzymes is a similar stabilization approach to osmolytes but utilizes a different mechanism. Amphiphilic surfactants can solubilize and stabilize enzymes either in aqueous[26-27] or organic[28] media by forming direct contact with the enzyme surface, either through hydrophobic interactions in aqueous media or polar interactions in organic solvent. The formation of micelles or shells around enzymes' surfaces has resulted in limited success with stabilization, and this approach has an advantage over osmolyte stabilization because surfactants can disperse enzymes in organic solvents; however, micelles are dynamic and thus leads to protein activity losses after short time periods in unfavorable conditions. Other

physical modification approaches include embedding the enzyme in a solid matrix, like acrylic gels.[29] Physical entrapment in a solid matrix increases enzyme stability by reducing conformational flexibility[30] and thermodynamic accessibility of unfolded states;[31] however, immobilization in a solid matrix also reduces apparent catalytic efficiency by orders of magnitude due to limited substrate accessibility to enzyme active site.[32]

Biological modification—altering the enzyme's primary sequence using random mutation/screening or by rational design—can also stabilize enzymes. Directed evolution has emerged as a powerful tool for enhancing enzyme activity and stability. Present-day natural enzymes are the product of billions of years of evolution, which has optimized enzyme performance through complex relationships between sequence/structure and activity/stability. Some new enzymes can even sprout up in a much shorter timespan—measured in years—in response to chemical cues introduced by human imposition on the environment. For instance, natural enzymes can now degrade the synthetic plastic PET,[33] which was synthesized for the first time less than 100 years ago. However, directed evolution in a laboratory setting speeds the process up even more, to a timescale of ~days. The process works by introducing a few mutations to a wild-type enzyme, screening for enhanced stability/activity, and then doing more rounds of mutations and screening.[34] Directed evolution is so useful because it eliminates the need to deeply understand complex relationships between sequence/structure and function for optimizing enzyme stability/activity. Selective mutations without directed evolution can also improve enzyme stability, as recently demonstrated in the case of PETase where thermal stability was enhanced by introducing metal-binding sites into the enzyme's structure.[35] De novo design involves taking functional protein motifs—like helices that facilitate metal-binding, for instance—and synthesizing non-natural enzymes.[36] Rational de novo design can also improve enzyme stability against thermal/solvent-induced denaturation. While directed evolution, rational selective mutations, and de novo design all have had immense success over the last several decades, they still have some significant drawbacks. Directed evolution can be time-consuming and require extensive resources, especially since the several rounds of synthesis are commonly carried out in bacteria. Selective mutations are not amenable as a generic enzyme stabilization approach given that it requires deep understanding of each individual enzyme (and hundreds or thousands of enzymes may be relevant for materials science!). De novo design may be limited by computational power for larger enzymes or enzyme complexes.

Finally, chemically modifying a wild-type enzyme by attaching polymers to their surfaces has also succeeded in increasing enzyme stability. Certain amino acids like lysine are inherently reactive for simple conjugation chemistries. PEGylation, the covalent linkage of poly(ethylene glycol) (PEG) to enzymes, is the most common covalent modification of enzymes.[37] PEGylation increases enzyme stability through a combination of several mechanisms. The presence of a bulky polymer at an enzyme's surface prevents autolysis by proteolytic enzymes like proteases (subtilisin, trypsin, etc) via steric hindrance.[38] It has also been suggested that PEGylation reduces conformational flexibility of enzymes, thereby increasing thermal stability in aqueous solutions.[39] Direct hydrogen bonding between the attached PEG and enzyme surface has also been implicated as a stabilizing factor.[40] Clearly, PEGylation is effective at improving enzyme stability in aqueous media, and since PEG is amphiphilic PEGylation may also successfully disperse enzymes in polymer processing solvents toward functional enzyme materials. However, PEGylation requires surface accessibility of reactive amino acids, which may not always be feasible. Further, PEG is

not soluble in some common solvents like toluene, which limits relevance for organic solvent dispersion.

1.5 Random heteropolymers stabilize enzymes

While each of the previous enzyme stabilization approaches has merit, problems still persist. Many of the biological and chemical modification approaches require changes to specific residues or sequences in a specific enzyme and thus cannot be easily scaled up as a broad stabilization approach. Other approaches—osmoloytes, small molecule surfactants, PEGylation—have limited or no ability to disperse and stabilize enzymes in organic solvents. The Xu group sought to address these issues by developing random heteropolymers (RHPs) that employ multiple noncovalent interactions to interact with enzymes' surfaces to stabilize the native state of enzymes in nonnative conditions (organic solvent, elevated temperature, etc).[41]

As previously described, enzymes are chemically diverse molecules due to the variety of functional groups present among the twenty amino acids. Enzyme surfaces are composed of heterogeneous chemical patches that are ~1-2 nm in diameter and interpatch distance (**Figure 1.4a and 1.4b**). The random heteropolymer was designed to match the statistical chemical patterning found on enzymes' surfaces and in enzyme primary sequences rather than aiming for sequence-specific polymers. The four monomers that comprise RHP include methyl methacrylate (MMA) as a flexible hydrophobic spacer, ethylhexyl methacrylate (EHMA) to interact with hydrophobic groups on enzymes' surfaces, oligoethylene glycol methacrylate (OEGMA) as a polar group that is well-known to stabilize enzymes, and sulfopropyl methacrylate (SPMA) as a negative group to interact with positive charges on enzymes' surfaces (**Figure 1.4c**). A small screening library determined that the best-performing RHP for enzyme stabilization had a composition of 50:20:25:5 MMA:EHMA:OEGMA:SPMA—any mention of "RHP" in the remainder of this dissertation, unless explicitly stated, refers to this composition.

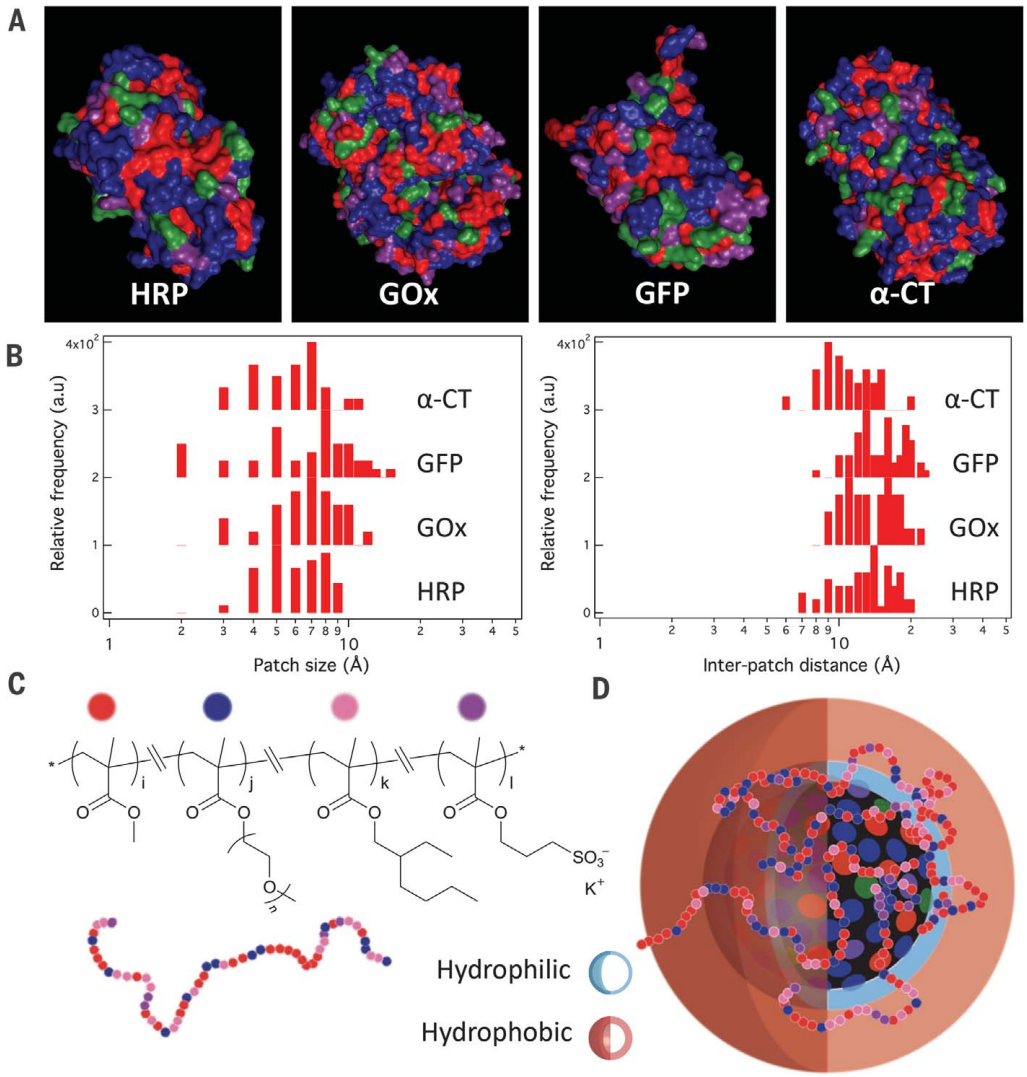

Figure 1.4 *(A) four common enzymes with different chemical function groups labelled using different colors; (B) average patch diameter (left) and interpatch distance (right) for the four proteins shown in "A"; (C) RHP chemical structure; (D) schematic of RHP coating an enzyme surface in an organic solvent*

All atom molecular dynamics (MD) simulations elucidate RHP-enzyme interactions in different media using horseradish peroxidase (HRP) as the model enzyme. In water, RHP-HRP forms dynamic interactions, and only ~40% of the enzyme surface is covered by HRP at the end of the 0.6 μs simulation. However, in toluene, the entire HRP surface is covered over the entire simulation. Hydrophilic monomers (OEGMA and SPMA) were found to orient toward the enzyme surface while the hydrophobic monomers preferentially pointed toward the nonpolar solvent, which agrees with the design. Moreover, ~50% of RHP-enzyme surface contact comes from hydrophilic monomer-hydrophilic amino acid interactions, which contribute the majority of the energetic stabilization in organic solvent (~800 kJ/mole).

Experimentally, the RHP has been shown to stabilize proteins in both aqueous and organic media. Membrane proteins expressed in buffer in the absence of a host cell can be unstable,[42] but it was hypothesized that the RHP may act as a chaperone to direct proper folding in cell-free expression. When blended at a 50:1 molar ratio of RHP:membrane protein, the protein folded properly with an order of magnitude higher efficiency than that of the protein expressed in presence of a liposome, as monitored by fluorescence of a GFP tag at the C-terminal. Moreover, the cell free-expressed membrane protein was able to retain its proton transport function after it was reconstituted in liposomes. Thus, it was determined that RHP can chaperone membrane proteins in aqueous media to fold properly, but the interactions are soft enough so as to not outcompete intramolecular protein interactions.

As of this writing, the RHP has been shown to solubilize and stabilize over 10 commercial enzymes in organic solvents. HRP was used first as a model enzyme, and it was shown that RHP/HRP forms <100nm clusters in toluene (**Figure 5a**). FTIR (**Figure 5b**) and UV-vis spectroscopy (**Figure 5c)** confirmed the retention of secondary and tertiary structure, respectively, and activity screening confirmed that HRP retained ~80% activity in toluene over 24 hours (**Figure 5d)**. This activity retention outperformed common commercial surfactants like small molecule and polymer reverse micelles, which both led to <20% activity retention over 24 hours. Other enzymes could be stabilized using the RHP and processed into functional polymeric materials, demonstrating the versatility afforded by solubilizing and stabilizing enzymes in different organic solvents. Thus, through a combination of simulation and experiment, it is confirmed that matching the statistical chemical heterogeneity of enzymes leads to RHPs that effectively stabilize enzymes in unfavorable conditions via multiple noncovalent interactions.

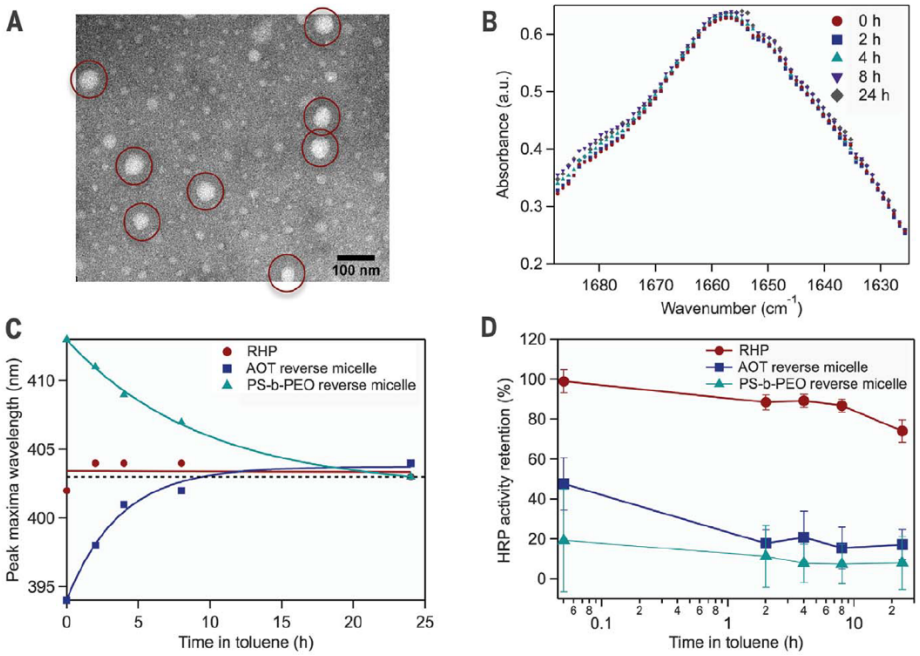

Figure 1.5 *(A) TEM of RHP-HRP cast from toluene; (B) FTIR spectra of RHP-HRP in toluene over 24 hours; (C) UV-vis wavelength peak over 24 hours in toluene for HRP dispersed via varying surfactants or RHP; (D) activity of HRP after dispersed in toluene by varying surfactants or RHP*

1.6 Subsequent chapters: random heteropolymers facilitate advances in enzyme stabilization

The RHP approach introduces numerous opportunities to use enzymes as material building blocks or improve their performance in otherwise unfavorable conditions. I have been interested in using the RHP to facilitate our understanding of enzyme behavior—stability, activity, and intermolecular interactions—in nonnatural environments and to develop enzyme-based materials. I have identified four different areas, all of which benefit from RHP enzyme stabilization and provide new insights into specific aspects of nonnatural enzymology. First, I will discuss enzyme stability and activity toward a small molecule substrate after embedding the enzyme in a solid matrix using organic solvent-based processing techniques, since organic solvent stability was the initial goal of the RHP design. I will then discuss how RHP can stabilize water-soluble enzymes in the presence of hydrophobic interfaces in aqueous media. Next, I will discuss how RHP-enzymes actually function in nonpolar organic solvents and how the RHP drives interfacial activation from nonpolar solvents. Finally, I will discuss embedded-enzyme behavior when the macromolecule embedding matrix is the substrate. I will highlight the scientific advances made in each of these different areas and demonstrate how RHPs have significantly improved the technological relevance of enzymes in traditional aqueous environments and non-traditional organic solvents or enzyme-embedded polymeric materials.

Chapter 2:
Solution-processing enzymes into functional polymeric materials

2.1 Introduction: enzyme incompatibility with organic solvent hinders material development

From the previous chapter, it is clear that enzymes possess many desirable traits to serve as building blocks for functional catalytic materials and as agents for biosynthesis (or bioremediation) of specific molecules. However, enzymes have evolved naturally in aqueous environments and as a result are largely incompatible with organic solvents. Many enzymes will denature in the presence of organic solvents[1] because the solvent molecules disrupt the intramolecular interactions that stabilize the native conformation. Some enzymes can maintain fractions of their native biological activity in organic solvents,[2] and in fact enzymatic reactions that are not possible in water can become enabled by switching the solvent from water to organic solvents.[3] Despite the possibility of maintaining some activity, water-soluble enzymes form > micron sized aggregates in organic solvents. These large aggregates significantly hinder the fabrication of enzyme-embedded polymeric materials with uniformly dispersed enzyme because most polymer processing techniques require organic solvents. Solubilizing and stabilizing enzymes in organic solvents for processing into polymeric materials, and subsequently understanding the behavior of enzymes in these nonnatural environments, can enable the fabrication of new enzyme-polymer hybrid materials.

Organophosphorus hydrolase (OPH) is a particularly relevant enzyme with which to serve as a material building block. OPH can rapidly and selectively neutralize neurotoxic organophosphate (OP) pesticides and chemical warfare agents,[4] so OPH-based materials can potentially serve as fabrics for breathable clothing that protects against neurotoxin exposure or porous membranes that filter contaminated water sources. Various approaches have been explored to develop these OPH-based materials for neurotoxin remediation. OPH has been covalently immobilized on the surface of solid polymers, including Nylon, polyurethane, and silicone.[5-7] These materials successfully retain varying levels of OPH activity; however, drawbacks exist to previous covalent approaches. OPH has a limited number of reactive functional groups exposed on its surface, so covalent immobilization leads to significant enzyme loss (over 50% of the initial OPH concentration and activity). Furthermore, many of the previously-reported OPH materials are not reusable and require cold storage (4 °C or lower). These storage requirements and limited reusability hinder the technological relevance of OPH-based materials: for example, protective clothing or on-demand filtration devices must remain reusable and stable at ambient temperature to successfully serve as functional materials. Physical entrapment of OPH using solid matrices like silk fibroin has been successful for creating OPH-based materials, but the matrix selection and material processing options are limited.[8]

Rather than covalent immobilization on polymer surfaces or physical encapsulation in fibroin matrices, incorporation of OPH in a polymer matrix via non-aqueous material processing affords more flexibility in matrix selection, structural control, and processing. Despite these advantages, incompatibility between enzymes and non-aqueous processing remains as a critical bottleneck to achieve technologically-relevant materials for bioremediation. For

instance, entrapping OPH in a fiber mat via electrospinning would ensure improved substrate accessibility to the enzyme due to the high surface area and porosity afforded by electrospun fibers.[9] Additionally, im- mobilizing OPH inside the fibers would reduce both the enzyme's tendency to aggregate[10] and susceptibility to degradation by proteases, enhancing longevity of the bioremediation agent. However, electrospinning is a non-aqueous processing technique and therefore is incompatible with OPH as well as many other biological building blocks. Given the past success with RHP solubilizing and stabilizing enzymes in organic solvents, we hypothesized that the same approach would enable fabrication of OPH-embedded electrospun fibers. We also sought to quantify the effects of embedding enzymes in polymeric materials on catalytic efficiency and stability.

2.2 Results and discussion: reusable enzymatic fiber mats degrade neurotoxins

Enzyme stabilization in organic solvents has been explored using small molecules and polymeric surfactants, but often leads to significant loss in enzymatic activity.[3] For OPH, dispersion in ethanol with a polymeric micelle leads to a 74% reduction of its native activity.[11] We hypothesized that RHP could stabilize OPH in a range of organic solvents given the previously-demonstrated ability to retain OPH fuction in toluene.[12] In order to fabricate technologically-relevant materials for OP bioremediation, it is requisite to understand and quantify how the RHP-OPH complexation affects OPH's structure and enzymatic activity in organic solvents, how the material fabrication process affects OPH activity, how the material morphology affects substrate accessibility, and how repeated use affects long-term performance of the material. Equally important is to design materials that are functional within the OP concentration regime relevant for practical needs such as trace pesticide removal from water sources and OP stockpile neutralization.

Polycaprolactone (PCL) is an ideal matrix to fabricate materials for OPH-based bioremediation. Its hydrophobicity should minimize protein leaching and facilitate diffusion of the hydrophobic substrate to improve its accessibility. Furthermore, PCL degrades in the environment in just a few years, mitigating environmental pollution from the material. OPH entrapment in PCL electrospun fibers requires dispersion and stabilization of the enzyme in organic media. As schematically shown in Figure 1, the OPH surface is chemically heterogeneous (**Figure 2.1a**). When the chemical diversity on a protein's surface and the functional side chain distribution along the RHP and OPH chains are matched, RHP can effectively complex with OPH and form a soft shell to mediate OPH−solvent interaction and stabilize OPH in a range of organic solvents.14 Dynamic light scattering (DLS) experiments showed that the RHP−OPH complexes were well dispersed in toluene, forming nanoparticles with a hydrodynamic diameter of ∼80 nm (**Figure 2.1a**). In contrast, pure OPH immediately precipitated in toluene. The dispersion of RHP−OPH in toluene enabled the fabrication of a threedimensional, self-standing fiber mat with integrated OPH. PCL fiber mats were successfully electrospun from a toluene-based solution (**Figure 2.1b**). The fibers possessed an average diameter of 3.8 ± 0.5 μm with a small population of sub-500 nm fibers for both pure PCL and PCL-RHP-OPH.

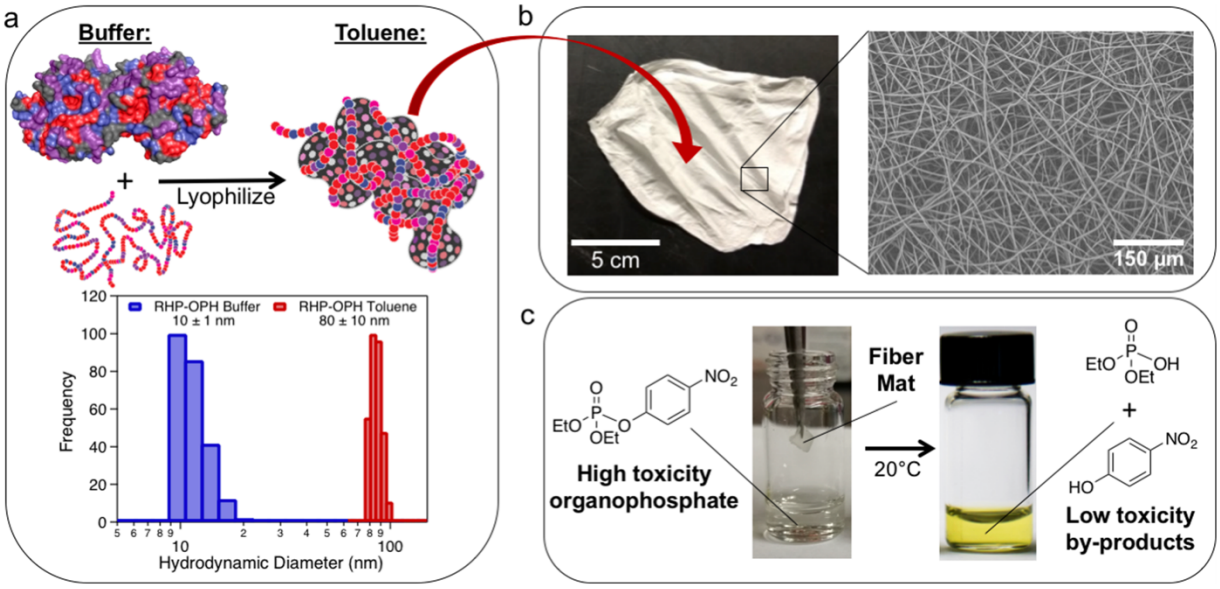

Figure 2.6 *Schematic demonstrating the PCL−RHP−OPH fabrication process and material functionality. (a) RHP−OPH colyophilized in aqueous solution and resuspended in toluene formed well-dispersed, ~80 nm clusters. (b) RHP−OPH was successfully incorporated inside of electrospun PCL fibers by simply mixing the complex with a PCL/toluene/DCM solution and electrospinning the solution. (c) the PCL−RHP−OPH fiber mat retained OPH's biological activity, converting highly toxic organophosphates (clear liquid) into low toxicity byproducts (bright yellow liquid)*

The PCL−RHP−OPH fiber mats were capable of degrading a range of OPs including methylparathion and paraoxon, two common insecticides that possess high acute toxicity to humans and wildlife (**Figure 2.1c**). Paraoxon was chosen as the target substrate for quantitative kinetic analysis because it has high water solubility compared to other OPs, eliminating the need to add organic solvents to the assay. Additionally, paraoxon is the active toxic metabolite that forms when other common insecticides (like parathion) are exposed to air,15 making paraoxon the relevant target for remediation. We performed kinetic analysis to decouple the effects of each step in the fiber mat fabrication process on OPH's catalytic activity. The results were in good agreement with Michaelis−Menten kinetics (**Figure 2.2a and Figure 2.2b**). The maximum reaction rate (Vmax) and substrate turnover rate (kcat) of RHP−OPH after 2 h of toluene suspension was 81% of that from RHP−OPH complexes in buffer. The inverse binding parameter Km, defined as the substrate concentration at one-half Vmax, increased by 1.4 times after 2 h toluene suspension, indicating slightly reduced binding affinity. The addition of 50 vol % dichloromethane (DCM) to toluene, which was necessary to facilitate electrospinning, had statistically insignificant effects on the kinetic parameters of RHP−OPH (80% Vmax of that from RHP−OPH in buffer, 1.1 times Km increase). The RHP−OPH complex exhibited good stability in toluene at room temperature, retaining over 80% of the initial activity of RHP−OPH in toluene after 24 h.

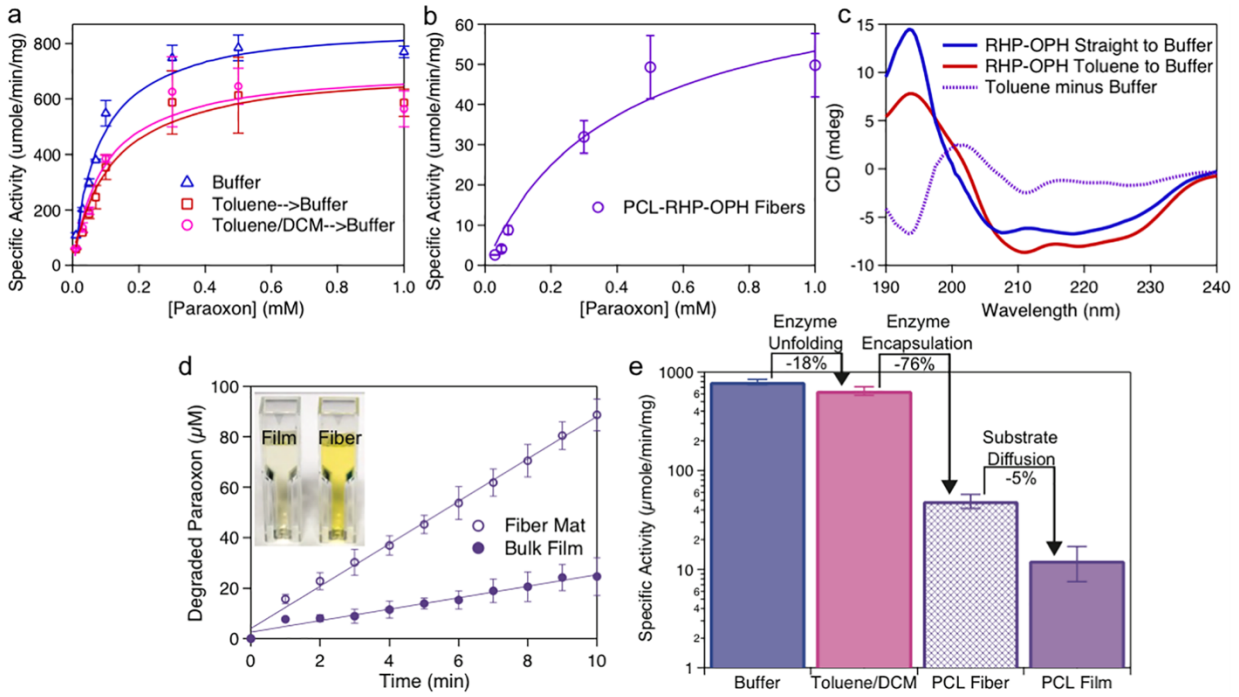

Figure 2.7 *(a) Michaelis−Menten plots for RHP−OPH 2 h suspension in different solvents (assayed in buffer at 20 °C using 50 ng/mL enzyme concentration). (b) Michaelis−Menten plot for PCL−RHP−OPH fibers (assayed in buffer at 20 °C using ∼1 mg fiber mats). (c) Circular dichroism spectra for RHP−OPH (0.15 mg/mL), showing slight conformational change after 2 h suspension in toluene. (d) Rate of hydrolysis for PCL−RHP−OPH fiber mats and bulk films at 20 °C, demonstrating a 4× higher activity for fiber mats of similar mass. (e) Summary of the effect of each processing step on the specific activity of OPH at 0.5 mM paraoxon concentration.*

OPH protein structure was analyzed via circular dichroism spectroscopy. The spectra of RHP−OPH in buffer displayed the widely reported α/β secondary structure of OPH (**Figure 2.2c**).[13-14] The spectra of RHP−OPH that was first suspended in toluene for 2 h exhibited some differences, which could indicate a slight conformational change of OPH.[15] This conformational change may potentially account for the slight increase in Km and reduction in Vmax after suspension in toluene.

RHP−OPH incorporated in PCL fibers possessed a Vmax of 76 ± 10 (μmol/min)/mg, which was 8.5% of the value of RHP−OPH in buffer. The Km of RHP−OPH entrapped in the PCL fibers was 4.8 times greater than that of RHP−OPH in buffer. This level of reduction in reaction rate and substrate affinity is common and expected for immobilized enzymes. The reduction can be attributed to limited substrate accessibility to the enzyme active site due to diffusion of the substrate through the material and steric constraints leading to reduced conformational flexibility of the enzyme.[5] To decouple the effect of material morphology on the macroscopic catalytic rate, a nonporous film with the same OPH loading (0.015 wt %) was fabricated from toluene/DCM solution. Electrospun fiber mats had 4 times higher specific activity than that of the nonporous bulk film (**Figure 2.2d**). This enhanced activity observed with the fiber mat can be attributed to the difference in substrate diffusion through the two materials. Electrospun fiber mats were ∼70%

porous on the basis of the measured apparent density of 0.35 g/ cm^3 while the solid films had negligible porosity (1.15 g/cm^3). The high fiber mat porosity improves substrate accessibility to the embedded OPH and therefore is critical to enhance the apparent activity of the functional material. **Figure 2.2e** summarizes the effect of each processing step on the specific activity of OPH, showing that the majority of the activity reduction occurs from embedding the enzyme inside the PCL matrix.

For PCL−RHP−OPH to be technologically relevant, it is critical that the fiber mat functions at both high and low OP concentrations. The fiber mat is capable of degrading high paraoxon concentrations (tested up to 30 mM), demonstrating the feasibility of using the material for bulk OP degradation. Alternatively, the reduced binding affinity of entrapped OPH raises concerns about the material's ability to degrade low concentrations of OPs. However, the fiber mat is still capable of degrading paraoxon at a concentration of 30 μM (or 8 ppm), which is 5 times lower than the reported oral toxicity level and 13 times lower than the reported dermal toxicity level for the average adult.[16] Thus, the PCL−RHP−OPH fiber mat can be employed as a useful bioremediation material for either degradation of neurotoxic stockpiles or purification of water containing subtoxic concentrations of neurotoxins.

Reusability and long-term stability are also critical characteristics for technologically relevant materials, particularly for those used in on-demand field applications that require repeated cycles. Protein leaching is an added concern for materials that employ noncovalent entrapment of proteins. The fiber mats possessed excellent stability after repeated daily use at room temperature over 3 months, retaining 42 ± 10% of their initial activity (**Figure 2.3a**) and exhibiting no visible signs of fiber disintegration (**Figure 2.3b**). Additionally, fiber mats that were stored dry had statistically insignificant differences in activity compared to that of the recycled mats (**Figure 2.3c**). This insignificant activity difference suggests that protein leaching out of the material likely plays a minimal role for the reduced activity of PCL−RHP−OPH fiber mats.

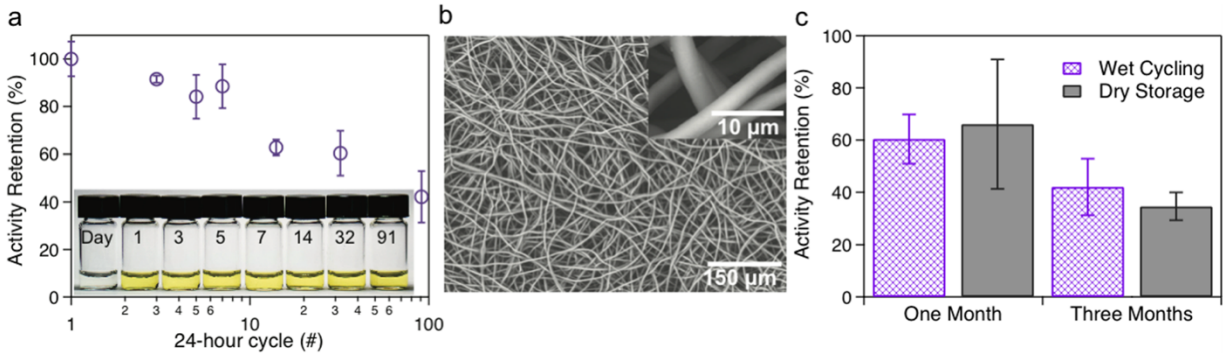

Figure 2.8 *(a) Activity retention for PCL−RHP−OPH fiber mats undergoing daily degradation cycles of 0.5 mM paraoxon at 20 °C. (b) SEM images of PCL−RHP−OPH fiber mat after 92 days of repeated daily use. (c) Activity retention for fiber mats undergoing repeated daily use or dry storage at 20 °C over 1 and 3 months.*

To put our enzyme-based material approach into perspective, we compare the performance of PCL−RHP−OPH fiber mats to that of materials made using other fabrication

techniques. Self-standing films containing only enzymes that were cross-linked with a small polymer surfactant retained 54% Vmax compared to that of the respective enzyme in solution.[17] Eliminating the traditional polymer matrix significantly enhanced substrate accessibility to the enzymes, leading to the high catalytic turnover rate. However, the films were mechanically brittle and had poor reusability, losing up to 31% Vmax after four 25 min cycles and limiting the technological relevance. Typical covalent attachment of enzymes to polymer surfaces results in a broad range of catalytic performance. Vmax retention for OPH-based covalent immobilization has been reported anywhere from 4%[5] to over 50%.[6] This high variability might be explainable by different immobilization reaction conditions: elevated temperature and high glutaraldehyde concentrations can denature enzymes, while more gentle reactions might lead to higher activity retentions. Few have reported on cyclic reusability for OPH-based materials, but most report the need for cold storage (4 °C or lower) to retain activity over time.[5, 18-20] The polyurethane foam-OPH material was stored dry at room temperature for 3 months and retained 51% Vmax, but the material lost 40% of its activity after just 6 paraoxon hydrolysis cycles in buffer.[21] Thus, although our approach of RHP−OPH entrapment inside of a PCL matrix results in a larger activity reduction than that observed in some other material approaches, the entrapment ensures excellent long-term stability and recyclability of the OPH-based material. Additionally, since no covalent reaction is necessary, the design principles demonstrated here can guide the production of other enzyme−polymer hybrid materials, resulting in similar catalytic performances.

2.3 Conclusions

We have reported the fabrication and characterization of a new OPH-based functional material that effectively degrades OP toxins. Kinetic and spectroscopic analysis of the material fabrication process indicated that dispersion of RHP−OPH in organic solvents slightly reduced the enzyme's catalytic efficiency, while entrapment inside the PCL matrix has a more substantial effect (as expected). The OPH-based functional fibers are capable of rapidly degrading both bulk and subtoxic OP concentrations. The fiber mats possess excellent stability, retaining 42% activity after 3 months of repeated daily use. Thus, noncovalent entrapment of OPH in electrospun fibers provides an alternative OPH-based material with large porosity and excellent reusability for on-demand OP bioremediation and trace pesticide removal from water sources. The reported studies provide critical guidance for fabricating functional enzymatic materials with excellent performance.

2.4 Experimental methods

Materials

All solvents were obtained from Fisher Chemical and were used without any further purification. PCL (80,000 g/mole) was purchased from Sigma-Aldrich. OPH expression and purification were carried out as previously reported.[8] TRIS-HCl buffer (50 mM and pH 9, with 100 mM NaCl and 100 μM CoCl2) was used to store the enzyme and run all activity assays. Paraoxon-ethyl ("paraoxon") was purchased from Sigma-Aldrich and stored neat at 4°C. Paraoxon solutions were prepared fresh prior to running assays in the TRIS buffer. The random heteropolymer was synthesized as previously reported.[12]

Methods

RHP-OPH complexes were prepared by mixing both compounds in deionized water and buffer, respectively and lyophilizing overnight in a 65/1 mass ratio. Dynamic light scattering measurements were conducted on a Brookhaven BI-200SM Light Scattering System at a 90° scattering angle. The concentration for each measurement was 2 mg/mL of polymer and 0.03 mg/mL of protein. Circular dichroism measurements were obtained on a JASCO J-1100 spectrophotometer with a 0.15 mg/mL OPH concentration in 10 mM TRIS buffer. The presented DLS data and CD spectra are averages of three measurements.

Electrospinning was carried out on a homemade apparatus. PCL electrospinning solution in toluene/DCM was prepared and stirred overnight at 250 RPM to ensure adequate dissolution of PCL in the solvent. The RHP-OPH complex was lyophilized overnight, resuspended in toluene, and then mixed and stirred with the electrospinning solution to give a final PCL concentration of 15 wt% PCL in 50/50 toluene/DCM by volume. The electrospun fibers were collected on a flat aluminum collector plate, and the operating parameters were as follows: 0.4 mL/hr, 15 cm, and 8 kV. Scanning electron microscope images were obtained on a Hitachi TM-1000 microscope with a 15-kV accelerating voltage. Bulk films were created by dropcasting the polymer solution onto a glass substrate and made uniform by dragging a doctor blade across the solution. Apparent density of fiber mats or bulk films was determined by measuring the weight of the sample and dividing by the sample's dimensions.

All activity assays were run in triplicate. A NanoDrop 2000 (0.1 cm pathlength, for paraoxon concentrations 0.1 mM and over) or Agilent 8453 (1 cm pathlength, for paraoxon concentrations under 0.1 mM) UV-vis spectrophotometer was used to obtain the absorbance measurements of p-nitrophenol, the product of paraoxon hydrolysis, at 410 nm. Beer-Lambert law was used to determine the *p*-nitrophenol concentration, using an extinction coefficient of 16,500 $M^{-1}cm^{-1}$. The assays were carried out at 20°C with the RHP-OPH mass ratio of 65/1. The enzyme concentration for all assays of OPH in paraoxon solution (Figure 2a) was 50 ng/mL. The specific activity of OPH in solution at each substrate concentration was determined by taking the slope of the linear portion of *p*-nitrophenol concentration versus time over 4 minutes and dividing by OPH mass, a standard assay for OPH. The specific activity of the fibers (Figure 2b) was measured by stirring the assay at 250 RPM in 0.5 mM paraoxon solution and taking the *p*-nitrophenol concentration after 10 minutes—a longer time period was used to account for the slower reaction rate. The relative activity between fiber mat and film (Figure 2d) was determined by taking the ratio of the paraoxon hydrolysis rate over ten minutes in 0.5 mM paraoxon/TRIS solution. Nonlinear regression via the Michaelis-Menten package in the PRISM software (version 7.0c) was used to obtain the kinetic parameters of OPH assays. All errors expressed are one standard deviation over the three measurements. Fiber mats and films were rinsed and fully wetted by DI water before running assays to ensure removal of any free OPH on the surface. The 24h toluene incubation experiment (Figure S2) was conducted as previously reported (TRIS-HCl buffer at pH 9, 10mM methylparathion substrate concentration, 20°C). Methylparathion was used to demonstrate ability to degrade different substrates. Relative activity retention was determined by normalizing activity at each given timepoint to the t=0h activity.

For the storage stability experiments (Figure 3), three PCL-RHP-OPH electrospun fiber mats were stored in separate aqueous 0.5 mM paraoxon/TRIS solutions. Every day the fiber mats were removed from their respective solutions, rinsed rigorously with deionized water, and placed in a fresh 0.5 mM paraoxon solution. The same assay described above was employed at each given timepoint to measure the reaction rate, and the rate at each timepoint was divided by the day 0 rate to determine relative activity retention. For the dry storage assays, fiber mat pieces from the same three samples used for the wet storage experiments were placed in a scintillation vial and stored on a benchtop at room temperature and ambient humidity.

Chapter 3:
Mediating the local microenvironment stabilizes enzymes at hydrophobic interfaces in water

3.1 Introduction: Conformational flexibility is important for substrate binding but can also drive instability in water

Flexibility is a hallmark of enzymes' conformational fingerprint.[1-5] Rather than maintaining a static native state structure, enzymes rapidly sample a number of microstates with local energy minima along the conformational energy landscape.[6] An enzyme's most populated conformational state is likely to be heavily sensitive to the local microenvironment, as demonstrated by the detailed studies on short, well-defined peptides. For instance, hydrophobic polymers conjugated to the surface of a helical peptide induce local conformational changes only in the immediate vicinity of the conjugation site because the peptide partially unfolds to mediate unfavorable polymer/water interactions.[7] When an organic co-solvent is added to water, the peptide's entire initial structure is maintained since the polymer has less unfavorable solvent interactions, demonstrating that the local peptide conformation is largely determined by short-range interactions. Peptides have also been designed such that they adopt a random coil conformation in water but fold into a helix or sheet near a water/nonpolar interface.[8] The specific structure adopted at the interface depends on the peptide's sequence such that favorable polar and nonpolar interactions are maximized, reflecting again how the local short-range interactions determine a peptide's conformational state.

While these and other examples[9-11] establish specific mechanistic insights about how microenvironments affect short peptides' conformational states, fewer details are known about enzymes' reliance on microenvironment due to their larger size and more complex network of intramolecular interactions and structures. Studying enzymes with well-defined structural motifs at their active sites may facilitate new insights into features that determine enzyme (in)stability in predominantly aqueous media. Hydrophobic interfaces are particularly interesting microenvironments given the prevalence of interfacial enzymology in Nature and the potential biotechnological relevance of maintaining interfacial enzymatic activity. For instance, stabilizing enzymes at interfaces can enable two-phase catalysis of hydrophobic substrates in water, which would avoid the use of toxic organic solvents that reduce enzymes' activity by several orders of magnitude due to conformational rigidification.[12]

Flexible loops are emerging as important structural motifs for enzyme activity. Surface-exposed loops can directly bind substrates, especially for enzymes like proteases[13] and RNAses[14] that require high flexibility to accommodate their bulky macromolecular substrates. Enzymes like organophosphorus hydrolase (OPH) can use active site loops to rapidly switch between microstate conformations during catalysis, optimizing geometric positioning at various stages along the catalytic pathway (i.e. for substrate diffusion in, transition state stabilization, and product release).[15] Loops that do not directly bind substrates can serve other functional roles, like facilitating conformational changes that expand active site accessibility.[16] Despite the utility of loops as functional motifs, numerous reports associate loops with enzyme instability. For instance, natural thermophilic enzymes typically have more rigid loop domains than their mesophilic

counterparts.[17] Additionally, artificial mutations that rigidify or delete loop segments protect enzymes against heat-[18-19] and organic solvent-[20]induced deactivation.

We hypothesized that enzymes with flexible loops as their primary binding site motifs may be susceptible to interface-induced activity changes due to the reduced barrier for local conformational changes relative to that of more rigid structural motifs. Indeed, many enzymes are known to adsorb to hydrophobic interfaces in water,[9, 21] and some enzymes exhibit drastic activity changes in the presence of hydrophobic interfaces. For instance, it is well established that lipases' activity is significantly enhanced as their active sites are opened up via lid displacement,[22] but other enzymes such as chymotrypsin and glucose oxidase have been shown to lose almost all activity at hydrophobic interfaces with little, if any, mechanistic insights to explain the instability.[23] We chose to study the stability of OPH in the presence of hydrophobic interfaces since loops comprise the entire substrate binding domain.[24] Furthermore, OPH catalyzes the breakdown of neurotoxic pesticides and chemical warfare agents that have little or no water solubility,[25] so manipulating OPH's stability at hydrophobic interfaces can enable two-phase catalysis approaches that safely and efficiently remediate bulk neurotoxin stockpiles in water as the substrate self-assembles into hydrophobic particles at high concentrations.

Here, we demonstrate that OPH undergoes interfacial inactivation in buffer, losing over 90% activity when its substrate self-assembles into hydrophobic suspended particles (**Figure 1a**). Noncovalent interactions with amphiphilic random heteropolymers (RHPs) prevent OPH interfacial inactivation, enabling rapid decontamination of high concentrations (>10 mM) of hydrophobic neurotoxins in water (**Figure 1b**). Specifically, RHP may stabilize OPH by mediating the microenvironment and dampening the enzyme's conformational flexibility, as suggested by the ~20°C increase in T_{50} (the temperature at which 50% activity loss occurs) and the significant tryptophan fluorescence quenching in the presence of RHP. The RHPs' hydrophobic characteristics are the dominant factor in determining the extent of OPH stabilization, with short hydrophobic segments preferred over long hydrophobic blocks, while electrostatics play no observable role. We show that chymotrypsin, which also utilizes surface-exposed binding site loops, is also protected against interfacial inactivation by RHP. The data reported here suggest that surface-exposed binding site loops may be a primary source of enzyme instability at hydrophobic interfaces and demonstrate that mediating loops' microenvironment can prevent interfacial inactivation.

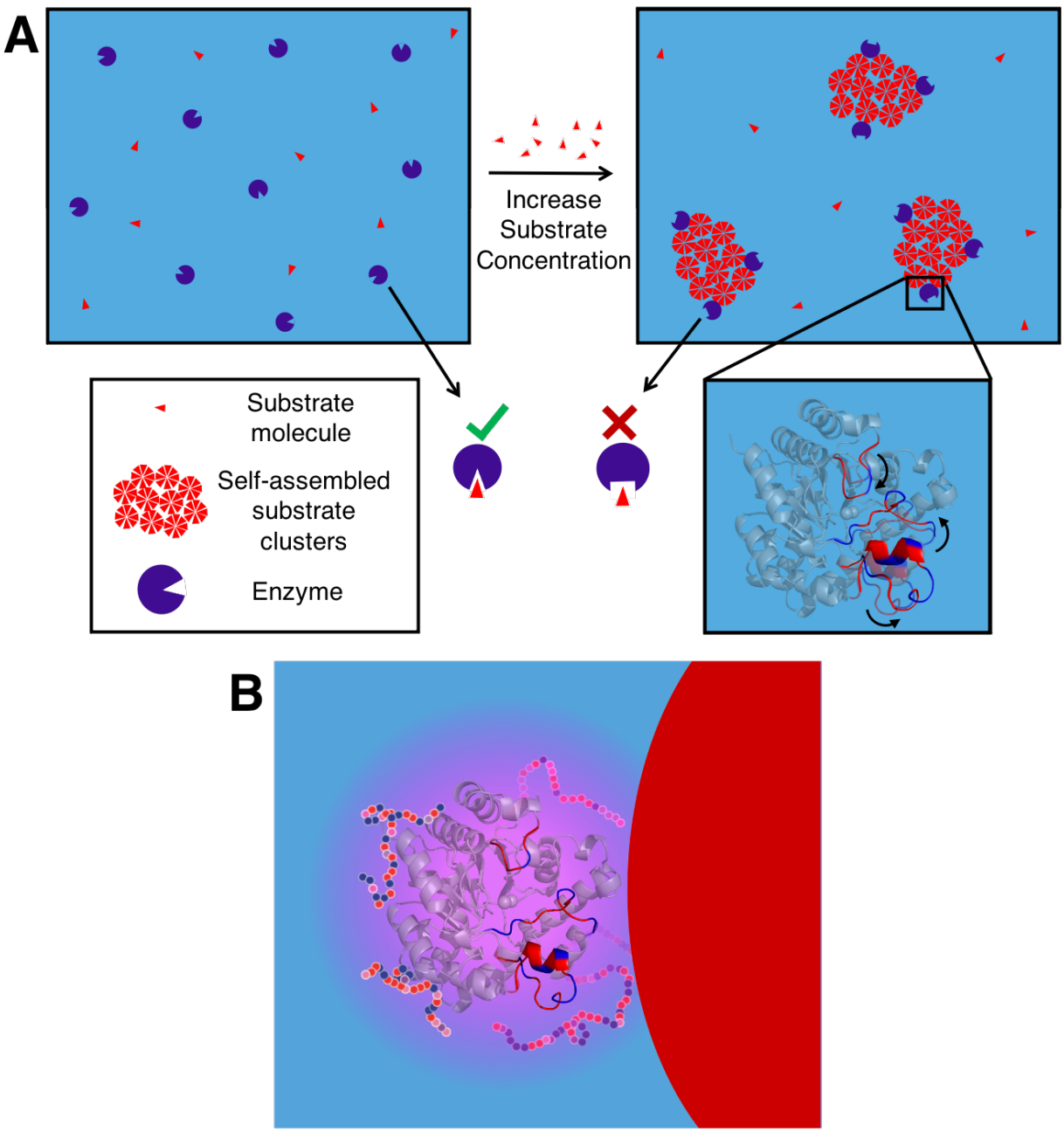

Figure 3.1 *Preventing interfacial inactivation of enzymes with RHP. (A) Enzymatic catalysis of small molecule substrates at low concentrations with active enzyme (blue). (B) The presence of hydrophobic precipitates at high substrate concentrations can lead to enzyme inactivation (red) of up to 100%. (C) Stabilizing enzymes with noncovalent polymer interactions may keep the enzyme active in the presence of hydrophobic precipitates.*

3.2 Results and discussion: Mediating OPH's microenvironment prevents interfacial inactivation in water

Since OPH's substrates are hydrophobic, we wanted to probe the enzyme's stability in the presence of hydrophobic interfaces to develop a bioremediation technique using two-phase catalysis in water while simultaneously testing whether enzymes with binding site loops may be prone to interfacial inactivation. OPH follows Michaelis-Menten kinetics at low substrate concentrations but loses >90% activity after the substrate, methylparathion, surpasses its solubility limit of ~0.5 mM and forms a suspension of 500-1,500 nm hydrophobic particles (**Figure 3.2a and Figure 3.2b**). UV-vis spectroscopy confirmed that at least ~0.5 mM of substrate remained dissolved in buffer for all substrate concentrations up to 10 mM. Thus, it is unlikely that substrate self-assembly and subsequent lack of accessibility to OPH can explain the activity loss at high substrate concentrations. Rather, OPH undergoes interfacial inactivation at hydrophobic surfaces in water.

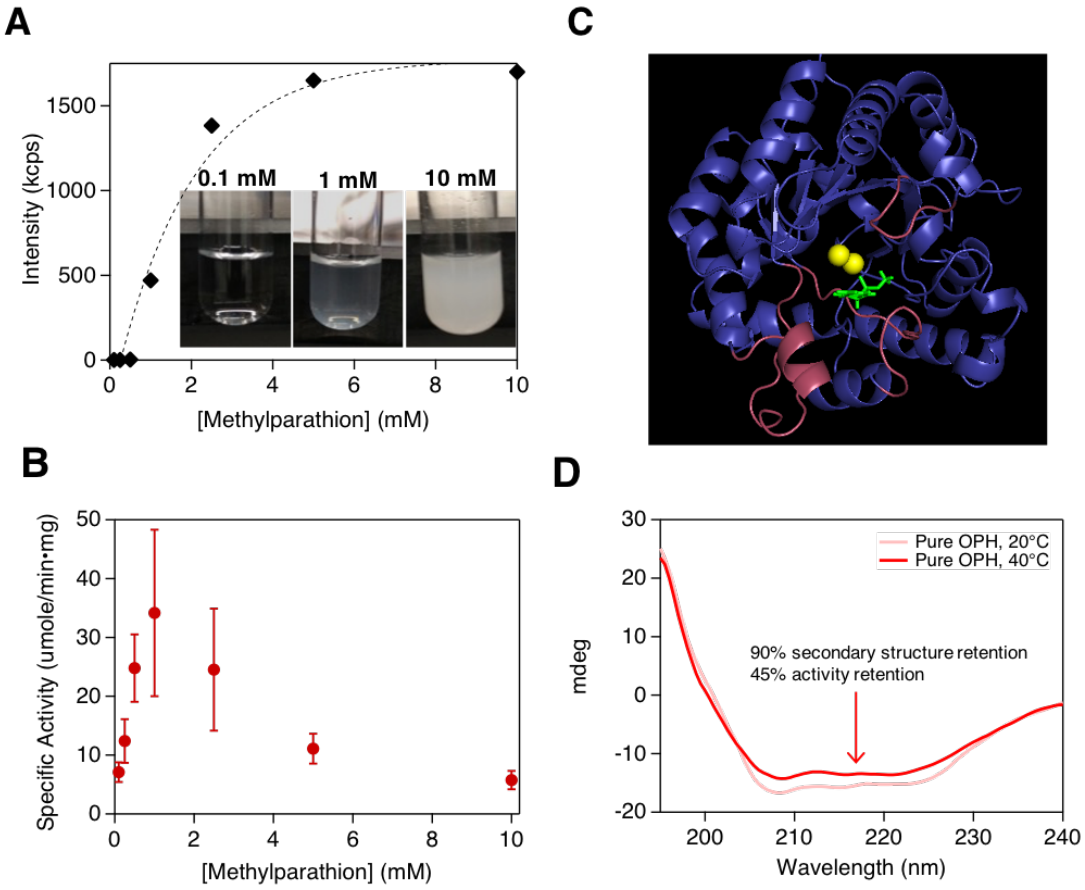

Figure 3.2 *(A) DLS turbidity data of methylparathion in buffer. (B) Specific activity of pure OPH as a function of substrate concentration, showing that OPH loses up to 90% activity in the presence of hydrophobic suspension. (C) Secondary structure representation of OPH highlighting the three flexible loops relevant for catalysis (substrate docking in green, zinc atoms in yellow). (D) Circular dichroism spectra of OPH in buffer as a function of temperature.*

Active site features may provide mechanistic insights into the driving forces for OPH interfacial inactivation. Our own docking simulations (**Figure 3.2c**) verify past experimental reports that highlight the importance of three surface-exposed loops for OPH catalytic activity. "Loop 7" (residues 256-276) mediates the opening to the binding pocket,[15] while the top binding loop (residues 129-135) and bottom binding loop (residues 300-312) contain key aromatic residues that bind and orient the substrate for catalysis by the bimetallic catalytic center.[26-27] Since each of these threes loops is surface-exposed, flexible, and amphiphilic, it is likely that they are particularly susceptible to local conformational changes during adsorption to hydrophobic interfaces, which could deactivate the enzyme without global unfolding of the native state. As further support for this explanation, OPH's structure and activity were quantified as a function of temperature without the hydrophobic suspension present. Despite retaining 90% of its native secondary structure (α-helices and β-sheets) at 40°C based on circular dichroism (CD) spectroscopy, OPH lost ~50% of its native activity (**Figure 3.2d**). Although this experiment cannot directly confirm loop displacement as the main source of OPH interfacial inactivation, it shows that significant portions of enzymatic activity can be lost due to subtle conformational changes (like loop displacement) that would not be detectable in CD spectroscopy since the global native structure is retained.

We hypothesized that mediating the microenvironment of OPH's surface using a polymer additive may be an effective method to prevent interfacial inactivation by reducing the number of accessible unfolded states. We mixed OPH in buffer with an amphiphilic random heteropolymer (RHP), which has previously been shown to protect enzymes' structure and activity[28] (including that of OPH[29]) in organic solvents. The RHP consists of four monomers: a hydrophobic spacer, a hydrophobic side group, a polar side group, and a negatively charged side group (**Figure 3.3a**). At large RHP excesses (>60:1 RHP:OPH), OPH retains its activity and follows a typical Michaelis-Menten profile even at high substrate concentrations in the presence of a hydrophobic suspension (**Figure 3.3b**). To understand how RHP prevents interfacial inactivation, OPH's microenvironment was qualitatively probed via fluorescence spectroscopy since OPH has four tryptophan residues, each of which is surface exposed. The fluorescence spectrum is significantly quenched in the presence of RHP (**Figure 3.3c**), which may be due to altered OPH conformational dynamics near the tryptophan residues[30] or to direct interactions between RHP and OPH's surface since -C=O, which is abundant in RHP, is a known quencher at distances <1 nm.[31] Interestingly, three of the four surface-exposed tryptophan residues exist in (Trp131 and Trp302) or directly adjacent to (Trp277) the substrate binding site loops, suggesting direct changes in the loops' microenvironment. Moreover, RHP significantly increases the thermal stability of OPH in non-destabilizing conditions (low substrate concentrations), increasing T_{50} by ~20°C (**Figure 3.3d**). Previous reports have shown that an increased density of contacts among residues in enzymes' loop regions leads to increased thermal stability,[17] and mutations that rigidified Loop 7 increased OPH's thermal stability.[15] Thus, our fluorescence and thermal stability data support a mechanism whereby RHP stabilizes OPH and prevents interfacial inactivation by directly interacting with OPH's surface and modulating its conformational fluctuations such that OPH can only sample a subpopulation of all available microstates, reducing the probability of loop displacement.

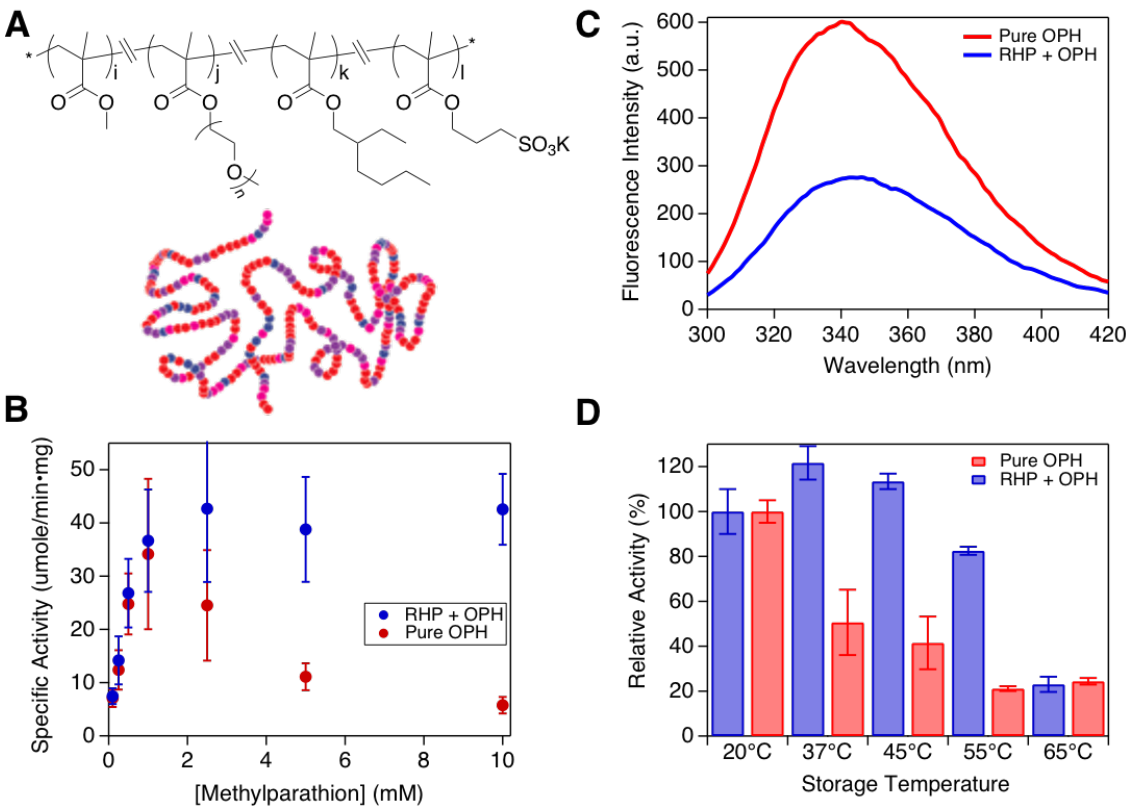

Figure 3.3 *(A) Chemical composition of RHP (top) and chemical heterogeneity of OPH. (B) Activity as a function of substrate concentration for pure OPH and RHP-OPH, showing Michaelis-Menten profile and full activity retention in presence of RHP. (C) Fluorescence spectra of pure OPH (red) and RHP-OPH (blue) monitoring the emission of Trp residues at ~340 nm. Reduction of fluorescence suggests altered microenvironment of Trp residues. (D) Activity during storage for 35 minutes at the specified temperature for pure OPH (red) and RHP-OPH (blue) in buffer and then assayed in non-denaturing conditions (low substrate concentration); T_{50} (50% reduction in activity) is shifted from ~40 °C for pure OPH to ~60 °C for RHP-OPH.*

To understand more deeply how RHP stabilizes OPH, we tested RHPs with different compositions. RHPs with a positively charged monomer substituted in for the negatively charged monomer stabilized OPH to the same extent, suggesting a limited role for specific electrostatic interactions in the stabilization process. Rather, it is likely that RHP's short hydrophobic segments can transiently interact with OPH's amphiphilic loops. To further test this hypothesis, we used RHPs with higher hydrophobic block content among their sequences (specific composition details in SI) (**Figure 3.4a**). The blocky RHP had limited stabilizing effects on OPH, retaining ~1/3 of the activity compared to OPH stabilized by the disperse RHP (**Figure 3.4b**). Furthermore, the blocky RHP only quenches tryptophan fluorescence in OPH by ~5% (**Figure 3.4c**), suggesting limited interactions with OPH's surface-exposed binding site loops compared to the disperse RHP. The high hydrophobic blockiness imparted by increasing the composition of RHP's most hydrophobic monomer from 20% (disperse RHP) to 40-50% (blocky RHP) may reduce the number of favorable RHP segments available to interact with OPH, especially since large hydrophobic sequences tend

to cause chain collapse in water. The improved stabilization for disperse RHP sequences is similar to results found in natural molecular chaperones, which facilitate the correct folding of proteins by presenting short hydrophobic segments spread out over a wide area to provide many low affinity interactions rather than a few high affinity interactions.[32]

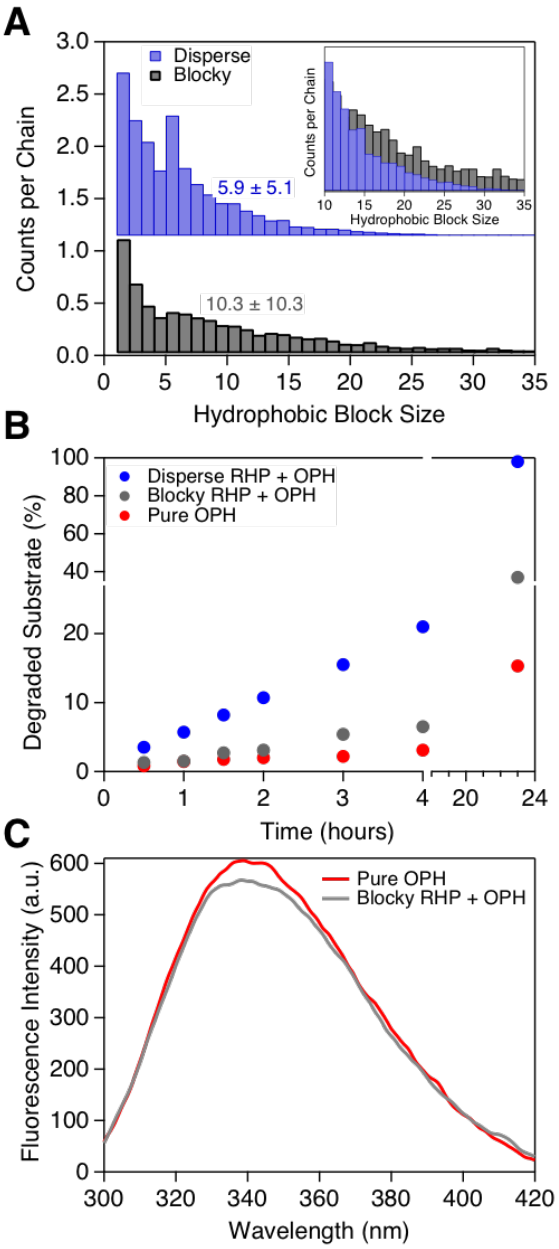

Figure 3.4 *(A) Sequence analysis showing the average block size for hydrophobic residues—the "blocky" sequence is nearly double the average block size of the disperse sequence. (B) Degraded substrate as a function of time for different OPH systems. (C) Fluorescence spectra show minimal quenching of Trp residues along OPH surface, indicating a lack of interactions with OPH's loop regions by the blocky RHP.*

We hypothesized that because of the weak and nonspecific interactions, RHP may prevent interfacial inactivation for other enzymes that utilize similar binding site motifs. Chymotrypsin is a nonspecific protease that is known to utilize two partially surface-exposed loops to bind its hydrophobic substrates[13] (**Figure 3.5a**), making it an apt choice to further explore the role of substrate binding loops in interfacial instability. We incubated chymotrypsin with or without RHP for 10 minutes in a buffer solution with suspended 2-methyoxynaphthalene (10 mM) and then tested the enzyme's ability to hydrolyze a small peptide substrate. Pure chymotrypsin had no detectable activity after incubating with the hydrophobic suspension, whereas RHP-chymotrypsin retained all of the enzyme's native activity (**Figure 3.5b**). Thus, RHP also prevents interfacial inactivation in chymotrypsin.

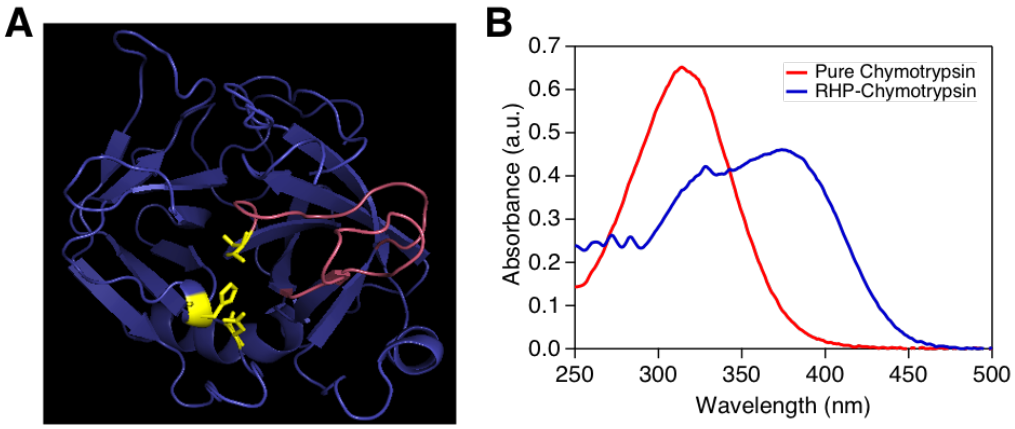

Figure 3.5 *(A) Crystal structure of chymotrypsin showing surface-exposed binding site loops. (B) Chymotrypsin assay in the presence of hydrophobic precipitates (product of substrate hydrolysis absorbs at ~380 nm) showing pure chymotrypsin loses all measurable activity in presence of hydrophobic precipitates but RHP prevents inactivation.*

Enzymes are complicated macromolecules, each one employing its unique and intricate network of interactions; it is therefore impossible to definitively conclude that a general structural motif at the binding site is responsible for interfacial inactivation, and other explanations are possible. For instance, both OPH and chymotrypsin exist natively as dimers, so it is possible that the activity loss at hydrophobic interfaces is due to disruption of the dimeric subunits' packing. However, both enzymes have been shown to remain active in the monomeric form.[33-34] Furthermore, crystallography studies[22] and molecular modeling[16] have established that lipases' binding site lids are displaced via interactions between loops and interfaces. Thus, experimental evidence here and previously established mechanisms elsewhere demonstrate that surface-exposed loops may be particularly susceptible to local conformational changes at hydrophobic interfaces, which can destabilize enzymes that use loops to directly bind substrates (OPH, chymotrypsin) or increase activity for enzymes that use loops to induce conformational changes that expand active site accessibility for buried active sites (lipases).

If surface-exposed binding site loops destabilize enzymes, it begs the question of why enzymes evolve these motifs for substrate binding in the first place. Chymotrypsin's natural substrates are large peptide chains, so a flexible binding site is likely required to accommodate the bulky substrate. Furthermore, although OPH's substrates are small molecules, its loop motif might remain as an artifact of its evolutionary origin since OPH is thought to have evolved from the same enzyme family as RNAses[35], which require high flexibility to accommodate bulky RNA chains. Regardless of evolutionary origin, OPH's catalytic process for small molecules substrates has clearly been enhanced by exploiting loop flexibility to balance conformations that promote substrate/product diffusion ("open state") and transition state stabilization ("closed state").[15] Thus, in Nature it appears that enzymes with surface-exposed binding site loops sacrifice stability for the conformational flexibility that is required to efficiently bind bulky macromolecular substrates and/or rapidly interconvert among substates to optimize geometric constraints along the catalytic pathway. Mediating the microenvironment of these loops while retaining enzyme solubility is an effective way to stabilize enzymes without sacrificing efficiency, as is commonly seen when enzymes are immobilized in solid matrices.[29, 36]

3.3 Conclusions

We have suggested a link between surface-exposed binding site loops and interfacial inactivation in enzymes. Noncovalent surface interactions with RHPs prevent interfacial inactivation in OPH and chymotrypsin, perhaps due to increased density of contacts in loop regions as suggested by the altered active site microenvironment. The RHP composition and sequence play key roles in enzyme stabilization: while electrostatics play a limited role, RHPs with blocky hydrophobic sequences are significantly less effective than disperse sequences, likely because disperse sequences are better able to present short hydrophobic segments that interact favorably with enzymes. The insights provided here offer a new approach for efficient two-phase enzymatic reactions of hydrophobic substrates in water and help to improve our understanding of structure/(in)stability relationships in enzymes.

3.4 Experimental methods

Materials:

Polymer synthesis and enzyme expression:
The random heteropolymers used in this work were synthesized using previously established methods.[28] Unless otherwise stated in the text, the RHP molar composition was 50:20:25:5 methyl methacrylate (MMA):ethylhexyl methacrylate (EHMA):oligoethylene glycol methacrylate (OEGMA):sulfopropyl methacrylate (SPMA). OPH from two different sources was tested to ensure that the interfacial inactivation was not an experimental artifact—both sources exhibited the same interfacial inactivation. One source was generously provided after expression and purification[37] from the Air Force Research Laboratory. The other source was expressed and purified in-house from an OPH plasmid. Briefly, protein was expressed in Rosetta2 cells, induced with 0.5 mM IPTG. Cells were supplemented with 10 μM $CoCl_2$ at time of inoculation and with a

further 90 μM after 4 h of induction. Cells were harvested after 21 h growth at 16°C. Purification was by Ni affinity, using standard buffers and protocols. The material eluting from the column was very cloudy indicating significant precipitation of the protein. However, after clarification, a moderate amount of protein remained in the soluble fraction. This protein was buffer exchanged into 50 mM TrisHCl pH 9.0, 0.1 mM $CoCl_2$, concentrated to 2 mg/ml (Coomassie assay), and frozen in 200 μl aliquots (at -80°C). Chymotrypsin from bovine pancreas and methylparathion were purchased from Sigma Aldrich and used as-is.

Enzyme crystal structures:
The crystal structures of OPH (1HZY) and chymotrypsin (4CHA) were downloaded from Protein Data Bank and analyzed using PyMol. Only one monomer subunit of the dimeric proteins is displayed in the paper in the interest of clarity.

Methods:

Turbidity of methylparathion solutions:
Turbidity was used to roughly quantify the solubility of the substrate at different concentrations. Dynamic light scattering (DLS) was conducted using a 90° detector angle, and the intensity at each substrate concentration is reported as an average of triplicate runs. DLS was also used to estimate the size of the suspended substrate particles at high substrate concentrations when methylparathion surpassed its solubility limit.

OPH assay conditions:
Consistent with past optimal assay conditions for OPH,[38] methylparathion was first dissolved in methanol and then mixed with TRIS-HCl buffer (pH 9) to give a final volume ratio of 90:10 buffer:methanol for each substrate concentration. To obtain the specific activity of OPH at each substrate concentration, ~100 ng/mL of OPH was mixed with the substrate and placed at 37°C for 9 minutes. The solution was then centrifuged for 1 minute to remove any suspended substrate and enable accurate quantification of product concentration using UV-vis spectroscopy. Specifically, the product concentration was quantified by monitoring the 410 nm wavelength with an absorption coefficient of 16,5000 M^{-1} cm^{-1} using a NanoDrop 2000 (0.1 cm pathlength, for high substrate concentrations) or Agilent 8453 (1 cm pathlength, for low substrate concentrations). All assays were run in triplicate.

Control experiment for OPH interfacial inactivation:
To further rule out substrate inhibition as the cause of OPH inactivation at higher concentrations, a control experiment was run using a hydrophobic non-substrate (2-methoxynapthalene). When OPH was incubated with 10 mM of 2-methoxynapthalene (which is beyond its solubility limit and thus formed a hydrophobic suspension) for 10 min, it lost 80% of its activity in the absence of RHP and retained all of its activity (within error) in the presence of RHP. This control experiment further supports interfacial inactivation as the explanation for loss of OPH activity (in the absence of RHP) at high substrate concentrations in buffer.

Circular dichroism:
OPH's secondary structure was quantified using a JASCO J-1100 spectrophotometer. An OPH stock solution was diluted with pure MilliQ water or RHP in MilliQ water (10 mg/mL) to give a

final enzyme concentration of ~0.2 mg/mL. Spectra presented are smoothed averages of three measurements.

Molecular docking studies:
Schrodinger's Glide docking software was used to probe interactions between OPH and methylparathion. Briefly, 1HZY from protein data bank was loaded into the Protein Preparation Wizard software and the structure was optimized following standard protocol.[39] The methylparathion molecule was then centered within the active site of an OPH monomeric unit, and Induced Fit Docking in Glide was used to run the docking simulations.[40] Poses with the top 7 docking scores were analyzed to qualitatively understand which residues interact with the substrate. The docking pose in Figure 2b is that of the most energetically-favorable pose for methylparathion in OPH. Qualitatively, Trp131, Phe132, Phe306, and Tyr309 interacted most frequently with methylparathion's aromatic group, which is consistent with past experimental crystallization studies.[26]

Tryptophan fluorescence:
A PerkinElmer LS-55 fluorescence spectrophotometer was used to monitor the inherent fluorescence emission of OPH's tryptophan residues. Briefly, OPH in TRIS buffer was mixed with either MilliQ water (for pure OPH) or RHP in MilliQ water (for RHP-OPH) to give a final enzyme concentration of ~0.1 mg/mL and, for RHP-OPH, a mass ratio of 25:1. A 260 nm wavelength was used to excite tryptophan's fluorescence, and spectra were recorded using 5 nm slit widths for emission and excitation windows. Similar qualitative trends for fluorescence quenching by RHPs were obtained regardless of TRIS:MilliQ ratio.

Effect of RHP composition on OPH stabilization:
As mentioned in the text, different RHP compositions were probed to understand interaction and stabilization mechanisms. All assays and fluorescence experiments were run identically for every RHP composition. The "disperse" RHP had composition of 50:25:20:5 MMA:OEGMA:EHMA:SPMA while the "blocky" RHP had composition of 20:25:50:5 MMA:OEGMA:EGMA:SPMA. The positively-charged RHP analogue had the same composition as the disperse RHP except with the positively-charged monomer dimethyl aminoethyl methacrylate (DMAEMA) substituted for the negatively charged SPMA.

RHP sequence analysis:
The polymer sequences with different monomer compositions were simulated with composition drift based on the Mayo-Lewis equation and Monte Carlo method, as previously reported.[41] The average degree of polymerization is 100 (MWD ~ 20k to 25k based on monomer composition). The hydrophobicity of monomer *i* is measured by the average hydrophilic-lipophilic balance (HLB) value of monomer *i*-2 to monomer *i*+2. A hydrophobic block is defined as a continuous subset of monomer sequence consisting of monomers whose average HLB value is below 9. The average size and size standard deviation of the hydrophobic blocks for each composition of polymers were calculated from a pool of 1000 chains using Python.

Chymotrypsin assay conditions:
A small peptide substrate (N-Succinyl-Ala-Ala-Pro-Phe p-nitroanilide) was used to quantify chymotrypsin activity by monitoring the release of 4-nitroaniline after hydrolysis. Since the

substrate has high water solubility, chymotrypsin (or RHP-chymotrypsin) was first incubated for 10 minutes in a 10 mM solution of 2-methyoxynaphthalene to probe chymotrypsin stability in the presence of a hydrophobic interface. The substrate was then added, and after 10 additional minutes a UV-vis spectrum was obtained on each sample. Prior to obtaining the UV-vis spectrum, the assay was centrifuged at 10,000 RPM for 1 minute to precipitate out the 2-methoxynapthalene particles in order to obtain a clean UV-vis spectrum.

Chapter 4:
Interfacial activation of enzymes in organic solvent modulated by random heteropolymers

4.1 Introduction: Enzymatic catalysis in nonaqueous solvents

Nonaqueous enzymology is becoming increasingly important for various industries[1-2] because of the unique advantages afforded over traditional aqueous enzymology. Retaining enzymatic activity in organic solvents enables high-throughput reactions on hydrophobic substrates that otherwise would precipitate in water.[3] Enzymatic reaction mechanisms (e.g. hydrolysis vs. condensation)[4] and substrate specificity[5] can be altered by switching the media from water to organic solvent due to changes in enzyme conformation, substrate availability, and binding affinity, among other factors.[6] Furthermore, enzymes' thermal stability is typically improved in organic solvents due to the conformational rigidity imparted by low dielectric media.[7]

Despite these crucial advances made over the last three decades, there still exist significant opportunities to expand our understanding of nonaqueous enzymology and manipulate enzymatic behavior in organic solvents. For instance, while insights have been established about generic features that determine enzyme activity in organic solvents—like the importance of a surface monolayer of water molecules[8]— little is known about how specific active site structural motifs enable (or prevent) nonaqueous enzymology. Furthermore, low dielectric environments increase the strength of polar and electrostatic interactions relative to those in water,[9] which may prove useful for manipulating enzymatic behavior in organic solvents by exploiting inter- or intra-molecular interactions. For example, selective binding of polymers near an enzyme's active site might outcompete substrate binding, thereby "turning off" enzymatic activity until an external stimulus triggers a change in polymer-enzyme interactions that activates the enzyme. In addition, the stronger intramolecular interactions that enzymes possess in organic solvents may disproportionately affect particular binding site functional motifs—like flexible loops—due to the rigidifying effect of low dielectric solvents. Thus, understanding how specific enzyme features behave in organic solvents may open new avenues to manipulate enzymatic behavior in ways that are not possible in water.

Oil/water interfaces are particularly interesting as a potential "trigger" with which to manipulate enzymatic behavior in organic solvent. As demonstrated in the last chapter, enzyme behavior at interfaces can vary greatly from that in bulk solvent. However, most reports studying enzymatic interfacial behavior focus on adsorption from the water phase to a water/oil (or water/hydrophobic solid) interface, which is driven primarily by hydrophobic interactions. Little work has been done on enzymatic adsorption to an oil/water interface from the organic phase because the driving force for adsorption is reduced since the solvent in which the enzyme is dispersed is hydrophobic. We hypothesized that the amphiphilic random heteropolymers (RHPs) previously described in this thesis may drive adsorption of enzymes to interfaces from organic solvent, especially since the RHPs coat much of the enzymes' surface based on MD simulations.[10] Here we show that RHPs can serve as molecular triggers for nonaqueous biocatalysis, keeping enzymatic activity dormant until being "turned on" by conformational changes induced at an oil/water interface. Furthermore, the enzyme organophosphorus hydrolase (OPH) has no activity

for any of its substrates in organic solvent. However, OPH becomes activated for hydrolysis after adsorbing to the oil/water interface with RHP and shows altered selectivity compared to that in water. Present studies demonstrate that modifying enzymes' surfaces via noncovalent interactions with surface-active polymers can drive interfacial adsorption and activation from organic solvent, providing a tool for manipulating enzymatic behavior in ways that are not possible in traditional aqueous media.

4.2 Results and discussion: Random heteropolymers drive interfacial activation of enzymes in organic solvent

Lipases' current importance in industrial nonaqueous enzymology[11] make them an ideal choice to study RHP-enzyme behavior in organic solvents. We first sought to understand RHP-BC-lipase activity toward a standard small molecule substrate. RHP-BC-lipase (80:1 by mass) was mixed in water, freeze-dried, and resuspended in toluene to give ~300 nm clusters. As shown in **Figure 4.1a**, RHP-BC-lipase has roughly two orders of magnitude higher activity than a pure BC-lipase suspension in toluene. Similar magnitudes of activity enhancement have previously been shown for pure enzymes suspended in organic solvents when excess water was added to sufficiently hydrate the enzymes' surfaces.[8] Indeed, we found in our own control experiments that addition of excess water to pure BC-lipase in toluene leads to similar activity as RHP-BC-lipase. This correlation between enzyme hydration and activity has been explained through flexibility arguments: in low dielectric solvents, enzymes become conformationally rigid due to increases in intramolecular interaction strength, but surface hydration enables sufficient flexibility to presumably overcome local energy minima and achieve the most catalytically-active conformation.[12] Therefore, we believe that RHP either forms permanent water bridges with the enzyme during freeze-drying or directly interacts with the enzyme's surface, thereby increasing the conformational flexibility of BC-lipase in nonpolar solvents without adding any additional water. Previous molecular dynamics simulations on the RHP system have shown that (1) RHP can cover most of an enzyme's surface in organic solvent, and (2) the majority of RHP-enzyme surface interactions comprise polar or electrostatic interactions in organic solvent.[10] These simulations support the notion that RHP can serve the same role as water by interacting with polar surface groups to impart flexibility and enhance enzymatic activity in nonaqueous solvent. Use of RHP rather than addition of excess water could be useful for reactions like transesterifications, where the presence of water is a significant hindrance to high product yield.[13]

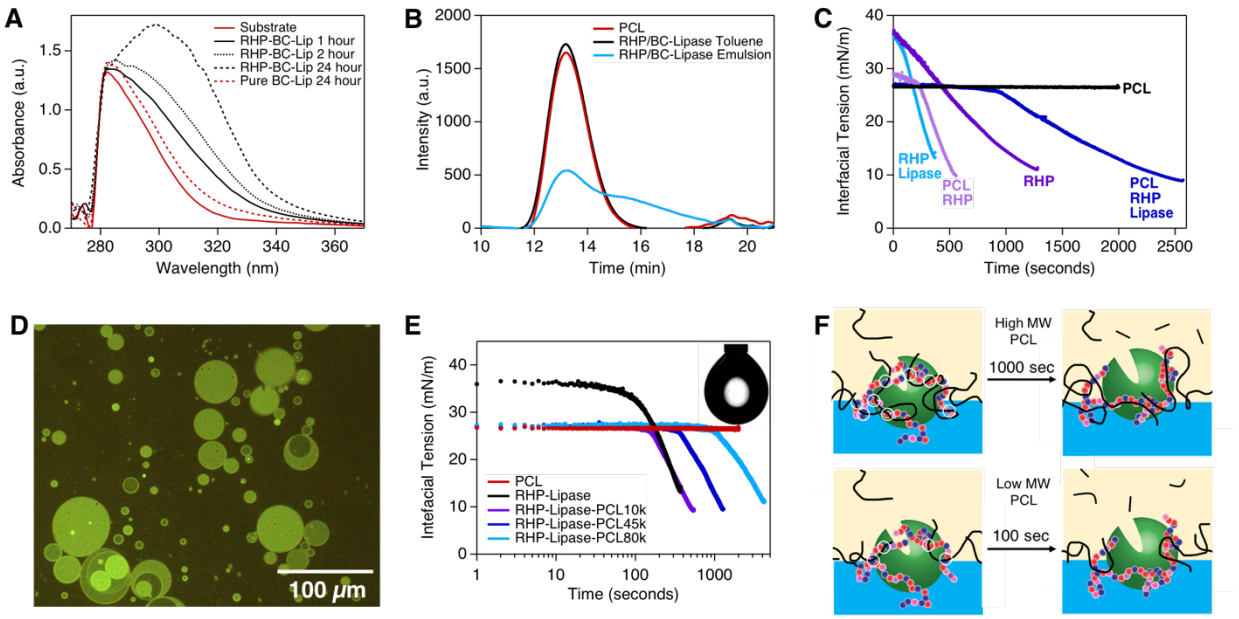

Figure 4.9 *RHP keeps BC-lipase dormant toward macromolecule hydrolysis in pure toluene, but activates the enzyme via adsorption at an oil/water interface. (A) Hydrolysis of p-nitrophenyl butyrate (280nm absorbance) to 4-nitrophenol (~305 nm absorbance) by pure lipase (red) or RHP-BC-lipase (black) in toluene showing that RHP enhances activity toward small molecule hydrolysis by roughly two orders of magnitude; (B) GPC curve of PCL (red), RHP-BC-lipase in toluene (black), or a toluene/water emulsion (blue); (C) interfacial tension of combinations of PCL, RHP, and BC-lipase in toluene probing the intermolecular interactions at a toluene/water interface; (D) fluorescence microscopy image of PCL-RHP-BC-lipase in toluene emulsified with water—the image was taken <20 seconds after emulsification occurred, suggesting that RHP-lipase are immediately present at the toluene/water interface; (E) interfacial tension of PCL-RHP-BC-lipase as a function of PCL molecular weight; (F) schematic illustrating that PCL per-chain entanglement density may dictate BC-lipase behavior at the interface*

After establishing RHP's ability to enhance activity toward small molecules, we tested RHP-BC-lipase reactivity toward PCL to understand whether the behavior in organic solvent differs for macromolecule substrates. Remarkably, RHP-BC-lipase exhibited no ability to hydrolyze PCL with 10 kDa, 45 kDa, or 80 kDa in toluene up to 1 week despite its high activity for small molecule hydrolysis (**Figure 4.1b**). Furthermore, pure BC-lipase suspended in toluene was capable of hydrolyzing PCL in just 24 hours via random chain scission, proving that the enzyme is inherently active toward PCL hydrolysis in toluene. The perimeter around BC-lipase's active site is amphiphilic, which may enable the RHP to outcompete PCL binding near the active site in toluene since RHP is amphiphilic while PCL is mostly hydrophobic. Thus, RHP seems to suppress enzymatic hydrolysis of macromolecule substrates in toluene by binding tightly to the enzyme's surface (particularly near the active site) and sterically precluding the macromolecule from reaching the catalytic residue. This explanation is supported by the fact that at the same RHP:enzyme ratios, the RHP has no effect on pure BC-lipase's ability to hydrolyze PCL in water via surface erosion, which suggests that RHP-enzyme interaction strength is reduced in water and

is consistent with our past results showing decreased enzyme surface coverage by RHP in water relative to toluene.[10]

We hypothesized that we could use an external stimulus to "turn on" PCL hydrolysis in toluene by altering the RHP-BC-lipase interactions via adsorption at an oil/water interface. Indeed, enzymes are known to undergo significant conformational changes at oil/water interfaces when they adsorb from the water phase,[14] and the amphiphilicity of the RHP chains may make RHP-enzyme clusters surface-active even in organic solvents (while enzymes typically do not adsorb to oil/water interfaces when they are dispersed in organic solvent[15]). As shown in **Figure 4.1b** (blue curve), when PCL-RHP-BC-lipase in toluene is emulsified by adding water and vortexing the mixture, PCL hydrolysis occurs rapidly (~50% of the initial chains cleaved within 24 hours) via random chain scission. This result indicates that RHPs can indeed serve as molecular triggers in toluene: the tight RHP binding near BC-lipase's active site prevents PCL hydrolysis until conformational changes occur in the RHP-enzyme complex due to adsorption at the oil/water interface.

To better understand how the RHP, enzyme, and macromolecule substrate interact at the interface, we used interfacial tensiometry as a model experiment. Briefly, PCL-RHP-BC-lipase were all dissolved (or dispersed) in toluene. A water droplet was then suspended in the toluene mixture, and the surface tension was monitored over time. As shown in **Figure 4.1c**, the water/toluene interfacial tension (ɣ) decreased from 36 to 27 mN/m when PCL was dissolved in toluene, but plummeted to ~10 mN/m with only lipase in the aqueous phase and to less than 5 mN/m with only RHP in toluene, reflecting the strong interfacial activity of both lipase and RHP. When all three components (PCL-RHP-BC-lipase) were dissolved in toluene, the interfacial tension initially started at 27 mN/m, the same starting value as pure PCL in toluene. The interfacial tension remained unchanged for a period of time but then dropped rapidly before plateauing at ~7mN/m over a long period. Furthermore, fluorescently labelled lipase was immediately concentrated at the toluene/water interface upon forming an emulsion, as shown in **Figure 4.1d**. Thus, the lipase/RHP complexes first dispersed in toluene should concentrate at the toluene/water interface due to their high interfacial activity. The interfacial tension during the steady period is similar to that of pure PCL, confirming that the PCL chains are associated with and wrap around lipase/RHP complexes. As the lipase degrades PCL at the interface, the short PCL chains desorb and expose the lipase/RHP complex. Thus, the RHP-lipase interactions are altered as the complexes adsorb to the toluene/water interface, enabling PCL hydrolysis from the toluene phase. Furthermore, tensiometry is validated as a useful tool to probe both the intermolecular interactions and reaction rates, simultaneously, for enzymes that hydrolyze surface-active components, which may be useful for lipid membrane-bound enzymes.

Tensiometry can also be used to understand how the physiochemical properties of the interface affect enzyme behavior. The results shown in **Figure 4.1e** demonstrate that the initial interfacial tension of PCL-RHP-BC-lipase is the same regardless of PCL's molecular weight for an equivalent PCL mass concentration (i.e. equivalent number of PCL monomers across all molecule weight samples). Interestingly, however, both the lag time and the slope of the tension reduction domain increase with increasing PCL molecular weight. The increased lag time may indicate that chain entanglements at the interface dictate RHP's ability to adjust its conformation: higher molecular weight chains have a higher per-chain entanglement density, which may hinder

RHP's ability to locally adjust its conformation at lipase's active site to start the PCL hydrolysis reaction (**Figure 4.1f**). The increased slope of the tension reduction domain likely indicates that a PCL chain only diffuses away from the interface once its molecular weight drops below a critical value, and since the hydrolysis mechanism is random scission, this critical value on average will be reached more quickly for PCL chains with lower starting molecular weight. Thus, these interfacial tensiometry experiments highlight that the physical properties of the macromolecular substrate can play a significant role in interfacial enzymatic catalysis because of the interplay among RHP, enzyme, and substrate interactions.

We tested PCL hydrolysis in toluene by another lipase, from *Candida Antarctica* (CA-lipase), to determine whether RHP-induced latency was specific to BC-lipase or applicable to other lipases. RHP does not induce latency for CA-lipase in toluene—rather, RHP-CA-lipase hydrolyzes PCL in pure toluene as well as at the oil/water interface. Contrary to the amphiphilic surface that surrounds BC-lipase's active site, CA-lipase possesses an active site perimeter that is completely hydrophobic aside from two charged amino acids. Thus, although the amphiphilic RHP likely binds somewhere on CA-lipase's surface in order to successfully disperse the enzyme in toluene, the RHP-enzyme binding sites may be spatially removed from CA-lipase's active site, allowing PCL to enter relatively unimpeded compared to BC-lipase.

Besides lipases, we also wanted to analyze the behavior of an enzyme that has never been shown to function in pure organic solvent to elucidate specific features that may inhibit nonaqueous enzymology and whether interfacial activation could occur in those cases. To the best of our knowledge, OPH has never been shown to function in pure organic solvents; however, there is a clear technological incentive to carry out nonaqueous enzymology using OPH since most of its neurotoxic substrates have little or no water solubility, making it difficult to efficiently neutralize bulk stockpiles via bioremediation in water. In stark contrast to lipases, neither pure OPH nor RHP-OPH suspended in toluene was able to hydrolyze its small molecule substrates, even when toluene was saturated with additional added water. This result suggests that some enzymes may be inherently incapable of functioning in nonaqueous media, even with sufficient water present to form a hydrating surface monolayer. OPH's binding domain is comprised of three surface-exposed flexible loops, whereas BC- and CA-lipase both have more rigid domains that are less surface exposed and consist of helices as well as loops. Thus, the flexible binding domain of OPH may become kinetically trapped in a conformationally-inactive state in the low dielectric environment of toluene that cannot be overcome even with a surface layer of hydrating water molecules, whereas lipases' domains may be rigid enough to not experience significant displacements and thus have a lower barrier to achieve their catalytically active conformation in toluene.

We hypothesized that adsorption from toluene to a toluene/water interface may result in conformational changes that activate OPH. As shown in **Figure 4.2a**, emulsifying RHP-OPH in toluene by adding 2.5 vol% water and vortexing the mixture did indeed activate OPH for hydrolysis of paraoxon. Furthermore, the apparent activity increased with increasing RHP concentration. We believe this dependence on RHP concentration indicates that OPH is only active at the interface: higher concentrations of RHP stabilize the emulsion more effectively, as shown visually in **Figure 4.2b** where significant phase separation occurred for a 10-1 RHP-OPH ratio after just a few minutes while 100-1 exhibited minimal phase separation over 24 hours (**Figure**

4.2c). As the toluene/water phases separate, RHP-OPH will be released back into the bulk toluene phase, where the enzyme is inactive; thus, emulsions stabilized by higher RHP concentrations possess higher surface areas on which OPH can remain adsorbed. As a control, we suspended OPH without RHP in toluene ("0-1" in **Figure 4.2b**) and attempted to form an emulsion under the same conditions, but the water and toluene immediately phase-separated and no activity was observed over 48 hours. Thus, RHP is crucial for activating OPH in nonaqueous enzymology: the RHP wraps around OPH's surface in toluene and then the RHP-OPH clusters adsorb strongly to the toluene/water interface, where OPH becomes activated for hydrolysis.

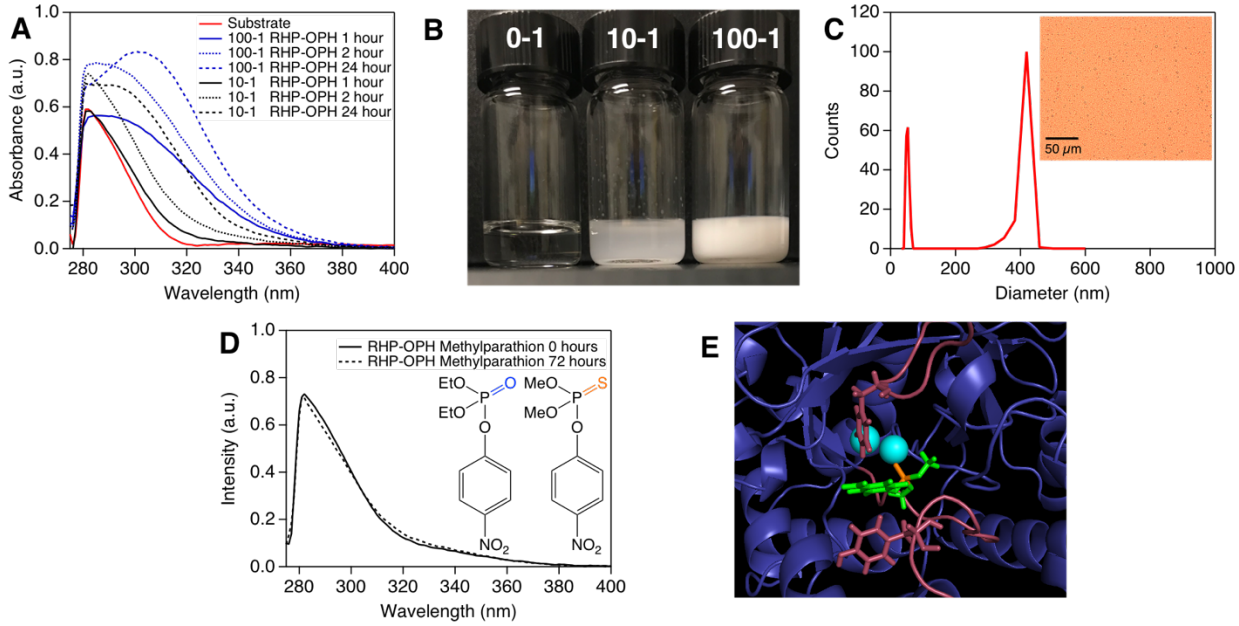

Figure 4.2 *RHP enables interfacial activation of OPH in organic solvent. (A) Hydrolysis of paraoxon by 10-1 (black) or 100-1 (blue) RHP-OPH in a toluene/water emulsion (2.5vol% water); (B) Picture demonstrating that increasing RHP concentrations stabilizes the water-in-toluene emulsion; (C) DLS graph showing that a 100-1 RHP-OPH ratio stabilizes ~400 nm water-in-toluene emulsions; (D) RHP-OPH can hydrolyze the P=O of paraoxon (left inset) but not P=S of methylparathion (right inset) within 3 days, suggesting the metal ions play a role in substrate binding in organic solvent; (E) Simulated crystal structure of OPH with methylparathion docked in its most energetically-favorable pose, demonstrating that, in water, aromatic stacking plays a key role in substrate binding / positioning.*

We tested OPH's interfacial activity for hydrolysis of methylparathion and paraoxon, two of OPH's most common substrates, with all components first dissolved/dispersed in toluene to understand whether there were differences in substrate selectivity relative to that in buffer. Despite hydrolyzing ~50% of paraoxon molecules in two hours, no activity was observed for methylparathion over 72 hours (**Figure 4.2d**). The main difference between methylparathion and paraoxon is the P=X bond that partakes in the hydrolysis reaction: methylparathion contains a P=S while paraoxon contains a P=O bond (**Figure 4.2d, inset**). In buffer, OPH binds its substrates primarily via aromatic stacking, which we confirmed in our own docking experiments (**Figure 4.2e**). However, when bound at a toluene/water interface starting from the toluene phase, aromatic stacking likely plays a minimal role in substrate binding. Rather, OPH's divalent metal ions at the

catalytic site may play a direct role in binding substrates from the organic solvent phase. The higher electronegativity of P=O relative to P=S may increase the binding interaction strength and enable catalysis. Thus, OPH's binding mode may differ when activated via interfacial adsorption from an organic solvent phase, highlighting the importance of the bimetallic active site not just for carrying out the catalytic step but also for enabling substrate binding.

The ability to program enzyme latency in organic solvents may represent an important advancement for solution-processing enzyme-based materials or storing enzyme-based formulations. Lipases are known to depolymerize polyesters, and we will discuss later in this thesis that we can embed lipases inside of polyesters using either solution- or melt-processing. Preventing hydrolysis during material processing is essential for maintaining optimal mechanical properties throughout the material's lifecycle. Furthermore, understanding how to properly trigger depolymerization in organic solvents may introduce new pathways for efficient hydrolysis of plastics that cannot be depolymerized to high extents by enzymes in the solid state (such as cellulose[16] or PET[17]). The recalcitrance of these plastics to enzymatic degradation typically stems from a high percent crystallinity, so dissolution in organic solvent may overcome that barrier. Finally, maintaining latency of enzymes with small molecule substrates, like OPH, can lead to formulations containing enzyme and substrate that are only activated when water is added, which may be particularly useful for developing more environmentally friendly pesticide formulations with OPH or devising other types of enzyme/substrate systems.

4.3 Conclusions

We have demonstrated, to the best of our knowledge, the first example of interfacial activation of enzymes from an organic solvent. The strong intermolecular interactions of RHPs with enzymes in low dielectric solvents can be exploited to maintain latency of BC-lipase toward macromolecule hydrolysis in the pure organic phase. Enzymatic activity can then be triggered as RHP-BC-lipase complexes adsorb to an oil/water interface, where they undergo conformational changes that enable macromolecule substrate binding and hydrolysis. Tensiometry can be used to directly and simultaneously monitor RHP/enzyme/substrate interactions and reaction rates at the interface, highlighting how the physiochemical properties at the interface dictate enzymatic activity. Furthermore, OPH becomes activated in organic solvent by adsorbing to the oil/water interface, which only occurs when complexed with surface-active RHPs. This interfacial activation likely occurs because the binding site loops obtain adequate flexibility to overcome a kinetic barrier and form a catalytically active conformation, which is not possible in the low dielectric media of toluene. The results in this chapter demonstrate that RHP is a useful tool with which to manipulate enzymatic behavior in nonaqueous media for enzymes that normally are active in organic solvents (lipases) and enzymes that are not (OPH).

4.4 Experimental Methods

Materials:

The RHPs were synthesized as previously reported.[10] Unless otherwise stated, the molar composition of the RHP was 50:20:25:5 MMA:EHMA:OEGMA:SPMA, and the molecular weight was 20 kDa. All PCL samples used here were purchased from Sigma Aldrich and used without further purification. Amano lipase PS from *Burkholderia cepacia* was purchased from Sigma Aldrich and purified following a previously reported procedure.[18] Lipase B from *Candida antarctica* was also purchased from Sigma Aldrich and used as purchased. Organophosphorus hydrolase was expressed in-house from a plasmid. Briefly, protein was expressed in Rosetta2 cells, induced with 0.5 mM IPTG. Cells were supplemented with 10 μM $CoCl_2$ at time of inoculation and with a further 90 μM after 4 h of induction. Cells were harvested after 21 h growth at 16°C. Purification was by Ni affinity, using standard buffers and protocols. The material eluting from the column was very cloudy indicating significant precipitation of the protein. However, after clarification, a moderate amount of protein remained in the soluble fraction. This protein was buffer exchanged into 50 mM TrisHCl pH 9.0, 0.1 mM $CoCl_2$, concentrated to 2 mg/ml (Coomassie assay), and frozen in 200 μl aliquots (at -80°C).

Methods:

Assay to probe RHP-BC-lipase activity against a small molecule substrate in toluene:
The small molecule ester 4-nitrophenyl butyrate was purchased from Sigma Aldrich and used as purchased. RHP and BC-lipase were mixed in a 100:1 mass ratio in water, freeze-dried overnight, and then resuspended directly in toluene. The substrate was dissolved separately in toluene, and the final assay conditions were as follows: room temperature, 2 mM substrate concentration, 5 ug/mL of BC-lipase. The reaction was monitored over time using UV-vis spectroscopy since the substrate absorbs around 280 nm and the product absorbs around 310 nm. The RHP-BC-lipase cluster size in toluene was measured using dynamic light scattering, as previously reported (DelRe et al., *in revision* at time of writing). The final BC-lipase concentration for DLS was 0.2 mg/mL.

Gel permeation chromatography (GPC) to probe RHP-BC-lipase and RHP-CA-lipase activity against a macromolecular substrate in toluene and at toluene/water interface:
PCL (Mn=80 kDa) was dissolved in toluene to give a concentration of 5 mg/mL. RHP and BC-lipase were mixed in water a 100-1 mass ratio, freeze-dried, and resuspended directly in the 5 mg/mL PCL/toluene solution to give a final concentration of 22 ug/mL of BC-lipase. To probe whether RHP-BC-lipase could hydrolyze PCL in pure toluene, the sample was left for up to 1 week, after which the toluene was evaporated at ambient temperature/pressure and the entire vial contents were resuspended in THF for GPC analysis. To probe RHP-BC-lipase hydrolysis of PCL at the interface, an equivalent volume of water was added to the PCL-RHP-BC-lipase in toluene solution and vortexed vigorously for 30 seconds. The toluene phase was evaporated at ambient conditions over 24 hours and then the water phase was freeze-dried. The vial contents were then resuspended directly in THF for GPC analysis. As a control to support hydrolysis at the interface / rule out hydrolysis in the water phase during drying, a sample was prepared by adding an equivalent volume of water to PCL-RHP-BC-lipase in toluene but without vortexing so that the

water and toluene phases remained separated and only a small interface relative to that of the emulsion was present. The contents of that control vial were dried in the exact same way as the emulsion, and GPC showed only minimal hydrolysis. Thus, it seems highly likely that hydrolysis occurs at the interface and is not an artifact of the drying procedure.

Experiments with CA-lipase were carried out using the exact same procedures as mentioned above. The RHP was mixed with CA-lipase commercial blend in a 1:1 mass ratio (~100:1 RHP:CA-lipase given the enzyme concentration in the commercial blend). The complex was then resuspended in toluene and the procedures outlined above were used to probe hydrolysis of PCL in toluene, a toluene/water emulsion, and a toluene/water phase separated interface control.

Fluorescence microscopy experiment to analyze interfacial adsorption:
To visually confirm RHP-enzyme adsorption to a toluene/water interface from the toluene phase, we tagged BC-lipase with a fluorescent dye, NHS-Fluorescein (5/6 carboxyfluorescein succinimidyl ester), by following the manufacturer's procedure. The solution with labelled lipase was then centrifuged in a 15 mL, 10,000 g/mole molecular weight cutoff filter for at least 3 cycles to remove excess dye from the labeled lipase.

For the emulsion experiments, RHP was mixed with fluorescent BC-lipase in water, freeze-dried, and resuspended in toluene to give a final lipase concentration of 50 ug/mL. MilliQ water (800 uL) was then added to the toluene solution containing RHP-BC-lipase, and the ensuing mixture was vortexed for 15 seconds. Fluorescence microscopy images were taken immediately after dropping 3 uL of the emulsion onto a microscope slide. A U-MWBS3 mirror unit with 460-490 nm excitation wavelengths was used to take the fluorescence microscopy images.

Interfacial tensiometry experiments:
Interfacial tension between a toluene and water phase was used to probe the intermolecular interactions among PCL-RHP-lipase. A MilliQ water droplet was dispensed by a 1mL syringe through a 1.27 mm-diameter needle and immersed in toluene. The droplet shape was captured by a CCD camera every second and fitted by Young-Laplace equation to obtain interfacial tension. For each sample, the measurement was repeated three times and showed good consistency and reproducibility.

RHP-lipase were mixed in a 10-1 mass ratio and lyophilized to remove the aqueous solvent. A different ratio was used here compared to actual degradation studies because any ratio over ~50-1 RHP-lipase resulted in unstable droplets, preventing accurate measurement. PCL was dissolved first in toluene at a 0.5 mg/mL concentration. The PCL/toluene solution was then used to directly disperse RHP-lipase, giving a final concentration of 0.005 mg/mL for RHP and 0.0005 mg/mL for lipase in toluene. The water droplet was immersed in toluene after all three components (PCL, RHP, and lipase) were dispersed in toluene.

Assay to probe RHP-OPH activity in toluene:
To analyze RHP-OPH (or pure OPH) activity in toluene and at a toluene/water interface, RHP and OPH were mixed in water, freeze-dried, and then resuspended directly in toluene. For the pure toluene assay, RHP-OPH (or pure OPH) were mixed with paraoxon dissolved in toluene to obtain final concentrations of 25 ug/mL OPH and 0.75 mM paraoxon. The reaction was carried out at

room temperature. For the interface analysis, the exact same procedure was followed, but then 2.5 vol% water was added and the mixture was vortexed vigorously for 30 seconds. Similar results were observed when the organic phase was swapped from toluene to butyl acetate.

Docking simulations of OPH: Schrodinger's Glide docking software was used to probe interactions between OPH and its substrate. Briefly, 1HZY from protein data bank was loaded into the Protein Preparation Wizard software and the structure was optimized following standard protocol.[19] The substrate molecule was then centered within the active site of an OPH monomeric unit, and Induced Fit Docking in Glide was used to run the docking simulations.[20] Poses with the top 7 docking scores were analyzed to qualitatively understand which residues interact with the substrate. The docking pose in Figure 2b is that of the most energetically-favorable pose for methylparathion in OPH. Qualitatively, residues Trp131, Phe132, Phe306, and Tyr309—all of which residue in flexible binding-site loops—interacted most frequently with methylparathion's aromatic group, which is consistent with past experimental crystallization studies.[21] Similar results were obtained when paraoxon was used as the substrate.

Chapter 5:
Nanoscopically-embedded enzymes enable bioplastics with on-demand degradation in water

5.1 Introduction: enzymatic degradation of plastics

When it comes to ecological harmony, we envy nature's ability to program numerous complex processes to achieve system-wide, long-term sustainability.[1-4] Synthetic biology opened a viable path to repurpose biomachineries toward new material development. Enzymes and/or biomachineries capable of reacting with plastics[5-7] can afford on-demand modification and/or programmable degradation to enhance plastics' environmental compatibility during manufacture/utilization.[8-10] Productions of polymers with enzymatic labile bonds such as polycaprolactone (PCL) and poly(lactic acid) (PLA) are rapidly increasing.[11] However, they are essentially non-degradable in landfills and/or compost facilities due to slow surface erosion. Embedding enzymes as micron-sized clusters has accelerated host plastic degradation, but they also produced secondary contaminations such as microplastic particles.[9, 12] To fulfill the promise of eco-friendly plastics, there is an urgent need to understand and manipulate biocatalysis with macromolecules being both the reaction substrates and host matrix.[13-14]

Enzymatic activity depends on the protein structure, substrate binding, and reactivity at the active site[15] as schematically shown in **Figure 5.1**. For enzymes embedded in semicrystalline polymers, which represent the majority of plastic produced,[16] substrate binding can be rate limiting due to the reduced mobilities of confined enzyme[10, 14, 17] and polymer[18-19] (**Figure 5.1a** and **Figure 5.1b**). The enzyme can either randomly bind and cleave a long chain or selectively bind to the chain end and catalyze depolymerization. While random chain scission is the more prevalent pathway, processive depolymerization is more desirable because it directly converts a polymer to high-value monomers with near-complete degradation. When enzymes are nanoscopically confined and co-reside with the chain ends, it becomes feasible to molecularly modulate the pathways of enzymatic degradation toward preferential chain-end mediated processive depolymerization. There are additional factors that are unique to biocatalysis by embedded enzymes (**Figure 5.1c**). Compatibilizers, needed to mediate enzyme/host interactions so as to disperse the enzyme, may compete for substrate binding and affect enzyme stability during plastic processing. Furthermore, the global entropic driving force for depolymerization depends on the polymer conformation of each chain. Local polymer chain packing affects the segmental mobility and chain end binding and thus, the depolymerization kinetics.[20-21] Quantitatively decoupling effects from these factors is requisite to holistically design plastic processing to achieve plastic circulatory lifecycle without compromising host properties and degradation latency during storage and usage.

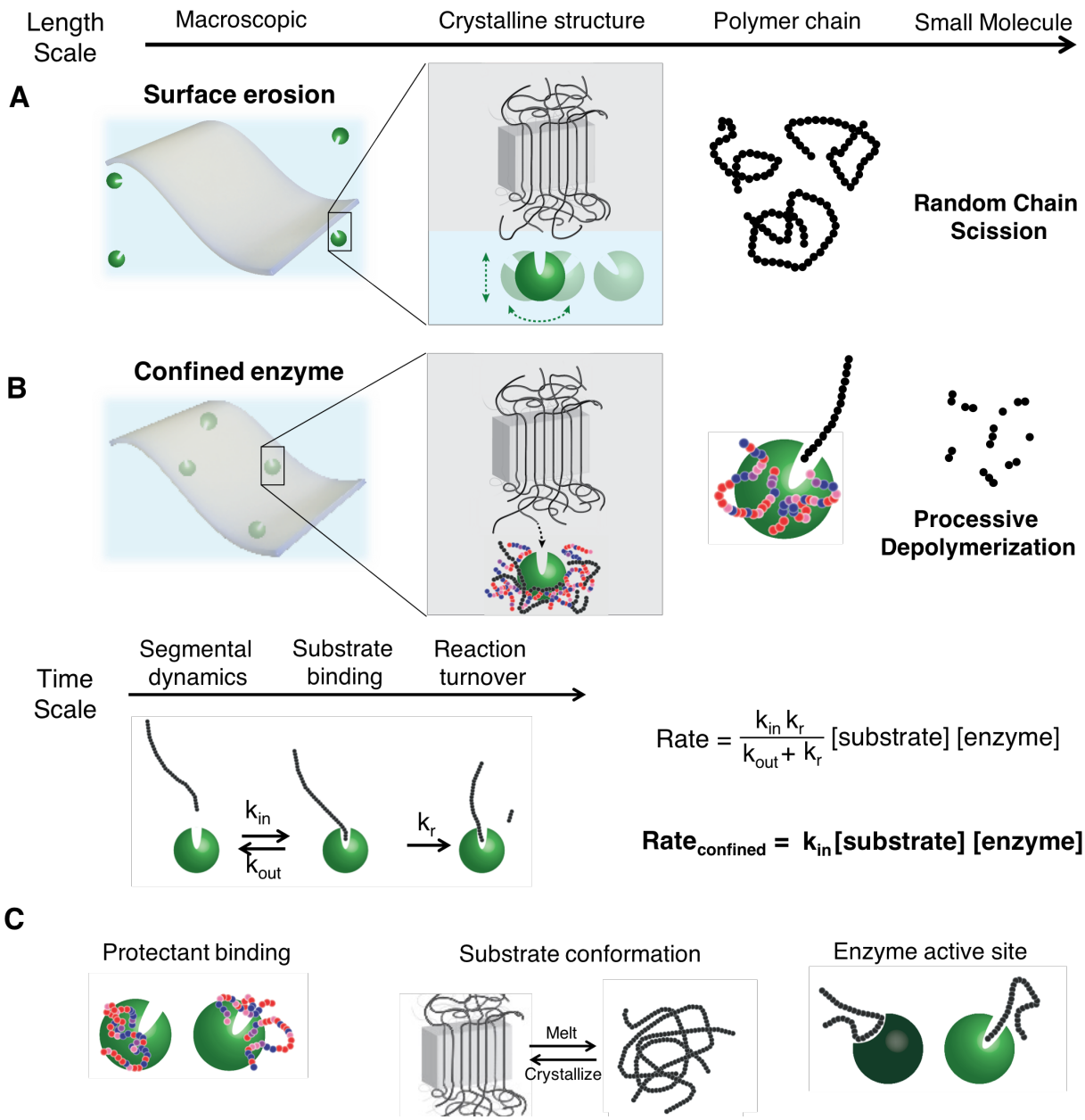

Figure 5.10 *Consideration of enzymology of embedded enzyme with macromolecular substrates. A) Schematically shows variation in the enzyme mobility may change the pathway of polymer degradation from random chain scission to processive depolymerization with nanoscopic confinements. B) Describes the reaction kinetic changes where macromolecular substrate binding becomes rate limiting factor for confined enzyme. C) Schematically shows additional factors to be considered to modulate enzymatic reactions toward polymer degradation.*

5.2 Results and discussion: degradation pathway of embedded enzymes depends on active site geometry and chemistry

Biodegradable plastics PCL and PLA are promised as suitable alternatives to commodity plastics,[4] but still suffer from lengthy degradation times (years). *Burkholderia cepacia* lipase (BC-lipase) and *Candida Antarctica* lipase (CA-lipase) were used since lipases broadly catalyze ester reactions.[22] Our previously described four-monomer random heteropolymer (RHP) was added to nanoscopically disperse lipases in polyesters.[8, 10] At 0.02-2 *wt*% loading, lipase nanoclusters are uniformly distributed throughout the PCL (**Figure 5.2a)**. Overlaid polarized optical microscope and fluorescence microscope images (**Figure 5.2b)** show that lipase is incorporated within crystalline spherulites. Transmission electron microscopy (TEM) images show RHP-BC-lipase clusters, ~50 nm to ~500 nm in size, are located between bundles of PCL lamellae (**Figure 5.2c)**. With enzyme loadings up to 2 *wt*%, there are less than 10% changes in the PCL's mechanical property and bulk crystallinity (**Figure 5.2d and Figure 5.2e)**. Small angle x-ray scattering (SAXS) showed similar PCL crystallization with lipase incorporation. These results underscore the importance of nanoscopic dispersion with minimal amount of additives to retain host properties.

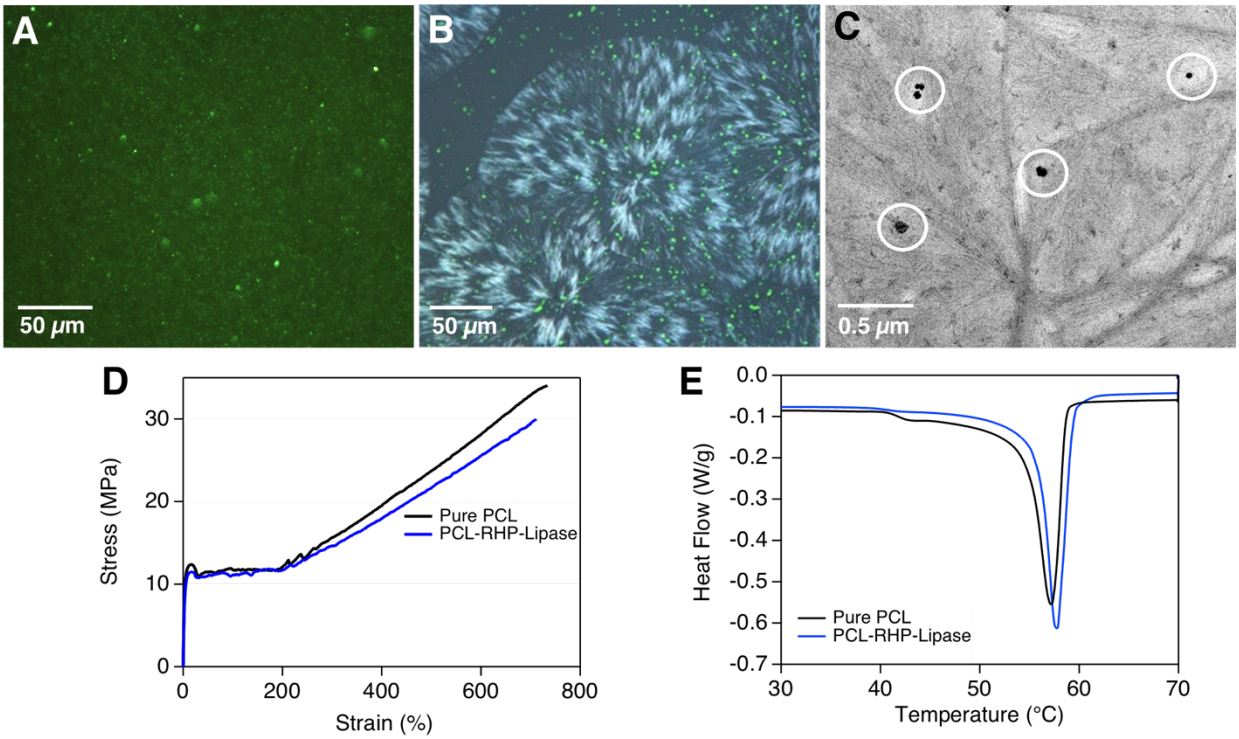

Figure 5.2 *Characterizing PCL-RHP-BC-lipase. (A) Fluorescence microscope image showing homogeneously distributed enzyme. (B) Polarized optical microscope overlaid with fluorescence microscope image showing incorporation of RHP-lipase within semicrystalline spherulites. (C) TEM image showing incorporation of RHP-lipase within semicrystalline matrix. (D) Stress-strain curve from tensile test of PCL and PCL-RHP-BC-lipase. (E) DSC curves of PCL and PCL-RHP-BC-lipase*

Semicrystalline PCL containing 0.02 *wt*% BC-lipase degrades internally once immersed in a 40 °C buffer solution rather than by a surface erosion. The degradation leads to ~95% weight loss after 24 hours. The increase in the SAXS intensity and the cross-sectional scanning electron microscopy (SEM) image of PCL-RHP-BC-lipase after ~25% mass (**Figure 5.3a)** confirm the internal nanoporous structures. After the PCL-RHP-BC-lipase sample disintegrates into microplastic particles (**Figure 5.3b**), the enzyme remained with the microparticles as determined by fluorescently-labelled lipase. In fact, the embedded lipase nanoclusters continue to degrade microplastics to achieve up to ~98% conversion over 1 week.

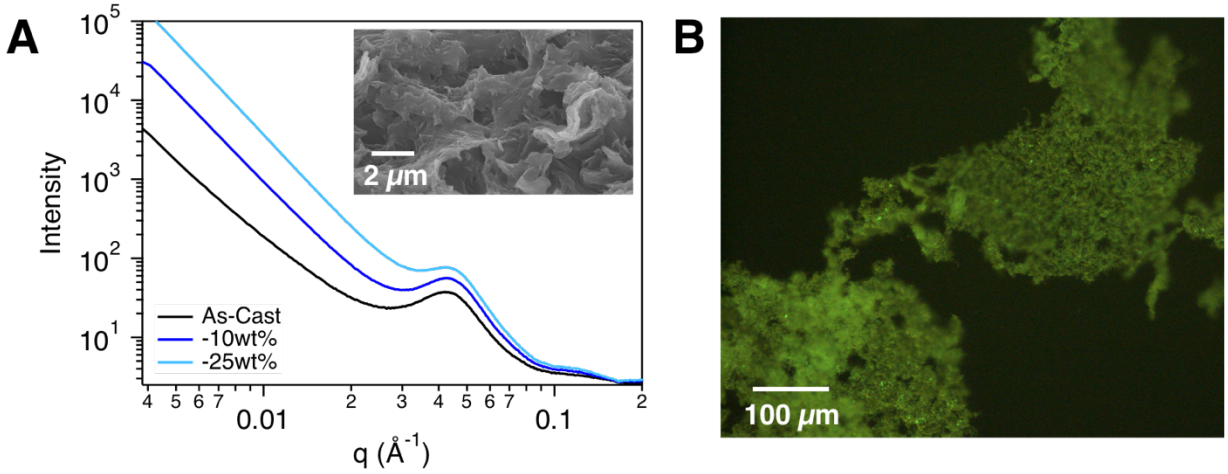

Figure 5.3 *Nanoscopically embedded BC-lipase depolymerizes PCL internally. (A) SAXS profile confirming nanoporous structure formation during internal degradation by confined enzyme (inset: cross-sectional SEM image after 50% weight loss confirming nanoporous structure formation). (B) fluorescence image showing confined BC-lipase remains with microplastics during degradation.*

As the degradation proceeded, the overall PCL crystallinity in PCL-RHP-BC-lipase didn't change when the degradation weight loss increased from 20% to 80% (**Figure 5.4a**). Thus, the PCL segments in both the amorphous and crystalline phases are degraded as opposed to mainly the amorphous segments. This is consistent with the SAXS results in Fig. 2D where the peak position associated with lamellar periodicity didn't change and only an increase in the scattering at small q. Gel permeation chromatography (GPC) analysis showed that the PCL molecular weight remains the same despite significant weight loss (**Figure 5.4b**). Liquid chromatograph-mass spectrometry (LC-MS) further confirmed the primary degradation by-products are small molecules, less than 500 Da in size, that can be readily repolymerized (**Figure 5.4c**). Control experiments with PCL degradation by random chain scission showed a wide range of high molecular weight oligomers. Thus, the degradation of PCL-RHP-BClipase should proceed via processive depolymerization as opposed to random chain scission.

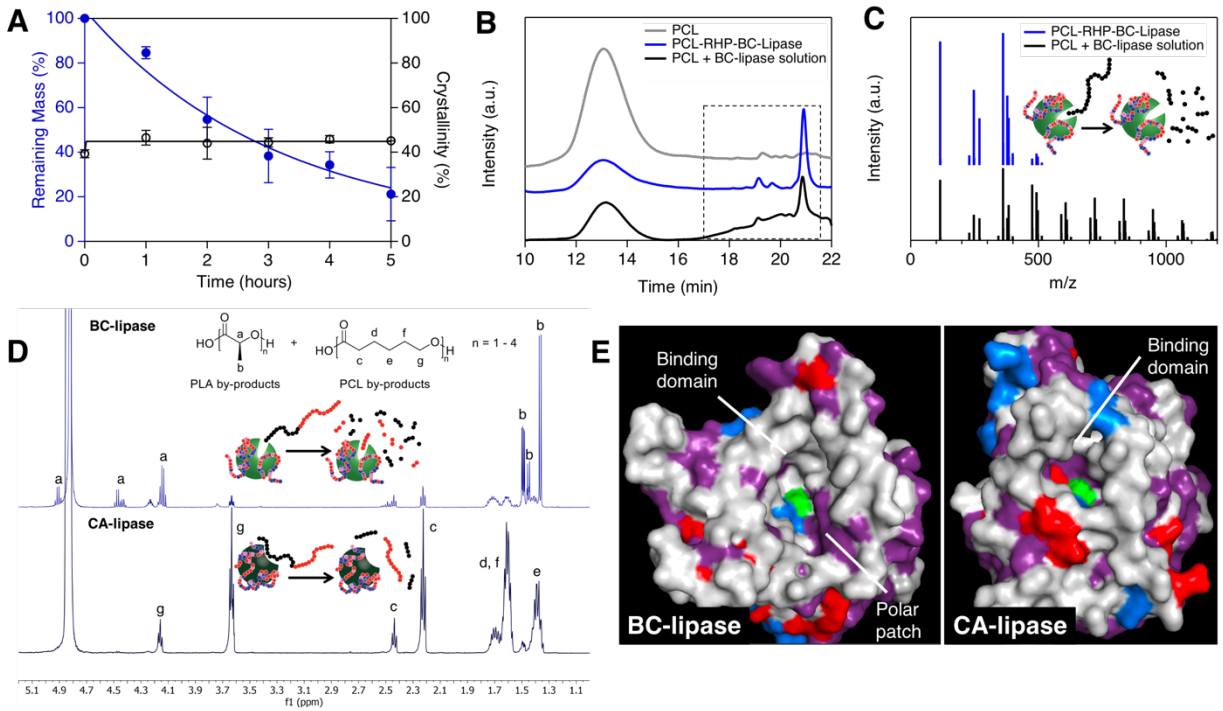

Figure 5.4 *Embedded BC-lipase depolymerizes polyesters via chain end-mediated processive degradation. A) Remaining mass (closed blue circles) and percent crystallinity (open black circles) as a function of degradation time in 37 °C buffer. B) GPC of surface erosion and confined degradation by BC lipase, including the remaining film and degraded by-product. C) Mass spectra of surface erosion and confined degradation by BC lipase, including the remaining film and degraded by-product. D) NMR spectra of degradation by-products of PCL-b-PLA diblock copolymer when blended with RHP/BC lipase and RHP/CA lipase, respectively. While both small molecule by- products of PCL and PLA were seen in BA lipase-containing blends, primarily PCL degradation was observed for CA lipase-containing blends. E) (Left) Surface representation of BC-lipase (3LIP entry on PDB) highlighting the hydrophobic (white) substrate binding domain and the polar (purple) patch across from the binding domain; catalytic serine residue is shown in green, while negative and positive residues are shown in red and blue, respectively. (Right) Surface representation of CA-lipase (1TCA entry on PDB) highlighting the hydrophobic binding domain with no obvious opportunity for processivity because the entire active site is surrounded by hydrophobic residues; residue color scheme is the same as that of BC-lipase.*

When BC-lipase nanoclusters are embedded in pure PLA or a PCL/PLA blend, no PLA hydrolysis was observed even though lipase is able to catalyze a broad range of hydrolysis reactions.[23-24] However, when the host matrix was switched to a PCL-b-PLA diblock copolymer (40,000-b-20,000 g/mole), ***both*** the PCL and PLA block were depolymerized into small molecule by-products in a similar molar proportion as the parent copolymer (**Figure 5.4d**). The results suggested that a PCL linkage to PLA alters the conformation such that the PLA block can be shuttled to the enzyme active site and depolymerized subsequently. This is strikingly similar to polyadenylation-induced processive mRNA degradation seen in biomacromolecules,[25-26] opening a useful route to expand substrate selection.

BC-lipase shares common traits with processive enzymes: [21, 27] it has a deep (up to 2 nm) and narrow (4.5 Å at the base) hydrophobic funnel from its surface to the catalytic triad,[28] which may facilitate substrate polymer chain sliding while preventing dissociation. Opposite to the hydrophobic binding patch, there is a large patch composed of six polar residues that can provide a driving force to pull the remaining chain forward after hydrolysis (**Figure 5.4e**). Once the chain end is bound, the BC-lipase processively catalyzes the depolymerization without releasing it.[27] Similar studies were carried out using CA-lipase that has a surface-exposed, shallow active site (~1nm from the surface) with no obvious residues that afford processivity (**Figure 5.4f**). With a similar nanoscopic dispersion, PCL-RHP-CA lipase degradation proceeded by random scission based on GPC. The CA-lipase-catalyzed degradation stops after just ~12% mass loss and the bulk PCL crystallinity increases as the degradation proceeds. In control experiments where CA-lipase nanoclusters were embedded in the PCL-b-PLA diblock copolymer, the PCL block was degraded with high selectivity and minimal PLA degradation was observed. The difference in the PCL degradation by the confined BC- and CA-lipase clearly demonstrates the importance of surface chemistry and shape of the enzyme active site to modulate polymeric substrate binding toward preferential chain end binding.

Control experiments were carried out to probe the role of the nanoscopic confinement of embedded enzymes. When PCL was immersed in BC-lipase solution, the degradation byproducts were oligomers with a wide molecular weight distribution. When BC-lipase was embedded in PCL at the same lipase loading but as micron-sized aggregates, the host degradation stopped after ~40 % mass loss and led to highly crystalline remaining plastic, consistent with previous reports. [9, 12] Due to enzyme leaching during degradation, the non-degraded bulk and microplastic particles remain in buffer. Furthermore, PCL-RHP-BC-lipase undergoes negligible degradation at room temperature after being incubated in buffer solution for >3 months, while BC-lipase in solution degrades pure PCL by surface erosion by ~30% in just 2 days. This was attributed to the hindered mobility of the embedded enzyme and PCL chain end that limits chain end binding to initiate depolymerization.

The turnover rate for embedded BC-lipase to degrade PCL is estimated to be ~30 s^{-1} for 0-3 hrs and reduces to ~12 s^{-1} after 3 hours. In control experiments, turnover rates were determined for BC-lipase in solution with small molecule substrate (~200 s^{-1}), BC-lipase in solution with a PCL film as substrate (~19 s^{-1}) and PCL-RHP-BC-lipase with small molecule substrate (~120 s^{-1}). For small molecule substrate, the embedded enzyme's apparent activity is approximately half that of enzyme in solution, which can be attributed to the hindered substrate diffusion by the host matrix. [17] The apparent activity of embedded enzyme is lower for the polymeric substrate than for small molecule substrate. We attribute this to much lower chain end concentration and a reduced diffusivity of polymer segment undergoing degradation in comparison to the small molecule. However, the embedded lipase shows a similar or higher apparent activity when compared with solution lipase against PCL where lipase has high rotational and translational freedom for substrate binding with much higher abundant substrates, i.e. polymer segment. Thus, the depolymerization kinetics is mainly governed by the substrate binding for embedded enzymes. With the chain end-mediated processive depolymerization, this rate limiting step is essentially removed for subsequent steps of depolymerization once the polymer chain end is bound.

Thus, to realize chain-end mediated processive depolymerization as the preferential degradation pathway, the enzyme should (1) have a substrate entrance that provides geometric restriction to sterically exclude the polymer's middle segments to reach the catalytic site and attractive interactions with the remaining chain end to ensure polymer chain sliding; and (2) be nanoscopically confined to co-reside with the polymer chain ends. Once chain-end mediated processive depolymerization becomes the preferential pathway, the host polymer degrades more readily with near complete polymer-to-small molecule conversion and eliminates microplastic particles. Kinetically, although the chain-end mediated depolymerization is disadvantaged by low substrate concentration of chain ends, the apparent degradation rate benefits from substrate shuttling and is comparable or slightly higher than that of random chain scission. When the concentration of small molecule substrates and polymer chain end is taken into consideration, the apparent enzyme activity actually benefits significantly from this degradation pathway.

5.3 Conclusions

Nanoscopically embedding enzymes in plastic matrices enables near complete depolymerization of the host matrix. The matrix's mechanical properties are largely retained upon addition of RHP-enzyme because of the low required additive concentration. The degradation kinetics and pathway depend on the enzyme active site features: a deep active site with appropriate chemical patterns enables processive behavior during degradation, leading to depolymerization of both amorphous and crystalline domains into small molecules by-products. However, we wondered what role the matrix characteristics played in the degradation, and whether polymer morphology could be exploited to achieve control over degradation. These results will be discussed in the remaining two chapters.

5.4 Experimental Methods

Materials:

The RHPs were synthesized as previously reported.[8] Unless otherwise stated, the molar composition of the RHP was 50:20:25:5 MMA:EHMA:OEGMA:SPMA, and the molecular weight was 70 kDa. PCL (80 kDa) was purchased from Sigma and used as-received. Amano lipase PS from *Burkholderia cepacia* was purchased from Sigma Aldrich and purified following a previously reported procedure.[29] However, the unpurified commercial blend behaved the same as the purified enzyme when embedded using RHP. Lipase B from *Candida antarctica* was also purchased from Sigma Aldrich and used as purchased.

Methods:

RHP-enzyme complexes

To form the RHP-enzyme complexes, RHP and enzymes were mixed in aqueous solution for 5 minutes at room temperature. The mixture was then flash-frozen in liquid nitrogen and lyophilized overnight to remove the water via sublimation. The remaining dried RHP-enzyme mixture was resuspended directly in the specified polymer solutions. Detailed information and composition for each blend is shown in Table S1.

RHP was mixed with purified BC-lipase in a mass ratio of 80:1. For commercial enzyme blends, the RHP to blend weight ratio was kept at 2:1. Dynamic light scattering (DLS) was used to obtain the complex's particle size after resuspending in toluene. DLS was run on a Brookhaven BI-200SM Light Scattering System using a 90° angle.

Processing and characterizing enzyme-embedded PCL via solution casting

To prepare films, PCL was dissolved in toluene at 4wt% concentration and stirred at 55°C for at least 4 hours to ensure complete dissolution. The polymer solution was then cooled to room temperature before resuspending the dried RHP-lipase complexes directly in the polymer solution at the specified enzyme concentration. Mixtures were vortexed for ~5 minutes before being cast directly on a glass plate and air dried in a chemical fume hood.

To probe the bulk distribution of enzyme in the films, purified lipase was fluorescently labeled. NHS-Fluorescein (5/6-carboxyfluorescein succinimidyl ester) was used to label lipase by following manufacturer's procedure. The solution was centrifuged in a 15 mL, 10,000 g/mole molecular weight cutoff filter for at least 3 cycles to remove excess dye from the labeled lipase. A U-MWBS3 mirror unit with 460-490 nm excitation wavelengths was used to take the fluorescence microscopy images. TEM images were taken on a JEOL 1200 microscope at 120 kV accelerating voltage. Vapor from a 0.5 *wt*% ruthenium tetroxide solution was used to stain the RHP-lipase and the amorphous PCL domains.

Crystallinity and mechanical properties of enzyme-embedded plastics were probed via differential scanning calorimetry (DSC) and tensile testing, respectively. For DSC, ~5 mg films were pressed

into aluminum pans and heated from 25 °C to 70 °C at a 2 °C min-1 scan rate. To quantify percent crystallinity, the sample's enthalpy of melting was normalized by 151.7 J g^{-1}, enthalpy of melting for 100% crystalline PCL.[30] There is no noticeable changes in the melting temperature and the percent crystallinity after incorporating up to 2 wt% enzyme. For uniaxial tensile tests, PCL solutions were cast directly in custom-designed Teflon molds with standard dog- bone shapes. There is <10% reduction in the modulus of PCL after embedding 2wt% enzyme. For small angle x-ray scattering (SAXS) studies, ~300μm thick films were cast in Teflon beakers. Samples were vacuum dried after degradation for at least 16 hours prior to running SAXS, which was conducted at beamline 7.3.3 at the Advanced Light Source (ALS) at the Lawrence Berkeley National Laboratory. X-rays with 1.24 Å wavelength and 2s exposure times were used. The scattered X-ray intensity distribution was detected using a high-speed Pilatus 2M detector. Images were plotted as intensity (I) vs q, where $q = (4\pi/\lambda)\sin(\theta)$, λ is the wavelength of the incident X-ray beam, and 2θ is the scattering angle. The sector-average profiles of SAXS patterns were extracted using Igor Pro with the Nika package. The same SAXS method was used to analyze the nanoporous structure of samples at different time points of the degradation process. To obtain the cross-sectional SEM image shown in the **inset** to **Figure 5.2d**, the degraded film was rinsed and fractured in liquid nitrogen to minimize fracture-induced morphological changes. The film was then mounted on an SEM stub and sputter coated with platinum. A Hitachi S-5000 SEM was used for imaging.

Degradation of PCL-RHP-BC-lipase

Degradation was carried out in sodium phosphate buffer (25 mM, pH 7.2). Data shown in **Figure 5.2a** was obtained at 37 °C. The mass loss for timepoints up to 5 hours was determined by drying the remaining film and measuring mass on a balance. The mass loss by weighing remaining film corresponded to the intensity reduction when integrating the GPC peaks, so GPC was used to estimate remaining PCL at 24 hours. Remaining PCL could also be weighed by centrifuging the solution at >10,000 RPM, decanting the supernatant, and recovering plastic at the bottom. The microplastic experiment shown in **Figure 5.2e** was run with a ~5 mg PCL-RHP-BC-lipase film (0.02 wt% enzyme) in 3 mL of buffer at 40 °C. The same experiment was run with fluorescently-labeled enzyme to track the enzyme in the film / microparticles during degradation.

Crystallinity change

At each timepoint from 0-5 hours, PCL-RHP-lipase remaining films were dried and analyzed via DSC. Percent crystallinity of the remaining film was determined as described above.

By-product analysis

Gel permeation chromatography (GPC) measurements were obtained using a total concentration of 2 mg/mL of remaining film and by-product in THF. 20 uL of solution was injected into an Agilent PolyPore 7.5x300 mm column. Liquid chromatography-mass spectrometry (LC-MS) measurements were obtained by resuspending degradation supernatant in acetonitrile/water (67/33 vol%) and running through an Agilent InfinityLab EC-C18, 2.7 μm column. Control experiments for surface erosion were run with ~0.15 mg/mL total BC-lipase blend concentration. The mass spectrum shown in **Figure 5.3c** is a combination of the major peaks seen in the chromatogram. Degradation products were dried via lyophilization overnight before resuspending in the proper solvent for GPC or LCMS. The by-products were repolymerized using a previously-reported

method[31] after recovering degraded PCL by-product from enzyme and buffer salts via phase extraction and filtration.

Degradation of PCL-b-PLLA using RHP-BC-lipase

RHP-BC-lipase was embedded in a PCL-b-PLA diblock blended with pure PLA for the testing. Pure PLA was blended with the diblock because the diblock on its own was too brittle to form a complete film after drying. The film was cast from a solution of 9 wt% PCL-b-PLA + 4 wt% pure PLA in dichloromethane. The film was allowed to degrade at 40 °C buffer for 24 hours, and the by-products were analyzed using NMR. BC-lipase degraded both blocks, whereas CA lipase could only degrade the PCL block with high efficiency. Similar results were obtained with a homemade PCL-b-PLA diblock without blending with pure PLA homopolymer.

Enzyme structural analysis

Crystal structures of BC-lipase and CA-lipase are taken from entries 3LIP and 1TCA in protein data bank, respectively. Hydrophobic residues (gray) are defined as the following amino acids: alanine, glycine, valine, leucine, isoleucine, phenylalanine, methionine, and proline. Aspartic acid and glutamic acid are defined as negative residues (red), while lysine, arginine, and histidine are defined as positive residues (blue). The remaining residues are considered polar uncharged residues (purple).

Differences in confined enzyme activity: BC-lipase vs. CA-lipase

CA lipase blend was embedded in PCL using a 2:1 mass ratio of RHP:CA lipase at a similar enzyme loading to BC lipase. Degradation seemingly proceeded via completely random scission, as indicated by a shift of GPC curve to lower average molecular weight over 2 weeks when CA lipase degraded ~12% of the PCL matrix.

Confinement length-scale affects degradation: nanoscopic vs. microscopic vs. surface erosion

Degradation was run in a 1 mL and 1 L container while shaking the container every few hours to demonstrate the effects of leaching and diffusion. PCL-RHP-BC-lipase degrades similarly in both volumes (~95% degradation in 24 hours). This confirms that PCL-RHP-lipase degradation has little reliance on buffer volume, consistent with primarily internal degradation and limited enzyme leaching.

As a control to reproduce experiments detailed in previous literature, Tween 80 was mixed with purified lipase in a 1:1 mass ratio. The resulting films were cast on glass slides, and degradation was carried out in 1 L buffer to probe the effects of leaching. In 1 L buffer, films with small molecule-embedded enzyme at the same enzyme loading as PCL-RHP-lipase degraded by ~40% in 1 day and then stopped degrading (monitored over 1 week), whereas in 1 mL buffer the small molecule-embedded film degraded similarly as RHP-embedded film (~95% in 24 hours). This reliance on buffer volume suggests that small molecule surfactant-embedded enzyme experiments previously reported in literature exhibit significant leaching, and in large volumes this enzyme leaching can prevent complete degradation of the film.

As a further control, pure PCL films were placed in 1 L buffer with an equivalent mass of total lipase as was present in the 10 mg PCL-RHP-lipase films. Pure PCL films exhibited negligible degradation in 1 L buffer over a week, whereas pure PCL films in 1 mL buffer with the same enzyme mass lost ~80% mass in 1 day. This buffer volume dependence is expected, because enzyme must diffuse to plastic surface in order to hydrolyze the plastic.

Kinetic analysis of BC-lipase in different environments with different substrates

Confined BC-lipase with PCL substrate

The slope of the degradation plot shown in **Figure 5.2a** was used to estimate the degradation rate for confined lipase at 37 °C. Two different slopes were obtained (0-3 hours and 3-5 hours) because the rate changed around 3 hours. The turnover rate was determined by dividing the number of PCL bonds broken per second by the total number of lipase molecule in the film, assuming an average trimer PCL by-product based on the LC-MS by-product analysis.

Dissolved BC-lipase with PCL substrate

Pure PCL films (~5 mg each) were placed in 1 mL buffer (37 °C) containing ~1 μg of lipase to mimic concentrations from degradation experiments of confined lipase (S5.1). The turnover rate provided in the text was determined by also assuming a trimer by-product, which may represent an upper bound since surface erosion can occur by random scission (larger oligomers generated per bond cleavage would serve to reduce the apparent turnover rate since more mass is lost per bond cleavage).

Dissolved BC-lipase with small molecule substrate

=A common small molecule substrate (4-nitrophenyl butyrate) was used to carry out a standard Michaelis-Menten kinetic study at 37°C. It was ensured that the small molecule substrate was completely dissolved in buffer at each substrate concentration prior to running the assay to rule out interfacial effects of soluble lipase, since lipase has been shown to undergo interfacial activation. Activity was quantified by using UV-vis spectroscopy to monitor the absorbance over 10 minutes at 410 nm, which is where the hydrolyzed by-product absorbs. Extinction coefficient for by-product concentration quantification was estimated as 16,500 M^{-1} cm^{-1}. PRISM software was used to fit the activity as a function of substrate concentration in order to obtain Vmax, the theoretical maximum reaction rate at saturated substrate concentration. Vmax was converted to a turnover rate by converting per-mass to per-lipase molecule.

Confined BC-lipase with small molecule substrate

The same small molecule assay described above was used to quantify activity of confined lipase in PCL.

Chapter 6:
Thermodynamic and kinetic control over plastic depolymerization by embedded enzymes

6.1 Introduction: semicrystalline morphology of polymers

In the previous chapter we considered how embedded enzymes' active sites control their reaction pathways with polymeric substrates. However, polymers are hierarchically structured molecules, and as such their arrangement should also play a key role enzyme/polymer interactions. The majority of commercial plastics are semicrystalline,[1] so understanding how semicrystalline polymers arrange is crucial to understand enzyme-based depolymerization.

Semicrystalline polymers generally have three levels of order (**Figure 6.1**).[2-3] At the smallest scale, polymer chains adapt their most favorable conformation to pack into a unit cell, which is similar to all crystalline materials. Unlike metallic or ceramic crystals, however, the unit cell packs in three dimensions to give rise to another structural component—thin, sheetlike structures called lamellae. These crystalline lamellae are typically separated by amorphous domains in a repeating, alternating structure (so crystalline-amorphous-crystalline-amorhous…). Finally, within a bulk polymer sample, the crystalline and amorphous layers will typically stack radially from a central nucleus to form what is known as a spherulite. The thickness of crystalline/amorphous domains as well as the spherulite size can be tuned by exploiting the thermodynamics and kinetics of crystallization via melt-processing.[4]

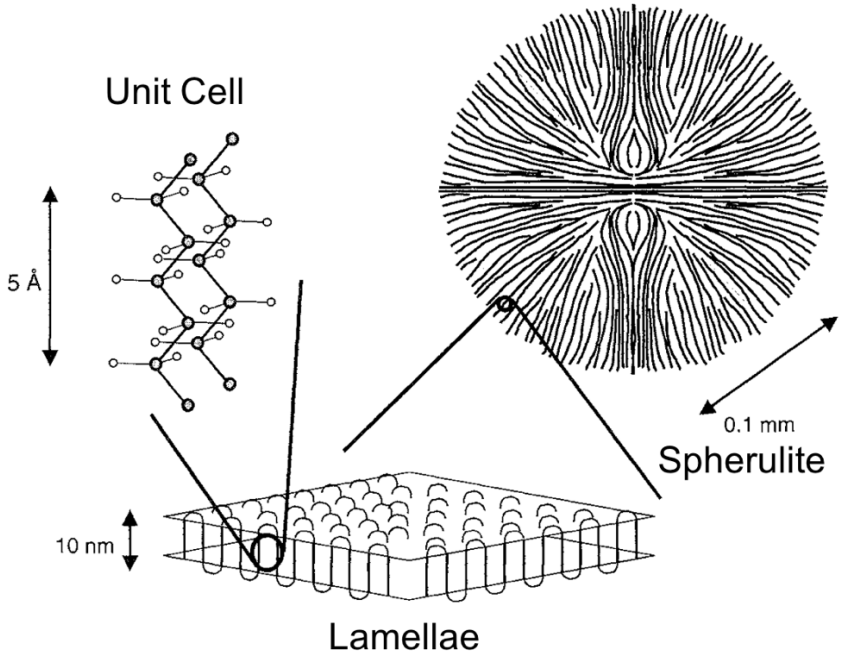

Figure 6.11 *Three levels of hierarchical order in semicrystalline polymers (image adapted from Hiemenz and Lodge's Polymer Chemistry, Second Edition)*

6.2 Results and discussion: hierarchical morphology and single-chain conformation dictate processive degradation by embedded enzymes

The exceptional thermal stability of RHP-BC-lipase embedded inside the melt—over 40% activity retention after 5 hours at 100°C—enables control over the semicrystalline architecture via melt processing. Given the processive mechanism of BC-lipase, we hypothesized that degradation would have a strong dependence on lamellae thickness because as lipase pulls the PCL chain, that force is countered by the inter-chain forces holding together the crystalline domain (and a thicker crystalline lamella would result in more local per-segment interactions) (**Figure 6.2a**). Indeed, PCL-RHP-BC-lipase films with thicker crystalline lamellae (T_c = 49 °C) undergo negligible degradation over 3 months in 37 °C buffer while films with thinner crystalline lamellae (T_c = 20 °C) degrade by up to ~95% in 24 hours (**Figure 6.2b and Figure 6.2c**). Note that all films regardless of lamellae thickness had similar percent crystallinities, ruling that out as a possible variable. The Tc = 49°C films had crystalline lamellae that were ~2 nm thicker than solution cast or Tc = 20 °C films, which corresponds to roughly 3 additional PCL repeat units per lamellae. Control experiments using CA-lipase showed degradation with no crystalline lamellae thickness dependence nor thermal treatment history dependence, likely because the degradation mechanism is random scission rather than processive and thus does not rely on pulling segments out of the crystalline domain. The lamellae thickness dependence of processive degradation can be exploited to program thermal treatment to spatially vary degradation within the same film (**Figure 6.2d**).

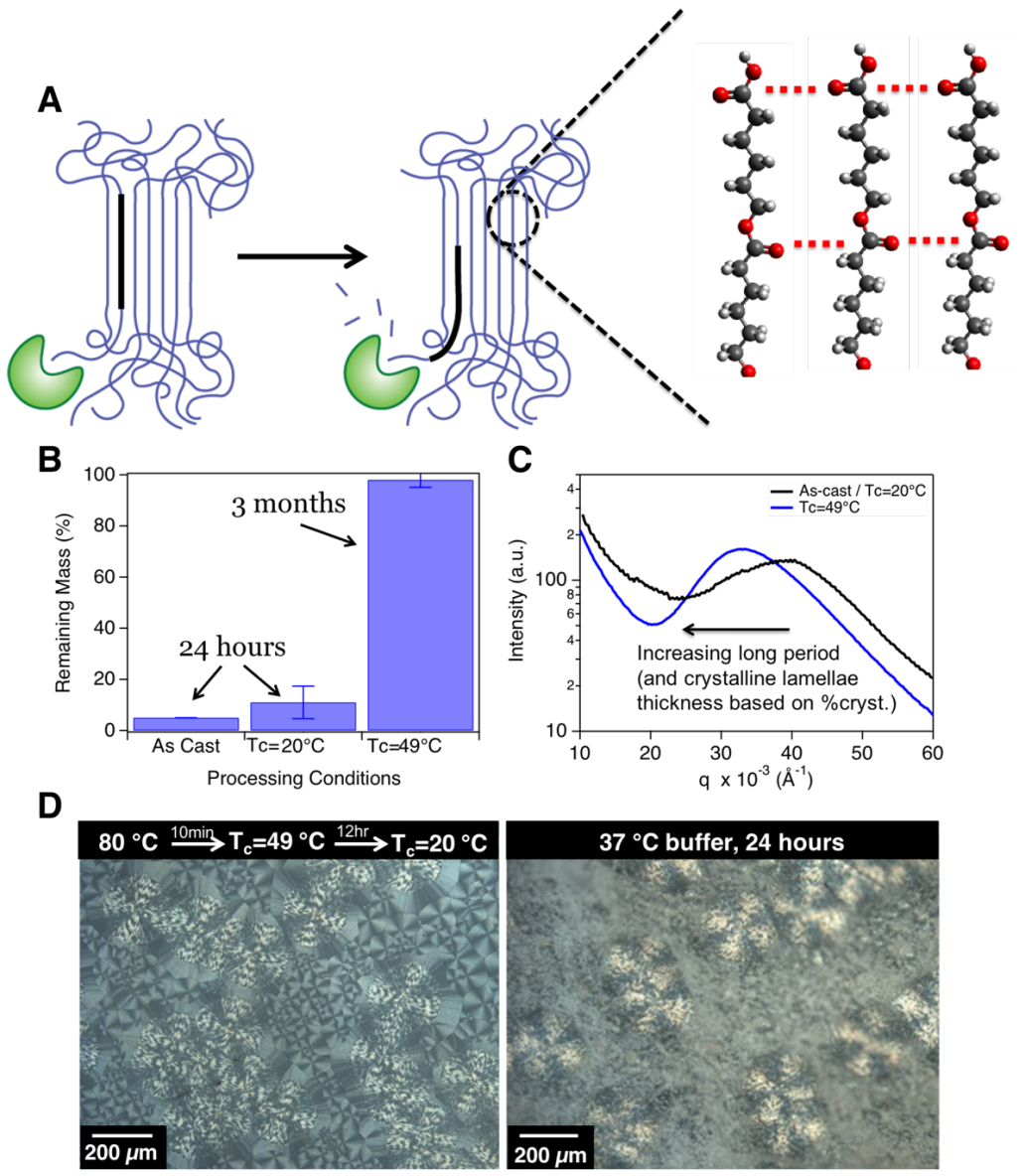

Figure 6.2 *Crystalline lamellae thickness determines embedded enzyme degradation. (A) Schematic of crystalline segments being pulled by processive mechanism; (B) Degradation in 37°C buffer for various processed films; (C) SAXS data for processed films; (D) Spatial control of PCL degradation based on thermal history*

Degradation kinetics by confined BC-lipase depend on the global driving force for depolymerization. There is a much lower conformational entropic penalty for a crystallized chain end to bind to an enzyme than an amorphous chain, provided sufficient mobility.[5] The degradation rate was lowest when PCL was fully melted (> 60 °C) although the confined enzyme had a higher activity for hydrolyzing a small molecule substrate at elevated temperatures, ruling out enzyme denaturation (**Figure 6.3a**). Degradation rate increased significantly before the onset of PCL melting (~43 °C) but exhibited an exponential decrease as the temperature exceeded 43 °C (**Figure 6.3b**). The high entropic penalty for enzyme binding overtakes the effects of increased chain

mobility, leading to large reductions in degradation rates at higher temperatures and eventually minimal degradation of PCL in the melt state. These results counter the long-standing opinion that crystallinity slows enzymatic degradation of both synthetic[6-7] and natural[8-9] polymers. Thus, chain-end mediated processive depolymerization leads to latency of embedded enzymes to ensure polymer integrity during melt processing and long-term storage.

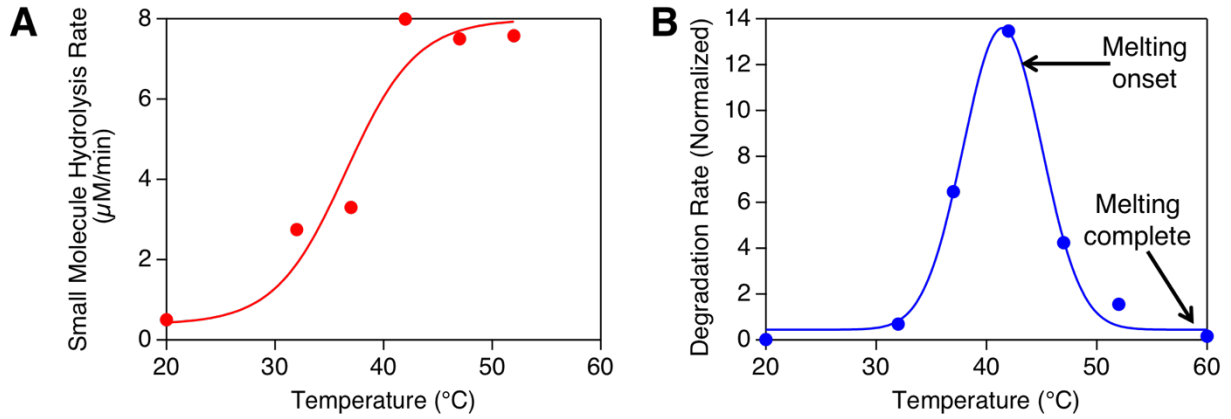

Figure 6.3 *Single chain conformation seems to dictate degradation by embedded BC-lipase. (A) Small molecule ester hydrolysis as a function of temperature showing that the enzyme is not deactivated at elevated temperatures. (B) Normalized degradation rate as a function of temperature*

We also exploited the molecular weight of the PCL matrix to further probe kinetics and thermodynamics of depolymerization by embedded BC-lipase. First, we used solution-cast films of varying molecular weights to alter the crystalline lamellae thickness in order to test the hypothesis that the dependence of degradation extent on lamellae thickness was a thermodynamic parameter dominated by overcoming the enthalpy of interchain forces in the crystalline domain. It is a known phenomenon in polymer science that crystalline lamellae thickness for solution-cast films is reduced as the polymer entanglement density is reduced.[10-11] This relationship arises because chain entanglements increase the free energy associated with the crystalline fold surface, so a higher entanglement density leads to higher crystalline surface free energy and thus to lamellae thickening to reduce surface-area-to-volume ratios. We cast three solutions—one each of PCL 80kDa, 45 kDa, and 10 kDa—whose concentrations are listed in **Table 6.1**. PCL is known to have an entanglement molecular weight—or the average molecular weight between entanglements, denoted as MW_e—of ~2.4 kDa in the melt. The MW_e for polymer solutions is dependent on the inherent MW_e in the melt divided by the concentration of the polymer in solution.[12] As shown in Table 6.1, the crystalline lamellae thickness (proportional to melt temperature by the Thompson-Gibbs equation) nicely scales with the average number of entanglements per chain.

***Table 6.1**: Characterization of PCL solution-cast films*

Sample	Concentration	MW_e (solution)	Entangle./chain	T_m (°C)
PCL-80 kDa	3 vol%	78 kDa	1.0	58.2
PCL-45 kDa	4.6 vol%	52 kDa	0.9	57.8
PCL-10 kDa	6 vol%	39 kDa	0.4	56.0

After successfully tuning lamellae thickness of solution-cast films via molecular weight and concentration, we first determined the lowest possible buffer temperature at which measurable degradation occurred for PCL 80kDa, which we found to be 32 °C. We then tested the degradation of the other two PCL molecular weight samples at that temperature, reasoning that if the lamellae thickness dependence was a thermodynamic phenomenon, then the extents of degradation should be higher for the 45 kDa sample and even higher still for the 10 kDa sample. Indeed, we found that relationship to be true, as demonstrated in **Figure 6.4a**. This experiment supports the thermodynamic explanation for lamellae thickness dependence of degradation by embedded BC-lipase.

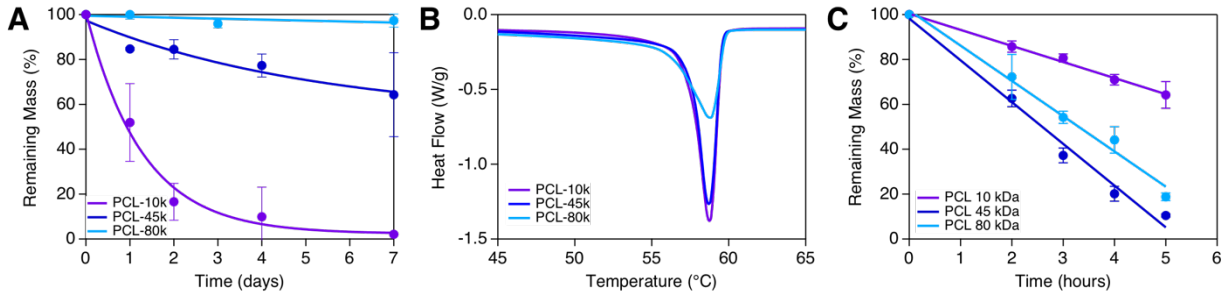

***Figure 6.4** Exploiting PCL molecular weight to understand thermodynamics and kinetics of enzyme-embedded depolymerization. (A) Degradation in 32 °C buffer for different solution-cast PCL films; (B) DSC curves showing ~identical melting temperatures (and thus crystalline lamellae thickness) for PCL films crystallized via melt-processing; (C) degradation of melt-processed films shown in "B" at 42 °C buffer*

Finally, we wanted to understand the primary kinetic factors governing degradation when all three PCL molecular weight samples had identical crystalline lamellae thicknesses. Through trial and error, we were able to achieve ~identical crystalline lamellae by crystallizing the 80 kDa and 45 kDa samples at Tc = 32 °C for 12 hours and the 10 kDa sample at Tc = 34.5 °C for 12 hours (**Figure 6.4b**). Samples were degraded in 42 °C buffer and the rates for one batch are shown in **Figure 6.4c**. The 80 kDa and 45 kDa samples have similar degradation rates, but the 10 kDa sample degrades at least 2 times slower. This data may suggest that chain-end binding is the rate-

limiting factor and/or may support processivity in the degradation process—as one crystalline stem is pulled out of the lamellae, the neighboring stem has fewer inter-chain interactions to overcome, and since adjacent reentry occurs for ~50% of crystalline stem segments,[13] higher MW chains may degrade faster for equivalent lamellae thicknesses due to processivity.

6.3 Conclusions

In this chapter we have delved deeper into the thermodynamics and kinetics that dictate depolymerization by embedded BC-lipase. We show that BC-lipase, due to its processive mechanism, has a strong dependence on crystalline lamellae thickness that can be exploited to achieve temporal and spatial depolymerization control. We also show that the single chain conformation of PCL affects degradation, and that contrary to most literature reports of plastics in enzyme solutions, crystalline domains actually help degradation to occur for enzyme-embedded materials. Finally, using PCL molecular weight as a handle, we showed that the lamellae thickness dependence is indeed likely to be a thermodynamic factor and that for equivalent lamellae thicknesses, chain end binding and/or processivity lead to higher molecular weight PCL being depolymerized faster. In the final chapter, we will demonstrate the importance of considering RHP not only for its effects on the enzyme but also for its effects on the matrix.

6.4 Experimental Methods

Materials

The RHPs were synthesized as previously reported.[8] Unless otherwise stated, the molar composition of the RHP was 50:20:25:5 MMA:EHMA:OEGMA:SPMA, and the molecular weight was 70 kDa. PCL (80 kDa, 45 kDa, and 10 kDa) was purchased from Sigma and used as-received. Note that films here denoted as "PCL-10 kDa" also have 15% (by mole) of 45 kDa chains added in — the pure 10 kDa film did not have adequate mechanical properties to remain as a freestanding film, so higher MW chains were added to eliminate leaching as a potential concern. Amano lipase PS from *Burkholderia cepacia* was purchased from Sigma Aldrich and purified following a previously reported procedure.[29] However, the unpurified commercial blend behaved the same as the purified enzyme when embedded using RHP. Lipase B from *Candida antarctica* was also purchased from Sigma Aldrich and used as purchased.

Methods

Enzyme-embedded films were created using the exact same procedure mentioned in Chapter 5, and all films in this chapter utilized 0.02 wt% BC-lipase concentrations (and 80-1 RHP-BC-lipase ratio). Melt-processed films were melted at 80 °C or 100 °C for 5 minutes and then recrystallized at the specified temperatures in the text. Lamellae thicknesses were estimated by combining the long period obtained via SAXS (procedure for data collection same as that in Chapter 5) with the percent crystallinity obtained from DSC. All other methods for degradation in this chapter were done using same conditions described in the "Experimental Methods" section of Chapter 5.

Chapter 7:
Synergistic enzyme mechanisms overcome additive-induced recalcitrance of plastic depolymerization by embedded enzymes

7.1 Introduction: additives affect the semicrystalline morphology of polymers

Throughout the thesis, we have considered how RHP-enzyme interactions stabilize enzymes in nonnatural environments and how enzyme-matrix interactions dictate depolymerization extents and pathways by embedded enzymes. However, for bioactive plastics, a third consideration—RHP-matrix interactions—may also play a crucial role in the system's behavior. The RHP is typically present in large excesses (~100:1) in order to disperse and stabilize enzymes in organic solvents and polymeric matrices, and thus there are likely to be free RHP molecules embedded inside the polymer matrix. As such, the RHP must be considered as a polymer additive in addition to its role as an enzyme protectant.

Additives have long been known to affect the morphology and properties of polymer matrices.[1-4] Since all matrices used during my dissertation work are semicrystalline, I will focus here on the role of additives only on semicrystalline morphology. It was shown in 1989 that the semicrystalline morphology of polyesters—and polycaprolactone (PCL) in particular—can undergo drastic changes in the presence of just small amounts (<5 wt%) of polymer additives.[5] As shown in **Figure 7.1a**, melt-crystallized pure PCL exhibited spherulites with a standard extinction cross pattern under a polarized optical microscope (POM). However, addition of just 1 wt% of polar polymer additives (poly vinyl chloride (PVC) or poly vinyl butyral (PVB)) led to a "banded" morphology of regularly spaced rings radiating from the center of the spherulite when recrystallized at the same temperature (**Figure 7.1b**). This banded ring pattern has been observed in other semicrystalline polymers and is attributed to cooperative bending and/or twisting of lamellae bundles.[6] Specifically, it is hypothesized that unbalanced stresses at the surface of a nascent crystalline lamellae cause the lamellae to bend, and this bending persists across bundles of lamellae because neighboring lamellae are connected through tie chains.[7] Unbalanced stresses at lamellae surfaces can arise from several sources,[8] but two primary explanations are generally considered in the literature. First, inherent chain tilt in the crystalline domains of some polymers cause different stress values at the top and bottom lamellae surfaces due to the difference in geometry at which the chains emerge from the respective surfaces (**Figure 7.1c**). In the case of additive-induced bending, however, the additive can transiently adsorb onto the surface of a growing lamellae during crystallization, thereby leading to different stresses at the site of additive adsorption compared to the rest of the lamellae, which causes the lamellae to bend.[5] Lamellae bending in PCL/additive blends is generally attributed to the transient adsorption argument, especially since two separate groups have confirmed via x-ray diffraction that PCL's unit cell structure does not change for banded (bent) versus non-banded (straight) spherulites (which suggests that chain tilt in the crystalline domain is equivalent for straight and bent lamellae).[5, 9]

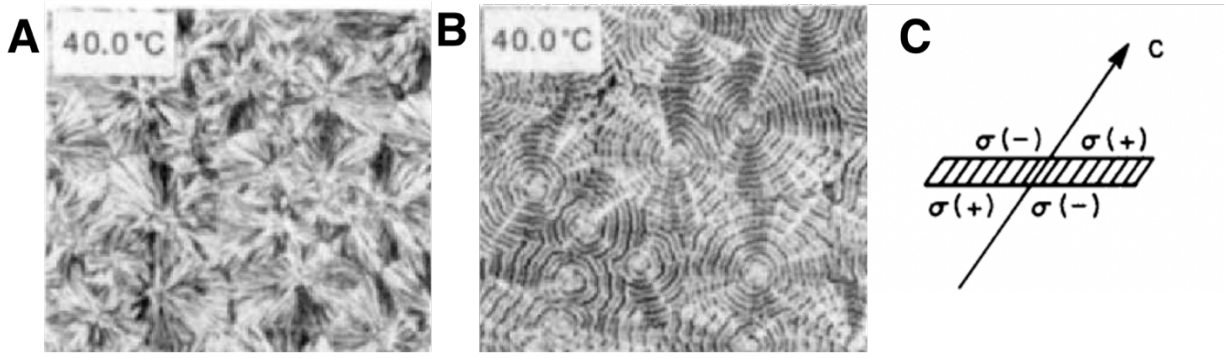

Figure 7.12 *(A) POM image of pure PCL exhibiting an extinction cross pattern, typical of most semicrystalline polymers; (B) POM image of PCL with 1 wt% of poly(vinyl chloride) added showing a regularly-textured banded pattern, indicative of lamellae bending and/or twisting; (C) illustration of why some polymers exhibit bent lamellae due to the inherent stress imbalance arising from geometric considerations of tilted chains (note that PCL additive-induced banding likely occurs due to transient adsorption of additive to the surface, not due to chain tilt); Figure 7.1A and B were adapted from ref[5] and Figure 7.1C was adapted from ref[6]*

Designing the next generation of degradable plastics requires us to consider additives given their ubiquity in plastic materials. Indeed, commercial plastics contain plasticizers to improve processability, fillers to improve mechanical strength, and antioxidants to prevent unwanted degradation during material usage, for instance. Given the prevalence of additives in existing commercial plastics, and that enzyme-dispersing agents like RHP can be considered as additives, we deemed it relevant to study the effects of RHP on the polymeric matrix and how those effects contribute to the material's depolymerization. Here, we demonstrate that low molecular weight (MW) RHPs cause recalcitrance during depolymerization by embedded enzymes, likely due to alterations to the semicrystalline morphology that may cause inaccessibility of PCL chain ends BC-lipase.

7.2 Results and discussion: molecular weight of random heteropolymer affects extent of degradation by embedded enzymes

All results from preceding chapters on the degradable bioactive plastics, unless otherwise specified, were carried out using 70 kDa MW RHPs to embed the enzyme inside PCL. We found that when keeping the RHP composition and the total RHP:BC-lipase mass ratio (80:1) constant but reducing the RHP molecular weight to 20 kDa, degradation by the embedded enzyme stops after ~70% mass loss (**Figure 7.2a**). Increasing the total concentration of 20 kDa MW RHP to give a 140:1 RHP:lipase ratio led to degradation stopping at even shorter extents—roughly after 35% mass loss. Thus, the low MW RHP causes depolymerization recalcitrance.

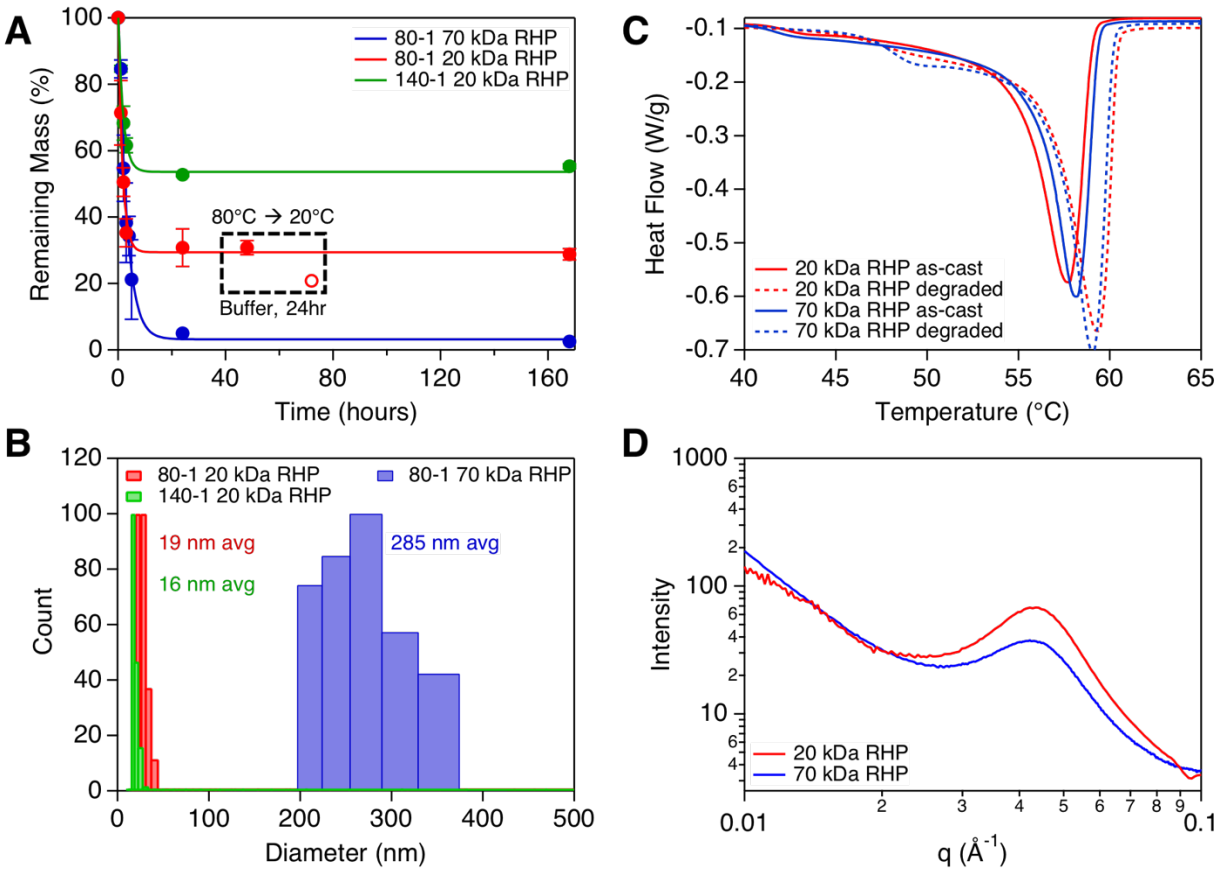

Figure 7.2 *(A) Remaining mass as a function of time for different PCL-RHP-BC-lipase films; the black box indicates the control experiment where the crystal structure of the remaining film was "reset" by melting and recrystallizing at room temperature followed by placing the remaining film back in buffer; (B) DLS of RHP-BC-lipase in toluene; (C) DSC curves of PCL-RHP-BC-lipase films, as-cast (solid) or after ~50% depolymerization (dotted lines); (D) SAXS curves of PCL-RHP-BC-lipase solution-cast films*

We ran a series of control experiments to understand why degradation stops for low MW RHP. We first confirmed that the embedded enzyme retained its inherent activity using a small molecule assay (data not shown). Next, we used DLS to determine whether the distribution of enzymes may be different in the solution-cast films—for instance, degradation may have stopped if the low MW RHP caused larger aggregates that prevented the enzymes from accessing large portions of the film. However, as shown in **Figure 7.2b**, reducing the MW of RHP actually led to much smaller RHP-BC-lipase clusters and better dispersion in toluene (the solvent used to cast the films), so lack of enzyme availability is unlikely to explain why degradation stops for low MW RHP. Interestingly, the 80-1 and 140-1 low MW RHP-lipase clusters have the same diameter within experimental error. The reason for the 10x reduction in RHP-lipase cluster size going from high MW to low MW RHP will be the subject of future studies. The main takeaway from these DLS results, however, is that a high proportion of the 20 kDa RHP likely exists in the PCL matrix after solution casting, since the 80-1 and 140-1 cluster sizes are the same within experimental error

(so when increasing the total RHP concentration from 80:1 to 140:1, the excess RHP likely exists in the PCL matrix). These results suggest that the reason for depolymerization recalcitrance for low MW RHP may have to do with RHP-induced effects on the crystalline matrix rather than RHP-enzyme interactions.

Given the degradation dependence on lamellae thickness due to the processive depolymerization mechanism that we demonstrated in previous chapters, we initially thought that the low MW RHP may cause lamellae thickening (either before or during degradation), which could then potentially explain the stopped degradation. However, differential scanning calorimetry (DSC) and small angle x-ray scattering (SAXS) data demonstrate that PCL-RHP-BC-lipase films have identical percent crystallinity, crystalline lamellae thickness, and crystal-amorphous long periods (**Figure 7.2c** and **Figure 7.2d**) both prior to and during degradation. Thus, bulk changes to the lamellae thickness are unlikely to explain the stopped degradation.

As a final control experiment to determine whether matrix effects contribute to the stopped degradation for low MW RHP, we "reset" the crystalline morphology after degradation stopped. Specifically, for the 80-1 low MW RHP-BC-lipase sample, we dried the remaining film after degradation stopped, melted the film at 80°C for 5 minutes, and then recrystallized the film at room temperature and put the film back in buffer. Resetting the crystal structure enabled degradation to continue (**Figure 7.2a, dotted box**), causing the remaining film to lose ~33% of its mass from the point at which degradation had initially stopped (i.e. from 30% remaining to 20% remaining mass). Taken together, our control experiments suggest that the low MW RHP causes some change in the semicrystalline structure of PCL that is not observable by bulk techniques like DSC or SAXS, but that prevent depolymerization by embedded BC-lipase from continuing after a certain point (~70% mass loss for 80-1, ~35% mass loss for 140-1).

We used transmission electron microscopy (TEM) and polarized optical microscopy (POM) to observe whether morphological changes occurred as a function of RHP MW. Indeed, TEM of solution-cast films showed that the low MW RHP caused significant curvature in the PCL crystalline lamellae, while pure PCL or PCL with high MW RHP had straight, continuous lamellae (**Figure 7.3a**). Thus, it seems as though the low MW RHP acts similarly to PVC/PVB additives mentioned in the introduction above,[5] adsorbing to the PCL lamellae surfaces and causing bending due to unbalanced surface stresses. Interestingly, the concentration of RHP in the matrix (1.5 wt%) is similar to that of the PVC/PVB additives from past reports (1 wt%).

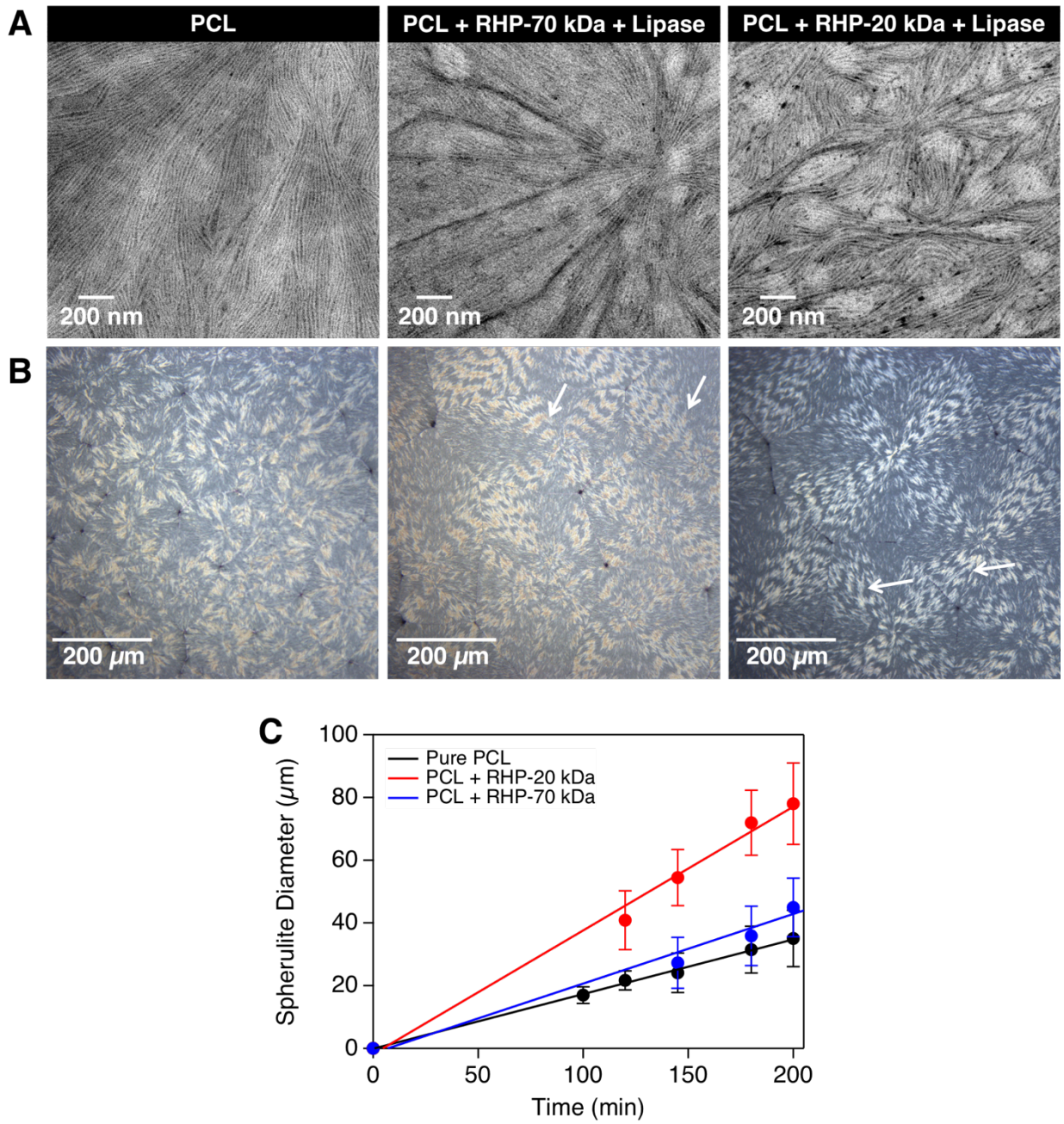

Figure 7.3 *(A) TEM images of solution cast films and (B) POM images of melt-crystallized (Tc= 49°C) films for PCL (left), PCL+ RHP-70 kDa+BC-lipase (middle), and PCL + RHP-20 kDa+BC-lipase (right); (C) Spherulite growth rates for PCL and PCL-RHP*

We used POM to confirm that the TEM results were representative of lamellae bending/twisting throughout the bulk film and not just a local artifact. Solution-cast films had spherulites that were too small for their textures to be observed using POM, so we used melt-processed films with a crystallization temperature of 49 °C. As shown in **Figure 7.3b**, pure PCL

possessed the same non-banded extinction cross patterns reported in literature (indicative of straight lamellae), but the PCL-low MW RHP-lipase films displayed a banded ring pattern, consistent with lamellae bending and/or twisting. Note that the PCL-high MW RHP-lipase films also displayed a banded pattern. The melt-processed films crystallize slowly and require at least 1 day to fully crystallize at 49 °C, whereas solution cast films crystallize over a period of minutes, so it is possible that some high MW RHP molecules have enough time to diffuse and/or adjust their conformation to adsorb transiently at the lamellae surface when crystallization occurs slowly enough (as is the case for 49 °C crystallized films), but crystallization from solution occurs so quickly that only the low MW RHPs can adsorb and cause lamellae bending. As support for this explanation, the growth rate of PCL + low MW RHP is approximately 2 times faster than that of pure PCL while the growth rate of PCL + high MW RHP is only marginally faster than that of pure PCL (**Figure 7.3c**) for the melt crystallized films. Increased growth rates have been observed previously for semicrystalline polymers containing plasticizers due to increased chain mobility as the local chain entanglements are disrupted by the plasticizing agent.[10] Our data suggests that the low MW RHP more effectively mixes with PCL at the molecular level, causing increased chain mobility and faster crystallization rates. This data indirectly supports the proposed explanation that, in solution cast films, the low MW RHP causes lamellae curvature because it more effectively mixes with PCL chains while the high MW RHP does not mix as well with PCL and therefore only alters the PCL matrix morphology for slow crystallization conditions.

7.3 Results and discussion: synergistic enzyme mechanisms overcome RHP-induced recalcitrance

Although the microscopy data presented in **Figure 7.3** demonstrate that low MW RHP causes bent/twisted lamellae for solution cast films, the observations still do not explain why the low MW RHP causes depolymerization recalcitrance. Here, using a lattice model, we consider how curvature may cause redistribution of chain ends in the amorphous domains, and since depolymerization is seemingly a chain end-based process, this redistribution of chain ends may explain the recalcitrance.

Consider a basic lattice model for a planar crystalline/amorphous structure and a curved crystalline/amorphous structure (**Figure 7.4a**). In a fixed volume, the planar structure has the same number of available lattice sites at each layer below the crystal/amorphous interface. However, due to geometric arguments, the number of available lattice sites for the curved structure decreases with each ensuing layer below the crystal/amorphous interface since each layer's lattice sites scales with $4\pi r^2$, the surface area of a sphere. For a radius of curvature of 100 nm, which is frequently observed for the lamellae in the TEM images, the number of available lattice sites decreases by ~8% just 4 nm below the crystal/amorphous interface. If we assume no changes to the unit cell structure in the curved crystalline regions, which has been confirmed in literature for PCL,[5, 9] then the density in the amorphous regions could theoretically increase to values greater than that of the crystalline domain since the same number of chains will emerge from the crystal domain but have a smaller volume to occupy. This high density of chain packing is energetically unfavorable, and polymers typically avoid density anomalies (higher density in amorphous than crystalline domains) by several morphological changes. Higher angles of chain tilt in the crystalline domain reduce the number of chains emerging into the amorphous region, thereby reducing the density.[11]

If the chain tilt remains constant, polymer chains can also increase the frequency of adjacent reentry back into the crystalline domain,[12] which helps alleviate density anomalies by also reducing the number of segments emerging into the amorphous region. Finally, if chain tilt and adjacent reentry frequency are assumed to be constant, polymers can concentrate their chain ends at the crystal/amorphous interface to reduce the segments in the amorphous region.[13]

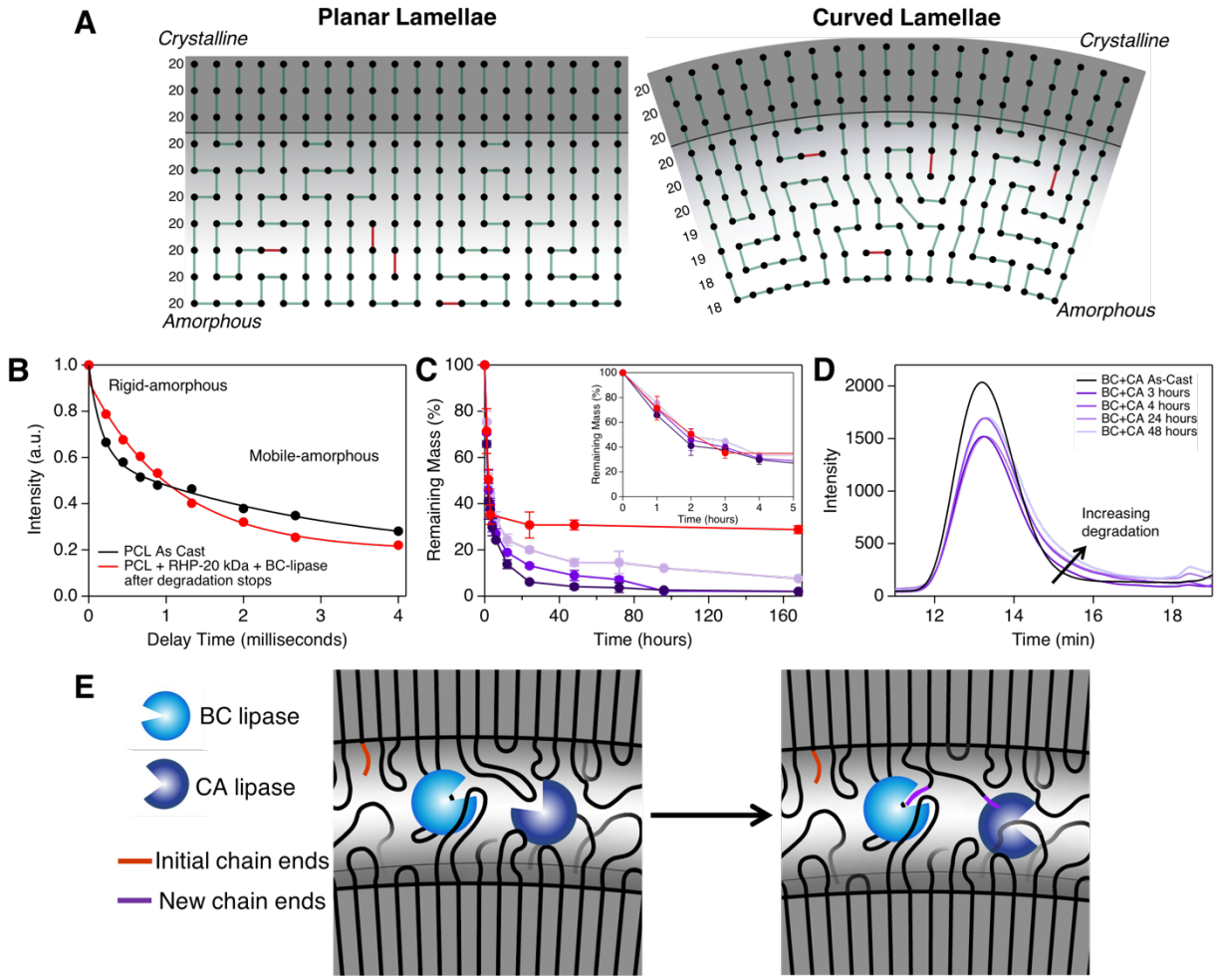

Figure 7.4 *(A) Lattice model for planar and curved semicrystalline morphologies; (B) T2 relaxation of solid-state ^{13}C NMR suggesting significant changes in the rigid-amorphous domain for PCL samples containing low MW RHP and BC-lipase that have stopped degrading; (C) Degradation over time for PCL and low MW RHP containing just BC-lipase (red) and BC-lipase plus varying concentrations of CA-Lipase (purple); (D) GPC curves of PCL+low MW RHP+BC-lipase+CA-lipase over time; (E) Proposed model suggesting that curved lamellae render a large portion of chain ends inaccessible to processive depolymerization by BC-lipase by pinning chain ends at the crystal-amorphous interface, but that CA-lipase can create new chain ends to overcome this barrier*

Since depolymerization by embedded BC-lipase is a chain end-mediated process that also requires pulling segments out of the crystalline domain, we hypothesized that any changes in the crystal/amorphous interface could explain why degradation stops for the low MW RHP (i.e. curved lamellae) samples. Solid-state ^{13}C NMR is a useful technique to probe the crystal/amorphous interfacial region. Specifically, the amorphous domain in semicrystalline polymers does not behave exactly like a pure amorphous polymer melt. Rather, there are two regions in the amorphous semicrystalline phase: a constrained "rigid amorphous region" that has significantly reduce mobility and exists immediately adjacent to the crystalline domain, and a non-constrained "mobile amorphous region" that has the same mobility as a pure amorphous melt that exists further from the crystalline domain.[14-16] The NMR T2 relaxation of amorphous segments in semicrystalline polymers decay with two different rates: segments in the rigid amorphous region have a rapid T2 decay while segments in the mobile amorphous region decay slowly.[17] We used this technique to probe whether changes occurred in the rigid amorphous region for low MW RHP samples after degradation stopped. We found a significant increase in mobility in the rigid amorphous region, as indicated by the reduction in the T2 decay rate (**Figure 7.4b**). Important controls are underway, but assuming the T2 relaxation rate reduction is reproducible and only occurs for low MW RHP samples, these changes may help explain the stopped degradation. For instance, increase in mobility in the rigid-amorphous domain could potentially arise from the chain end segments being pinned at the crystal-amorphous interface, which would prevent accessibility to the embedded BC-lipase and thus prevent degradation for a large number of chains. Note that when we say "chain ends" we do not mean the monomer at the chain end, but rather the entire unentangled segment at the chain end, because that entire segment has higher mobility than the bulk segments of the chain. Since PCL has an entanglement molecular weight of ~2,400 g/mole, chain end segments account for 6% of PCL 80 kDa chains, and chain end segments are preferentially excluded from crystalline domains due to the energetic penalty associated with incorporating defects into crystals[13] (so 12% of the amorphous segments comprise chain end segments). Thus, it is possible that pinning the chain ends in the rigid-amorphous domain could account for such a significant change in rigid-amorphous mobility.

To explore the hypothesis that chain end redistirubtion and inaccessibility is the cause of degradation stopping for low MW RHP, we embedded both BC- and CA-lipase together. From Chapter 5, we showed that CA-lipase alone only degrades ~12-15% of PCL when it is embedded inside the matrix because it cleaves chains via random scission and is not processive, but we hypothesized that embedding BC- and CA-lipase together could potentially overcome depolymerization recalcitrance for the low MW RHP samples because CA-lipase could create more chain ends that BC-lipase could then grab and degrade processively. Indeed, we found that addition of CA-lipase results in a higher extent of degradation in a manner that depends on CA-lipase concentration (**Figure 7.4c**). Importantly, the degradation rate is identical at early timepoints, and the rate then slows down significantly around the same time (3-4 hours) that the low MW RHP sample containing only BC-lipase stops degrading altogether (**Figure 7.4c inset**). The rate kinetics suggest that at early stages (<3-4 hours), degradation occurs primarily via BC-lipase processive depolymerization, but then when no chain ends are accessible any longer (i.e. when PCL containing BC-lipase alone would stop degrading altogether), the rate slows down significantly as CA-lipase creates more chain ends that must diffuse to the BC-lipase active site. GPC analysis supports this explanation. At early timepoints, there is no change in the MW distribution of the PCL matrix, consistent with processive depolymerization; however, after ~3

hours, the MW distribution shifts significantly to the right and broadens, indicative of random chain scission (**Figure 7.4d**). Taken together, the rate kinetics and GPC analysis suggest that embedding BC- and CA-lipase together enables a synergistic depolymerization approach that overcomes recalcitrance that arises from chain end inaccessibility (**Figure 7.4e**).

7.4 Conclusions

Synergistic enzyme mechanisms during surface erosion have previously been shown to increase the extent of degradation of recalcitrant polymers such as cellulose[18] or PET.[19-20] Our detailed studies here shed light on potential mechanistic explanations for additive-induced recalcitrance in polyesters and provide an approach to overcome such a barrier by exploiting synergistic mechanisms. Given the prevalence of additives in the plastics industry in general, and the necessity of using additives to embed enzymes inside plastic matrices in particular, the insights provided here may greatly enhance the technological relevance of enzymatic plastic depolymerization in settings outside of academic laboratories.

7.5 Experimental Methods

Materials:

All materials used in this chapter are described in the "experimental methods" section of Chapter 5.

Methods:

DLS was used to obtain the complex's particle size after resuspending in toluene. DLS was run on a Brookhaven BI-200SM Light Scattering System using a 90° angle. DSC scans were carried out using 2°C / min scan rate. For SAXS studies, ~300μm thick films were cast in Teflon beakers. Samples were vacuum dried after degradation for at least 16 hours prior to running SAXS, which was conducted at beamline 7.3.3 at the Advanced Light Source (ALS) at the Lawrence Berkeley National Laboratory. X-rays with 1.24 Å wavelength and 2s exposure times were used. The scattered X-ray intensity distribution was detected using a high-speed Pilatus 2M detector. Images were plotted as intensity (I) vs q, where $q = (4\pi/\lambda)\sin(\theta)$, λ is the wavelength of the incident X-ray beam, and 2θ is the scattering angle. The sector-average profiles of SAXS patterns were extracted using Igor Pro with the Nika package.

TEM images were taken on a JEOL 1200 microscope at 120 kV accelerating voltage. Vapor from a 0.5 *wt*% ruthenium tetroxide solution was used to stain the RHP-lipase and the amorphous PCL domains. The growth rate of melt-processed films was obtained by taking POM images at the specified timepoints and measuring the size of ~10 spherulites per time point.

Solid-state NMR measurements were conducted using a Bruker AV-500 (500 MHz) spectrometer. PCL films were cut into small pieces and subsequently packed into a half rotor. ^{13}C chemical shifts were referenced to tetramethylsilane (TMS) using the methylene peak of adamantane (38.48 ppm). All measurements were conducted at room temperature and magic angle

spinning (MAS) rate of 9kHz. Recycle delay was set to 2s, which is sufficient for saturation recovery of the amorphous chains (T_1 = 0.19s) but not the crystalline domains (T_1 = 28s and 276s).[17] ^{13}C spin-spin relaxation (T_2) was obtained using Hahn echo through direct excitation. The experiment included 8 delays synchronized to the MAS rotor period. T_2 calculations of PCL were centered on the methylene peak at 64.26 ppm to avoid peak overlap with other groups. Integrals were obtained by line fitting a Gaussian peak from 60-70 ppm. T_2 relaxation times were obtained by fitting magnetization decay vs delay time to a two-component exponential curve.

Afterword

Throughout this thesis, we have provided fundamental insights into enzyme stabilization that enable us to manipulate enzymatic pathways, activity, and stability in nonnatural and/or unfavorable environments. While we have suggested a link between active site loops and instability at hydrophobic interfaces in water / inactivity in nonpolar organic solvents, it will be interesting to see if these trends hold across different enzymes. More in-depth biochemical characterization techniques may provide stronger insights into the role of loops on enzyme behavior in different liquid microenvironments.

Our insights have also opened up new opportunities for studying enzymatic behavior in solid matrices. While we have shown that lipases and proteases can withstand high temperatures exceeding 100 °C inside polymer melts, it will be interesting to understand how the specific microenvironment within the matrix affects enzyme stability. Enzyme confinement typically leads to thermodynamic stabilization based on entropy—fewer unfolded states are accessible for confined enzymes—but the enthalpic contribution of the microenvironment will certainly contribute to the enzyme's stability. Random heteropolymers offer a unique opportunity to study these enthalpic effects by tuning the accessible intermolecular interactions with confined enzymes. High-throughput approaches may also allow us to study how enzyme active site features correlate with melt stability

From a technological perspective, it will be interesting to understand how our self-degrading bioactive plastics behave in different environmentally relevant conditions. Composting experiments are currently underway to understand how much moisture is required for the embedded enzymes to carry out depolymerization, and it would be interesting to explore efficient recovery approaches to isolate the small molecule by-products from water after depolymerization is complete. These experiments combined with a deeper understanding of enzymes' stability in polymer melts at high temperatures will expand the technological relevance of our system and could introduce a pathway toward commercialization. Finally, our finding that crystallinity can actually facilitate depolymerization compared to the melt state for specific conditions may lead to new ways of thinking in the plastic degradation field, which currently focuses heavily on reducing the plastic's crystallinity in order to break it down into its building blocks.

Enzymes are clearly capable of retaining high activity in solid materials, and in fact the enzymatic behavior can be tuned by controlling the hierarchical and single chain structure of the plastic matrix using standard polymer processing techniques. We have just scratched the surface of enzyme-embedded materials with the embedding matrix as the substrate, and I anticipate many exciting scientific and technological advances in this area moving forward!

References

Chapter 1

1. Davis, B. G.; Borer, V., Biocatalysis and enzymes in organic synthesis. *Nat Prod Rep* **2001,** *18* (6), 618-640.
2. Brocklehurst, K., Evolution of Enzyme Catalytic Power - Characteristics of Optimal Catalysis Evaluated for Simplest Plausible Kinetic-Model. *Biochem J* **1977,** *163* (1), 111-116.
3. Dill, K.; Chan, H. S., On the Origins of Structure in Globular-Proteins. *Biochemistry-Us* **1990,** *29* (8), 2183-2183.
4. Dill, K. A., Dominant Forces in Protein Folding. *Biochemistry-Us* **1990,** *29* (31), 7133-7155.
5. Alberts, B.; Johnson, A.; Lewis, J.; Morgan, D.; Raff, M.; Roberts, K.; Walter, P., Molecular Biology of the Cell, Sixth Edition. *Molecular Biology of the Cell, Sixth Edition* **2015**, 1-1342.
6. Kamerlin, S. C. L.; Warshel, A., At the dawn of the 21st century: Is dynamics the missing link for understanding enzyme catalysis? *Proteins* **2010,** *78* (6), 1339-1375.
7. Warshel, A., Electrostatic origin of the catalytic power of enzymes and the role of preorganized active sites. *J Biol Chem* **1998,** *273* (42), 27035-27038.
8. Jindal, G.; Warshel, A., Misunderstanding the preorganization concept can lead to confusions about the origin of enzyme catalysis. *Proteins* **2017,** *85* (12), 2157-2161.
9. Austin, R. H.; Beeson, K. W.; Eisenstein, L.; Frauenfelder, H.; Gunsalus, I. C., Dynamics of Ligand-Binding to Myoglobin. *Biochemistry-Us* **1975,** *14* (24), 5355-5373.
10. Mccammon, J. A.; Gelin, B. R.; Karplus, M., Dynamics of Folded Proteins. *Nature* **1977,** *267* (5612), 585-590.
11. Makinen, M. W.; Houtchens, R. A.; Caughey, W. S., Structure of Carboxymyoglobin in Crystals and in Solution. *P Natl Acad Sci USA* **1979,** *76* (12), 6042-6046.
12. Frauenfelder, H.; Sligar, S. G.; Wolynes, P. G., The Energy Landscapes and Motions of Proteins. *Science* **1991,** *254* (5038), 1598-1603.
13. Yang, H.; Luo, G. B.; Karnchanaphanurach, P.; Louie, T. M.; Rech, I.; Cova, S.; Xun, L. Y.; Xie, X. S., Protein conformational dynamics probed by single-molecule electron transfer. *Science* **2003,** *302* (5643), 262-266.
14. Lu, H. P.; Xun, L. Y.; Xie, X. S., Single-molecule enzymatic dynamics. *Science* **1998,** *282* (5395), 1877-1882.
15. Bhabha, G.; Lee, J.; Ekiert, D. C.; Gam, J.; Wilson, I. A.; Dyson, H. J.; Benkovic, S. J.; Wright, P. E., A Dynamic Knockout Reveals That Conformational Fluctuations Influence the Chemical Step of Enzyme Catalysis. *Science* **2011,** *332* (6026), 234-238.
16. Pisliakov, A. V.; Cao, J.; Kamerlin, S. C. L.; Warshel, A., Enzyme millisecond conformational dynamics do not catalyze the chemical step. *P Natl Acad Sci USA* **2009,** *106* (41), 17359-17364.
17. Adamczyk, A. J.; Cao, J.; Kamerlin, S. C. L.; Warshel, A., Catalysis by dihydrofolate reductase and other enzymes arises from electrostatic preorganization, not conformational motions. *P Natl Acad Sci USA* **2011,** *108* (34), 14115-14120.
18. Singh, B. K.; Walker, A., Microbial degradation of organophosphorus compounds. *Fems Microbiol Rev* **2006,** *30* (3), 428-471.

19. Tokiwa, Y.; Calabia, B. P.; Ugwu, C. U.; Aiba, S., Biodegradability of Plastics. *Int J Mol Sci* **2009,** *10* (9), 3722-3742.
20. Panke, S.; Wubbolts, M., Advances in biocatalytic synthesis of pharmaceutical intermediates. *Curr Opin Chem Biol* **2005,** *9* (2), 188-194.
21. Klibanov, A. M., Why are enzymes less active in organic solvents than in water? *Trends Biotechnol* **1997,** *15* (3), 97-101.
22. Mozhaev, V. V.; Khmelnitsky, Y. L.; Sergeeva, M. V.; Belova, A. B.; Klyachko, N. L.; Levashov, A. V.; Martinek, K., Catalytic Activity and Denaturation of Enzymes in Water Organic Cosolvent Mixtures - Alpha-Chymotrypsin and Laccase in Mixed Water Alcohol, Water Glycol and Water Formamide Solvents. *Eur J Biochem* **1989,** *184* (3), 597-602.
23. Arakawa, T.; Timasheff, S. N., The Stabilization of Proteins by Osmolytes. *Biophys J* **1985,** *47* (3), 411-414.
24. Santoro, M. M.; Liu, Y. F.; Khan, S. M. A.; Hou, L. X.; Bolen, D. W., Increased Thermal-Stability of Proteins in the Presence of Naturally-Occurring Osmolytes. *Biochemistry-Us* **1992,** *31* (23), 5278-5283.
25. Gekko, K.; Timasheff, S. N., Mechanism of Protein Stabilization by Glycerol - Preferential Hydration in Glycerol-Water Mixtures. *Biochemistry-Us* **1981,** *20* (16), 4667-4676.
26. Tribet, C.; Audebert, R.; Popot, J. L., Amphipols: Polymers that keep membrane proteins soluble in aqueous solutions. *P Natl Acad Sci USA* **1996,** *93* (26), 15047-15050.
27. Gohon, Y.; Popot, J. L., Membrane protein-surfactant complexes. *Curr Opin Colloid In* **2003,** *8* (1), 15-22.
28. Goto, M.; Kamiya, N.; Miyata, M.; Nakashio, F., Enzymatic Esterification by Surfactant-Coated Lipase in Organic Media. *Biotechnol Progr* **1994,** *10* (3), 263-268.
29. Yang, Z.; Mesiano, A. J.; Venkatasubramanian, S.; Gross, S. H.; Harris, J. M.; Russell, A. J., Activity and Stability of Enzymes Incorporated into Acrylic Polymers. *Journal of the American Chemical Society* **1995,** *117* (17), 4843-4850.
30. Bismuto, E.; Martelli, P. L.; De Maio, A.; Mita, D. G.; Irace, G.; Casadio, R., Effect of molecular confinement on internal enzyme dynamics: Frequency domain fluorometry and molecular dynamics simulation studies. *Biopolymers* **2002,** *67* (2), 85-95.
31. Zhou, H. X.; Dill, K. A., Stabilization of proteins in confined spaces. *Biochemistry-Us* **2001,** *40* (38), 11289-11293.
32. Kuchler, A.; Yoshimoto, M.; Luginbuhl, S.; Mavelli, F.; Walde, P., Enzymatic reactions in confined environments. *Nat Nanotechnol* **2016,** *11* (5), 409-420.
33. Yoshida, S.; Hiraga, K.; Takehana, T.; Taniguchi, I.; Yamaji, H.; Maeda, Y.; Toyohara, K.; Miyamoto, K.; Kimura, Y.; Oda, K., A bacterium that degrades and assimilates poly(ethylene terephthalate). *Science* **2016,** *351* (6278), 1196-1199.
34. Arnold, F. H., Directed Evolution: Bringing New Chemistry to Life. *Angew Chem Int Edit* **2018,** *57* (16), 4143-4148.
35. Tournier, V.; Topham, C. M.; Gilles, A.; David, B.; Folgoas, C.; Moya-Leclair, E.; Kamionka, E.; Desrousseaux, M. L.; Texier, H.; Gavalda, S.; Cot, M.; Gu?mard, E.; Dalibey, M.; Nomme, J.; Cioci, G.; Barbe, S.; Chateau, M.; Andr?, I.; Duquesne, S.; Marty, A., An engineered PET depolymerase to break down and recycle plastic bottles. *Nature* **2020,** *580* (7802), 216-+.
36. DeGrado, W. F.; Summa, C. M.; Pavone, V.; Nastri, F.; Lombardi, A., De novo design and structural characterization of proteins and metalloproteins. *Annu Rev Biochem* **1999,** *68*, 779-819.

37. Veronese, F. M.; Pasut, G., PEGylation, successful approach to drug delivery. *Drug Discov Today* **2005,** *10* (21), 1451-1458.
38. Yang, Z.; Domach, M.; Auger, R.; Yang, F. X.; Russell, A. J., Polyethylene glycol-induced stabilization of subtilisin. *Enzyme Microb Tech* **1996,** *18* (2), 82-89.
39. Baillargeon, M. W.; Sonnet, P. E., Polyethylene-Glycol Modification of Candida-Rugosa Lipase. *J Am Oil Chem Soc* **1988,** *65* (11), 1812-1815.
40. Gaertner, H. F.; Puigserver, A. J., Increased Activity and Stability of Poly(Ethylene Glycol)-Modified Trypsin. *Enzyme Microb Tech* **1992,** *14* (2), 150-155.
41. Panganiban, B.; Qiao, B. F.; Jiang, T.; DelRe, C.; Obadia, M. M.; Nguyen, T. D.; Smith, A. A. A.; Hall, A.; Sit, I.; Crosby, M. G.; Dennis, P. B.; Drockenmuller, E.; de la Cruz, M. O.; Xu, T., Random heteropolymers preserve protein function in foreign environments. *Science* **2018,** *359* (6381), 1239-+.
42. Tate, C. G., Practical Considerations of Membrane Protein Instability during Purification and Crystallisation. *Methods Mol Biol* **2010,** *601*, 187-203.

Chapter 2

1. Mozhaev, V. V.; Khmelnitsky, Y. L.; Sergeeva, M. V.; Belova, A. B.; Klyachko, N. L.; Levashov, A. V.; Martinek, K., Catalytic Activity and Denaturation of Enzymes in Water Organic Cosolvent Mixtures - Alpha-Chymotrypsin and Laccase in Mixed Water Alcohol, Water Glycol and Water Formamide Solvents. *Eur J Biochem* **1989,** *184* (3), 597-602.
2. Klibanov, A. M., Why are enzymes less active in organic solvents than in water? *Trends Biotechnol* **1997,** *15* (3), 97-101.
3. Klibanov, A. M., Improving enzymes by using them in organic solvents. *Nature* **2001,** *409* (6817), 241-246.
4. Singh, B. K.; Walker, A., Microbial degradation of organophosphorus compounds. *Fems Microbiol Rev* **2006,** *30* (3), 428-471.
5. Caldwell, S. R.; Raushel, F. M., Detoxification of Organophosphate Pesticides Using a Nylon Based Immobilized Phosphotriesterase from Pseudomonas-Diminuta. *Appl Biochem Biotech* **1991,** *31* (1), 59-73.
6. LeJeune, K. E.; Russell, A. J., Covalent binding of a nerve agent hydrolyzing enzyme within polyurethane foams. *Biotechnol Bioeng* **1996,** *51* (4), 450-457.
7. Gill, I.; Ballesteros, A., Degradation of organophosphorous nerve agents by enzyme-polymer nanocomposites: Efficient biocatalytic materials for personal protection and large-scale detoxification. *Biotechnol Bioeng* **2000,** *70* (4), 400-410.
8. Dennis, P. B.; Walker, A. Y.; Dickerson, M. B.; Kaplan, D. L.; Naik, R. R., Stabilization of Organophosphorus Hydrolase by Entrapment in Silk Fibroin: Formation of a Robust Enzymatic Material Suitable for Surface Coatings. *Biomacromolecules* **2012,** *13* (7), 2037-2045.
9. Reneker, D. H.; Chun, I., Nanometre diameter fibres of polymer, produced by electrospinning. *Nanotechnology* **1996,** *7* (3), 216-223.
10. Kim, M.; Gkikas, M.; Huang, A.; Kang, J. W.; Suthiwangcharoen, N.; Nagarajan, R.; Olsen, B. D., Enhanced activity and stability of organophosphorus hydrolase via interaction with an amphiphilic polymer. *Chem Commun* **2014,** *50* (40), 5345-5348.

11. Mills, C. E.; Obermeyer, A.; Dong, X. H.; Walker, J.; Olsen, B. D., Complex Coacervate Core Micelles for the Dispersion and Stabilization of Organophosphate Hydrolase in Organic Solvents. *Langmuir* **2016,** *32* (50), 13367-13376.
12. Panganiban, B.; Qiao, B. F.; Jiang, T.; DelRe, C.; Obadia, M. M.; Nguyen, T. D.; Smith, A. A. A.; Hall, A.; Sit, I.; Crosby, M. G.; Dennis, P. B.; Drockenmuller, E.; de la Cruz, M. O.; Xu, T., Random heteropolymers preserve protein function in foreign environments. *Science* **2018,** *359* (6381), 1239-+.
13. Zheng, J. Y.; Constantine, C. A.; Rastogi, V. K.; Cheng, T. C.; DeFrank, J. J.; Leblanc, R. M., Secondary structure of organophosphorus hydrolase in solution and in Langmuir-Blodgett film studied by circular dichroism spectroscopy. *J Phys Chem B* **2004,** *108* (44), 17238-17242.
14. Chen, B. W.; Lei, C. H.; Shin, Y. S.; Liu, J., Probing mechanisms for enzymatic activity enhancement of organophosphorus hydrolase in functionalized mesoporous silica. *Biochem Bioph Res Co* **2009,** *390* (4), 1177-1181.
15. Whitmore, L.; Wallace, B. A., Protein secondary structure analyses from circular dichroism spectroscopy: Methods and reference databases. *Biopolymers* **2008,** *89* (5), 392-400.
16. Lewis, R. J.; Sax, N. I., *Sax's dangerous properties of industrial materials*. 9th ed.; Van Nostrand Reinhold: New York, 1996.
17. Sharma, K. P.; Collins, A. M.; Perriman, A. W.; Mann, S., Enzymatically Active Self-Standing Protein-Polymer Surfactant Films Prepared by Hierarchical Self-Assembly. *Adv Mater* **2013,** *25* (14), 2005-2010.
18. Pedrosa, V. A.; Paliwal, S.; Balasubramanian, S.; Nepal, D.; Davis, V.; Wild, J.; Ramanculov, E.; Simonian, A., Enhanced stability of enzyme organophosphate hydrolase interfaced on the carbon nanotubes. *Colloid Surface B* **2010,** *77* (1), 69-74.
19. Lu, H. D.; Wheeldon, I. R.; Banta, S., Catalytic biomaterials: engineering organophosphate hydrolase to form self-assembling enzymatic hydrogels. *Protein Eng Des Sel* **2010,** *23* (7), 559-566.
20. Du, D.; Chen, W. J.; Zhang, W. Y.; Liu, D. L.; Li, H. B.; Lin, Y. H., Covalent coupling of organophosphorus hydrolase loaded quantum dots to carbon nanotube/Au nanocomposite for enhanced detection of methyl parathion. *Biosens Bioelectron* **2010,** *25* (6), 1370-1375.
21. LeJeune, K. E.; Mesiano, A. J.; Bower, S. B.; Grimsley, J. K.; Wild, J. R.; Russell, A. J., Dramatically stabilized phosphotriesterase-polymers for nerve agent degradation. *Biotechnol Bioeng* **1997,** *54* (2), 105-114.

Chapter 3

1. Austin, R. H.; Beeson, K. W.; Eisenstein, L.; Frauenfelder, H.; Gunsalus, I. C., Dynamics of Ligand-Binding to Myoglobin. *Biochemistry-Us* **1975,** *14* (24), 5355-5373.
2. Mccammon, J. A.; Gelin, B. R.; Karplus, M., Dynamics of Folded Proteins. *Nature* **1977,** *267* (5612), 585-590.
3. Adamczyk, A. J.; Cao, J.; Kamerlin, S. C. L.; Warshel, A., Catalysis by dihydrofolate reductase and other enzymes arises from electrostatic preorganization, not conformational motions. *P Natl Acad Sci USA* **2011,** *108* (34), 14115-14120.
4. Bhabha, G.; Lee, J.; Ekiert, D. C.; Gam, J.; Wilson, I. A.; Dyson, H. J.; Benkovic, S. J.; Wright, P. E., A Dynamic Knockout Reveals That Conformational Fluctuations Influence the Chemical Step of Enzyme Catalysis. *Science* **2011,** *332* (6026), 234-238.

5. Hammes, G. G.; Benkovic, S. J.; Hammes-Schiffer, S., Flexibility, Diversity, and Cooperativity: Pillars of Enzyme Catalysis. *Biochemistry-Us* **2011,** *50* (48), 10422-10430.
6. Frauenfelder, H.; Sligar, S. G.; Wolynes, P. G., The Energy Landscapes and Motions of Proteins. *Science* **1991,** *254* (5038), 1598-1603.
7. Dube, N.; Presley, A. D.; Shu, J. Y.; Xu, T., Amphiphilic Peptide-Polymer Conjugates with Side-Conjugation. *Macromol Rapid Comm* **2011,** *32* (4), 344-353.
8. Degrado, W. F.; Lear, J. D., Induction of Peptide Conformation at Apolar Water Interfaces .1. A Study with Model Peptides of Defined Hydrophobic Periodicity. *J Am Chem Soc* **1985,** *107* (25), 7684-7689.
9. Xu, G. F.; Wang, W. X.; Groves, J. T.; Hecht, M. H., Self-assembled monolayers from a designed combinatorial library of de novo beta-sheet proteins. *P Natl Acad Sci USA* **2001,** *98* (7), 3652-3657.
10. Bowerman, C. J.; Nilsson, B. L., A Reductive Trigger for Peptide Self-Assembly and Hydrogelation. *J Am Chem Soc* **2010,** *132* (28), 9526-9527.
11. Pappas, C. G.; Shafi, R.; Sasselli, I. R.; Siccardi, H.; Wang, T.; Narang, V.; Abzalimov, R.; Wijerathne, N.; Ulijn, R. V., Dynamic peptide libraries for the discovery of supramolecular nanomaterials. *Nat Nanotechnol* **2016,** *11* (11), 960-967.
12. Klibanov, A. M., Why are enzymes less active in organic solvents than in water? *Trends Biotechnol* **1997,** *15* (3), 97-101.
13. Hedstrom, L.; Szilagyi, L.; Rutter, W. J., Converting Trypsin to Chymotrypsin - the Role of Surface Loops. *Science* **1992,** *255* (5049), 1249-1253.
14. Redko, Y.; de la Sierra-Gallay, I. L.; Condon, C., When all's zed and done: the structure and function of RNase Z in prokaryotes. *Nat Rev Microbiol* **2007,** *5* (4), 278-286.
15. Jackson, C. J.; Foo, J. L.; Tokuriki, N.; Afriat, L.; Carr, P. D.; Kim, H. K.; Schenk, G.; Tawfik, D. S.; Ollis, D. L., Conformational sampling, catalysis, and evolution of the bacterial phosphotriesterase. *P Natl Acad Sci USA* **2009,** *106* (51), 21631-21636.
16. Trodler, P.; Schmid, R. D.; Pleiss, J., Modeling of solvent-dependent conformational transitions in Burkholderia cepacia lipase. *Bmc Struct Biol* **2009,** *9*.
17. Henzler-Wildman, K. A.; Lei, M.; Thai, V.; Kerns, S. J.; Karplus, M.; Kern, D., A hierarchy of timescales in protein dynamics is linked to enzyme catalysis. *Nature* **2007,** *450* (7171), 913-U27.
18. Thompson, M. J.; Eisenberg, D., Transproteomic evidence of a loop-deletion mechanism for enhancing protein thermostability. *J Mol Biol* **1999,** *290* (2), 595-604.
19. Yu, H. R.; Yan, Y. H.; Zhang, C.; Dalby, P. A., Two strategies to engineer flexible loops for improved enzyme thermostability. *Sci Rep-Uk* **2017,** *7*.
20. Chen, K. Q.; Arnold, F. H., Tuning the Activity of an Enzyme for Unusual Environments - Sequential Random Mutagenesis of Subtilisin-E for Catalysis in Dimethylformamide. *P Natl Acad Sci USA* **1993,** *90* (12), 5618-5622.
21. Beverung, C. J.; Radke, C. J.; Blanch, H. W., Protein adsorption at the oil/water interface: characterization of adsorption kinetics by dynamic interfacial tension measurements. *Biophys Chem* **1999,** *81* (1), 59-80.
22. Brzozowski, A. M.; Derewenda, U.; Derewenda, Z. S.; Dodson, G. G.; Lawson, D. M.; Turkenburg, J. P.; Bjorkling, F.; Hugejensen, B.; Patkar, S. A.; Thim, L., A Model for Interfacial Activation in Lipases from the Structure of a Fungal Lipase-Inhibitor Complex. *Nature* **1991,** *351* (6326), 491-494.

23. Ghatorae, A. S.; Guerra, M. J.; Bell, G.; Halling, P. J., Immiscible Organic-Solvent Inactivation of Urease, Chymotrypsin, Lipase, and Ribonuclease - Separation of Dissolved Solvent and Interfacial Effects. *Biotechnol Bioeng* **1994,** *44* (11), 1355-1361.
24. Zheng, F.; Zhan, C. G.; Ornstein, R. L., Theoretical studies of reaction pathways and energy barriers for alkaline hydrolysis of phosphotriesterase substrates paraoxon and related toxic phosphofluoridate nerve agents. *J Chem Soc Perk T 2* **2001,** (12), 2355-2363.
25. Singh, B. K.; Walker, A., Microbial degradation of organophosphorus compounds. *Fems Microbiol Rev* **2006,** *30* (3), 428-471.
26. Chen-Goodspeed, M.; Sogorb, M. A.; Wu, F. Y.; Hong, S. B.; Raushel, F. M., Structural determinants of the substrate and stereochemical specificity of phosphotriesterase. *Biochemistry-Us* **2001,** *40* (5), 1325-1331.
27. Hong, S. B.; Raushel, F. M., Stereochemical constraints on the substrate specificity of phosphotriesterase. *Biochemistry-Us* **1999,** *38* (4), 1159-1165.
28. Panganiban, B.; Qiao, B. F.; Jiang, T.; DelRe, C.; Obadia, M. M.; Nguyen, T. D.; Smith, A. A. A.; Hall, A.; Sit, I.; Crosby, M. G.; Dennis, P. B.; Drockenmuller, E.; de la Cruz, M. O.; Xu, T., Random heteropolymers preserve protein function in foreign environments. *Science* **2018,** *359* (6381), 1239-+.
29. DelRe, C.; Huang, C.; Li, T.; Dennis, P.; Drockenmuller, E.; Xu, T., Reusable Enzymatic Fiber Mats for Neurotoxin Remediation in Water. *Acs Appl Mater Inter* **2018,** *10* (51), 44216-44220.
30. Reshetnyak, Y. K.; Koshevnik, Y.; Burstein, E. A., Decomposition of protein tryptophan fluorescence spectra into log-normal components. III. Correlation between fluorescence and microenvironment parameters of individual tryptophan residues. *Biophys J* **2001,** *81* (3), 1735-1758.
31. Qiu, W. H.; Li, T. P.; Zhang, L. Y.; Yang, Y.; Kao, Y. T.; Wang, L. J.; Zhong, D. P., Ultrafast quenching of tryptophan fluorescence in proteins: Interresidue and intrahelical electron transfer. *Chem Phys* **2008,** *350* (1-3), 154-164.
32. Karagoz, G. E.; Duarte, A. M. S.; Akoury, E.; Ippel, H.; Biernat, J.; Luengo, T. M.; Radli, M.; Didenko, T.; Nordhues, B. A.; Veprintsev, D. B.; Dickey, C. A.; Mandelkow, E.; Zweckstetter, M.; Boelens, R.; Madl, T.; Rudiger, S. G. D., Hsp90-Tau Complex Reveals Molecular Basis for Specificity in Chaperone Action. *Cell* **2014,** *156* (5), 963-974.
33. Nichol, L. W.; Jackson, W. J. H.; Winzor, D. J., Preferential Binding of Competitive Inhibitors to Monomeric Form of Alpha-Chymotrypsin. *P Aust Biochem Soc* **1972,** *5* (Nmay), 13-&.
34. Liu, E. J.; Jiang, S. Y., Expressing a Monomeric Organophosphate Hydrolase as an EK Fusion Protein. *Bioconjugate Chem* **2018,** *29* (11), 3686-3690.
35. Zhang, H.; Yang, L.; Yan, L. F.; Liao, R. Z.; Tian, W. Q., Evolution of phosphotriesterase activities of the metallo-beta-lactamase family: A theoretical study. *J Inorg Biochem* **2018,** *184*, 8-14.
36. Yang, Z.; Mesiano, A. J.; Venkatasubramanian, S.; Gross, S. H.; Harris, J. M.; Russell, A. J., Activity and Stability of Enzymes Incorporated into Acrylic Polymers. *J Am Chem Soc* **1995,** *117* (17), 4843-4850.

Chapter 4

1. Wells, A.; Meyer, H. P., Biocatalysis as a Strategic Green Technology for the Chemical Industry. *Chemcatchem* **2014,** *6* (4), 918-920.
2. Truppo, M. D., Biocatalysis in the Pharmaceutical Industry: The Need for Speed. *Acs Med Chem Lett* **2017,** *8* (5), 476-480.
3. Klibanov, A. M., Why are enzymes less active in organic solvents than in water? *Trends Biotechnol* **1997,** *15* (3), 97-101.
4. Margolin, A. L.; Klibanov, A. M., Peptide-Synthesis Catalyzed by Lipases in Anhydrous Organic-Solvents. *J Am Chem Soc* **1987,** *109* (12), 3802-3804.
5. Zaks, A.; Klibanov, A. M., Substrate-Specificity of Enzymes in Organic-Solvents Vs Water Is Reversed. *J Am Chem Soc* **1986,** *108* (10), 2767-2768.
6. Klibanov, A. M., Improving enzymes by using them in organic solvents. *Nature* **2001,** *409* (6817), 241-246.
7. Volkin, D. B.; Staubli, A.; Langer, R.; Klibanov, A. M., Enzyme Thermoinactivation in Anhydrous Organic-Solvents. *Biotechnol Bioeng* **1991,** *37* (9), 843-853.
8. Zaks, A.; Klibanov, A. M., The Effect of Water on Enzyme Action in Organic Media. *J Biol Chem* **1988,** *263* (17), 8017-8021.
9. Walker, D. A.; Kowalczyk, B.; de la Cruz, M. O.; Grzybowski, B. A., Electrostatics at the nanoscale. *Nanoscale* **2011,** *3* (4), 1316-1344.
10. Panganiban, B.; Qiao, B. F.; Jiang, T.; DelRe, C.; Obadia, M. M.; Nguyen, T. D.; Smith, A. A. A.; Hall, A.; Sit, I.; Crosby, M. G.; Dennis, P. B.; Drockenmuller, E.; de la Cruz, M. O.; Xu, T., Random heteropolymers preserve protein function in foreign environments. *Science* **2018,** *359* (6381), 1239-+.
11. Krishna, S. H.; Karanth, N. G., Lipases and lipase-catalyzed esterification reactions in nonaqueous media. *Catal Rev* **2002,** *44* (4), 499-591.
12. Poole, P. L.; Finney, J. L., Hydration-Induced Conformational and Flexibility Changes in Lysozyme at Low Water-Content. *Int J Biol Macromol* **1983,** *5* (5), 308-310.
13. Suwannakarn, K.; Lotero, E.; Ngaosuwan, K.; Goodwin, J. G., Simultaneous Free Fatty Acid Esterification and Triglyceride Transesterification Using a Solid Acid Catalyst with in Situ Removal of Water and Unreacted Methanol. *Ind Eng Chem Res* **2009,** *48* (6), 2810-2818.
14. Beverung, C. J.; Radke, C. J.; Blanch, H. W., Protein adsorption at the oil/water interface: characterization of adsorption kinetics by dynamic interfacial tension measurements. *Biophys Chem* **1999,** *81* (1), 59-80.
15. Louwrier, A.; Drtina, G. J.; Klibanov, A. M., On the issue of interfacial activation of lipase in nonaqueous media. *Biotechnol Bioeng* **1996,** *50* (1), 1-5.
16. Beckham, G. T.; Crowley, M. F., Examination of the alpha-Chitin Structure and Decrystallization Thermodynamics at the Nanoscale. *J Phys Chem B* **2011,** *115* (15), 4516-4522.
17. Austin, H. P.; Allen, M. D.; Donohoe, B. S.; Rorrer, N. A.; Kearns, F. L.; Silveira, R. L.; Pollard, B. C.; Dominick, G.; Duman, R.; El Omari, K.; Mykhaylyk, V.; Wagner, A.; Michener, W. E.; Amore, A.; Skaf, M. S.; Crowley, M. F.; Thorne, A. W.; Johnson, C. W.; Woodcock, H. L.; McGeehan, J. E.; Beckham, G. T., Characterization and engineering of a plastic-degrading aromatic polyesterase. *Proc Natl Acad Sci U S A* **2018**.
18. Bornscheuer, U.; Reif, O. W.; Lausch, R.; Freitag, R.; Scheper, T.; Kolisis, F. N.; Menge, U., Lipase of Pseudomonas-Cepacia for Biotechnological Purposes - Purification, Crystallization and Characterization. *Bba-Gen Subjects* **1994,** *1201* (1), 55-60.

19. Sastry, G. M.; Adzhigirey, M.; Day, T.; Annabhimoju, R.; Sherman, W., Protein and ligand preparation: parameters, protocols, and influence on virtual screening enrichments. *J Comput Aid Mol Des* **2013,** *27* (3), 221-234.
20. Sherman, W.; Day, T.; Jacobson, M. P.; Friesner, R. A.; Farid, R., Novel procedure for modeling ligand/receptor induced fit effects. *J Med Chem* **2006,** *49* (2), 534-553.
21. Chen-Goodspeed, M.; Sogorb, M. A.; Wu, F. Y.; Hong, S. B.; Raushel, F. M., Structural determinants of the substrate and stereochemical specificity of phosphotriesterase. *Biochemistry-Us* **2001,** *40* (5), 1325-1331.

Chapter 5

1. Tokiwa, Y.; Calabia, B. P.; Ugwu, C. U.; Aiba, S., Biodegradability of Plastics. *Int J Mol Sci* **2009,** *10* (9), 3722-3742.
2. Jambeck, J. R.; Geyer, R.; Wilcox, C.; Siegler, T. R.; Perryman, M.; Andrady, A.; Narayan, R.; Law, K. L., Plastic waste inputs from land into the ocean. *Science* **2015,** *347* (6223), 768-771.
3. Ivleva, N. P.; Wiesheu, A. C.; Niessner, R., Microplastic in Aquatic Ecosystems. *Angew Chem Int Edit* **2017,** *56* (7), 1720-1739.
4. Haider, T.; Volker, C.; Kramm, J.; Landfester, K.; Wurm, F. R., Plastics of the future? The impact of biodegradable polymers on the environment and on society. *Angew Chem Int Ed Engl* **2018**.
5. Austin, H. P.; Allen, M. D.; Donohoe, B. S.; Rorrer, N. A.; Kearns, F. L.; Silveira, R. L.; Pollard, B. C.; Dominick, G.; Duman, R.; El Omari, K.; Mykhaylyk, V.; Wagner, A.; Michener, W. E.; Amore, A.; Skaf, M. S.; Crowley, M. F.; Thorne, A. W.; Johnson, C. W.; Woodcock, H. L.; McGeehan, J. E.; Beckham, G. T., Characterization and engineering of a plastic-degrading aromatic polyesterase. *Proc Natl Acad Sci U S A* **2018**.
6. Arnold, F. H., Directed Evolution: Bringing New Chemistry to Life. *Angew Chem Int Edit* **2018,** *57* (16), 4143-4148.
7. Yoshida, S.; Hiraga, K.; Takehana, T.; Taniguchi, I.; Yamaji, H.; Maeda, Y.; Toyohara, K.; Miyamoto, K.; Kimura, Y.; Oda, K., A bacterium that degrades and assimilates poly(ethylene terephthalate). *Science* **2016,** *351* (6278), 1196-1199.
8. Panganiban, B.; Qiao, B. F.; Jiang, T.; DelRe, C.; Obadia, M. M.; Nguyen, T. D.; Smith, A. A. A.; Hall, A.; Sit, I.; Crosby, M. G.; Dennis, P. B.; Drockenmuller, E.; de la Cruz, M. O.; Xu, T., Random heteropolymers preserve protein function in foreign environments. *Science* **2018,** *359* (6381), 1239-+.
9. Ganesh, M.; Dave, R. N.; L'Amoreaux, W.; Gross, R. A., Embedded Enzymatic Biomaterial Degradation. *Macromolecules* **2009,** *42* (18), 6836-6839.
10. DelRe, C.; Huang, C.; Li, T.; Dennis, P.; Drockenmuller, E.; Xu, T., Reusable Enzymatic Fiber Mats for Neurotoxin Remediation in Water. *Acs Appl Mater Inter* **2018,** *10* (51), 44216-44220.
11. Lambert, S.; Wagner, M., Environmental performance of bio-based and biodegradable plastics: the road ahead. *Chem Soc Rev* **2017,** *46* (22), 6855-6871.
12. Khan, I.; Nagarjuna, R.; Dutta, J. R.; Ganesan, R., Enzyme-Embedded Degradation of Poly(epsilon-caprolactone) using Lipase-Derived from Probiotic Lactobacillus plantarum. *Acs Omega* **2019,** *4* (2), 2844-2852.

13. Zhou, H. X.; Dill, K. A., Stabilization of proteins in confined spaces. *Biochemistry-Us* **2001,** *40* (38), 11289-11293.
14. Kuchler, A.; Yoshimoto, M.; Luginbuhl, S.; Mavelli, F.; Walde, P., Enzymatic reactions in confined environments. *Nat Nanotechnol* **2016,** *11* (5), 409-420.
15. Johnson, K. A.; Goody, R. S., The Original Michaelis Constant: Translation of the 1913 Michaelis-Menten Paper. *Biochemistry-Us* **2011,** *50* (39), 8264-8269.
16. Zhao, D.; Gimenez-Pinto, V.; Jimenez, A. M.; Zhao, L. X.; Jestin, J.; Kumar, S. K.; Kuei, B.; Gomez, E. D.; Prasad, A. S.; Schadler, L. S.; Khani, M. M.; Benicewicz, B. C., Tunable Multiscale Nanoparticle Ordering by Polymer Crystallization. *Acs Central Sci* **2017,** *3* (7), 751-758.
17. Yang, Z.; Mesiano, A. J.; Venkatasubramanian, S.; Gross, S. H.; Harris, J. M.; Russell, A. J., Activity and Stability of Enzymes Incorporated into Acrylic Polymers. *Journal of the American Chemical Society* **1995,** *117* (17), 4843-4850.
18. Flory, P. J.; Yoon, D. Y., Molecular Morphology in Semi-Crystalline Polymers. *Nature* **1978,** *272* (5650), 226-229.
19. Flory, P. J.; Yoon, D. Y.; Dill, K. A., The Interphase in Lamellar Semicrystalline Polymers. *Macromolecules* **1984,** *17* (4), 862-868.
20. Payne, C. M.; Himmel, M. E.; Crowley, M. F.; Beckham, G. T., Decrystallization of Oligosaccharides from the Cellulose I beta Surface with Molecular Simulation. *J Phys Chem Lett* **2011,** *2* (13), 1546-1550.
21. Beckham, G. T.; Matthews, J. F.; Peters, B.; Bomble, Y. J.; Himmel, M. E.; Crowley, M. F., Molecular-Level Origins of Biomass Recalcitrance: Decrystallization Free Energies for Four Common Cellulose Polymorphs. *J Phys Chem B* **2011,** *115* (14), 4118-4127.
22. Tokiwa, Y.; Suzuki, T., Hydrolysis of Polyesters by Lipases. *Nature* **1977,** *270* (5632), 76-78.
23. Kawai, F.; Nakadai, K.; Nishioka, E.; Nakajima, H.; Ohara, H.; Masaki, K.; Iefuji, H., Different enantioselectivity of two types of poly(lactic acid) depolymerases toward poly(L-lactic acid) and poly(D-lactic acid). *Polym Degrad Stabil* **2011,** *96* (7), 1342-1348.
24. Liu, L.; Li, S.; Garreau, H.; Vert, M., Selective enzymatic degradations of poly(L-lactide) and poly(epsilon-caprolactone) blend films. *Biomacromolecules* **2000,** *1* (3), 350-9.
25. Xu, F. F.; Cohen, S. N., Rna Degradation in Escherichia-Coli Regulated by 3' Adenylation and 5' Phosphorylatian. *Nature* **1995,** *374* (6518), 180-183.
26. Sarkar, N., Polyadenylation of mRNA in prokaryotes. *Annu Rev Biochem* **1997,** *66*, 173-197.
27. Horn, S. J.; Sikorski, P.; Cederkvist, J. B.; Vaaje-Kolstad, G.; Sorlie, M.; Synstad, B.; Vriend, G.; Varum, K. M.; Eijsink, V. G. H., Costs and benefits of processivity in enzymatic degradation of recalcitrant polysaccharides. *P Natl Acad Sci USA* **2006,** *103* (48), 18089-18094.
28. Pleiss, J.; Fischer, M.; Schmid, R. D., Anatomy of lipase binding sites: the scissile fatty acid binding site. *Chem Phys Lipids* **1998,** *93* (1-2), 67-80.
29. Bornscheuer, U.; Reif, O. W.; Lausch, R.; Freitag, R.; Scheper, T.; Kolisis, F. N.; Menge, U., Lipase of Pseudomonas-Cepacia for Biotechnological Purposes - Purification, Crystallization and Characterization. *Bba-Gen Subjects* **1994,** *1201* (1), 55-60.
30. Wurm, A.; Zhuravlev, E.; Eckstein, K.; Jehnichen, D.; Pospiech, D.; Androsch, R.; Wunderlich, B.; Schick, C., Crystallization and Homogeneous Nucleation Kinetics of Poly(epsilon-caprolactone) (PCL) with Different Molar Masses. *Macromolecules* **2012,** *45* (9), 3816-3828.

31. Ajioka, M.; Suizu, H.; Higuchi, C.; Kashima, T., Aliphatic polyesters and their copolymers synthesized through direct condensation polymerization. *Polym Degrad Stabil* **1998,** *59* (1-3), 137-143.

Chapter 6

1. Zhao, D.; Gimenez-Pinto, V.; Jimenez, A. M.; Zhao, L. X.; Jestin, J.; Kumar, S. K.; Kuei, B.; Gomez, E. D.; Prasad, A. S.; Schadler, L. S.; Khani, M. M.; Benicewicz, B. C., Tunable Multiscale Nanoparticle Ordering by Polymer Crystallization. *Acs Central Sci* **2017,** *3* (7), 751-758.
2. Flory, P. J.; Yoon, D. Y., Molecular Morphology in Semi-Crystalline Polymers. *Nature* **1978,** *272* (5650), 226-229.
3. Flory, P. J., Thermodynamics of Crystallization in High Polymers .4. A Theory of Crystalline States and Fusion in Polymers, Copolymers, and Their Mixtures with Diluents. *J Chem Phys* **1949,** *17* (3), 223-240.
4. Alfonso, G. C.; Russell, T. P., Kinetics of Crystallization in Semicrystalline Amorphous Polymer Mixtures. *Macromolecules* **1986,** *19* (4), 1143-1152.
5. Varmanair, M.; Pan, R.; Wunderlich, B., Heat-Capacities and Entropies of Linear, Aliphatic Polyesters. *J Polym Sci Pol Phys* **1991,** *29* (9), 1107-1115.
6. Li, S. M.; McCarthy, S., Influence of crystallinity and stereochemistry on the enzymatic degradation of poly(lactide)s. *Macromolecules* **1999,** *32* (13), 4454-4456.
7. Tokiwa, Y.; Calabia, B. P.; Ugwu, C. U.; Aiba, S., Biodegradability of Plastics. *Int J Mol Sci* **2009,** *10* (9), 3722-3742.
8. Beckham, G. T.; Matthews, J. F.; Peters, B.; Bomble, Y. J.; Himmel, M. E.; Crowley, M. F., Molecular-Level Origins of Biomass Recalcitrance: Decrystallization Free Energies for Four Common Cellulose Polymorphs. *J Phys Chem B* **2011,** *115* (14), 4118-4127.
9. Hall, M.; Bansal, P.; Lee, J. H.; Realff, M. J.; Bommarius, A. S., Cellulose crystallinity - a key predictor of the enzymatic hydrolysis rate. *Febs J* **2010,** *277* (6), 1571-1582.
10. Darras, O.; Seguela, R., Surface Free-Energy of the Chain-Folding Crystal Faces of Ethylene Butene Random Copolymers. *Polymer* **1993,** *34* (14), 2946-2950.
11. Sirotkin, R. O.; Brooks, N. W., The dynamic mechanical relaxation behaviour of polyethylene copolymers cast from solution. *Polymer* **2001,** *42* (24), 9801-9808.
12. Huang, Q.; Mednova, O.; Rasmussen, H. K.; Alvarez, N. J.; Skov, A. L.; Almdal, K.; Hassager, O., Concentrated Polymer Solutions are Different from Melts: Role of Entanglement Molecular Weight. *Macromolecules* **2013,** *46* (12), 5026-5035.
13. Mansfield, M. L., Monte-Carlo Study of Chain Folding in Melt-Crystallized Polymers. *Macromolecules* **1983,** *16* (6), 914-920.

Chapter 7

1. Liu, X. L.; Huettner, S.; Rong, Z. X.; Sommer, M.; Friend, R. H., Solvent Additive Control of Morphology and Crystallization in Semiconducting Polymer Blends. *Adv Mater* **2012,** *24* (5), 669-+.

2. Li, J. M.; Ma, P. L.; Favis, B. D., The role of the blend interface type on morphology in cocontinuous polymer blends. *Macromolecules* **2002,** *35* (6), 2005-2016.
3. Balazs, A. C.; Emrick, T.; Russell, T. P., Nanoparticle polymer composites: Where two small worlds meet. *Science* **2006,** *314* (5802), 1107-1110.
4. Lin, Y.; Boker, A.; He, J. B.; Sill, K.; Xiang, H. Q.; Abetz, C.; Li, X. F.; Wang, J.; Emrick, T.; Long, S.; Wang, Q.; Balazs, A.; Russell, T. P., Self-directed self-assembly of nanoparticle/copolymer mixtures. *Nature* **2005,** *434* (7029), 55-59.
5. Keith, H. D.; Padden, F. J.; Russell, T. P., Morphological-Changes in Polyesters and Polyamides Induced by Blending with Small Concentrations of Polymer Diluents. *Macromolecules* **1989,** *22* (2), 666-675.
6. Keith, H. D.; Padden, F. J., Twisting Orientation and the Role of Transient States in Polymer Crystallization. *Polymer* **1984,** *25* (1), 28-42.
7. Lotz, B.; Cheng, S. Z. D., A critical assessment of unbalanced surface stresses as the mechanical origin of twisting and scrolling of polymer crystals. *Polymer* **2005,** *46* (3), 577-610.
8. Lotz, B.; Cheng, S. Z. D., Comments on: 'A critical assessment of unbalanced surface stresses: Some complementary considerations', by DC Bassett. *Polymer* **2006,** *47* (9), 3267-3270.
9. Ong, C. J.; Price, F. P., Blends of Poly(Epsilon-Caprolactone) with Polyvinyl-Chloride) .2. Crystallization Kinetics. *J Polym Sci Pol Sym* **1977,** (63), 59-75.
10. Reinsch, V. E.; Rebenfeld, L., Crystallization Processes in Poly(Ethylene-Terephthalate) as Modified by Polymer Additives and Fiber Reinforcement. *J Appl Polym Sci* **1994,** *52* (5), 649-662.
11. Gautam, S.; Balijepalli, S.; Rutledge, G. C., Molecular simulations df the interlamellar phase in polymers: Effect of chain tilt. *Macromolecules* **2000,** *33* (24), 9136-9145.
12. Flory, P. J., On Morphology of Crystalline State in Polymers. *J Am Chem Soc* **1962,** *84* (15), 2857-&.
13. Fritzsching, K. J.; Mao, K.; Schmidt-Rohr, K., Avoidance of Density Anomalies as a Structural Principle for Semicrystalline Polymers: The Importance of Chain Ends and Chain Tilt. *Macromolecules* **2017,** *50* (4), 1521-1540.
14. Flory, P. J.; Yoon, D. Y.; Dill, K. A., The Interphase in Lamellar Semicrystalline Polymers. *Macromolecules* **1984,** *17* (4), 862-868.
15. Yoon, D. Y.; Flory, P. J., Chain Packing at Polymer Interfaces. *Macromolecules* **1984,** *17* (4), 868-871.
16. Cheng, S. Z. D.; Pan, R.; Wunderlich, B., Thermal-Analysis of Poly(Butylene Terephthalate) for Heat-Capacity, Rigid-Amorphous Content, and Transition Behavior. *Makromol Chem* **1988,** *189* (10), 2443-2458.
17. Kuwabara, K.; Kaji, H.; Horii, F.; Bassett, D. C.; Olley, R. H., Solid-state C-13 NMR analyses of the crystalline-noncrystalline structure for metallocene-catalyzed linear low-density polyethylene. *Macromolecules* **1997,** *30* (24), 7516-7521.
18. Resch, M. G.; Donohoe, B. S.; Baker, J. O.; Decker, S. R.; Bayer, E. A.; Beckham, G. T.; Himmel, M. E., Fungal cellulases and complexed cellulosomal enzymes exhibit synergistic mechanisms in cellulose deconstruction. *Energ Environ Sci* **2013,** *6* (6), 1858-1867.
19. Knott, B. C.; Erickson, E.; Allen, M. D.; Gado, J. E.; Graham, R.; Kearns, F. L.; Pardo, I.; Topuzlu, E.; Anderson, J. J.; Austin, H. P.; Dominick, G.; Johnson, C. W.; Rorrer, N. A.; Szostkiewicz, C. J.; Copie, V.; Payne, C. M.; Woodcock, H. L.; Donohoe, B. S.; Beckham, G. T.; McGeehan, J. E., Characterization and engineering of a two-enzyme system for plastics depolymerization. *Proc Natl Acad Sci U S A* **2020,** *117* (41), 25476-25485.

20. Meyer-Cifuentes, I. E.; Werner, J.; Jehmlich, N.; Will, S. E.; Neumann-Schaal, M.; Ozturk, B., Synergistic biodegradation of aromatic-aliphatic copolyester plastic by a marine microbial consortium. *Nat Commun* **2020,** *11* (1), 5790.